



Kent Academic Repository

Marsh, Jack (2021) *Synthesis & Characterization of supramolecular polypeptide network using PP II and Zinc at the water/oil interface*. Master of Science by Research (MScRes) thesis, University of Kent,.

Downloaded from

<https://kar.kent.ac.uk/89663/> The University of Kent's Academic Repository KAR

The version of record is available from

<https://doi.org/10.22024/UniKent/01.02.89663>

This document version

UNSPECIFIED

DOI for this version

Licence for this version

CC BY (Attribution)

Additional information

Versions of research works

Versions of Record

If this version is the version of record, it is the same as the published version available on the publisher's web site. Cite as the published version.

Author Accepted Manuscripts

If this document is identified as the Author Accepted Manuscript it is the version after peer review but before type setting, copy editing or publisher branding. Cite as Surname, Initial. (Year) 'Title of article'. To be published in *Title of Journal*, Volume and issue numbers [peer-reviewed accepted version]. Available at: DOI or URL (Accessed: date).

Enquiries

If you have questions about this document contact ResearchSupport@kent.ac.uk. Please include the URL of the record in KAR. If you believe that your, or a third party's rights have been compromised through this document please see our [Take Down policy](https://www.kent.ac.uk/guides/kar-the-kent-academic-repository#policies) (available from <https://www.kent.ac.uk/guides/kar-the-kent-academic-repository#policies>).



**Synthesis & Characterization of supramolecular polypeptide network using PP II and
Zinc at the water/oil interface**

Jack Marsh

MRes Chemistry

September 2019

This dissertation is submitted in part fulfilment of the requirements of the University of Kent
for the degree of Master of Research in Chemistry.

School of Physical science university of Kent

Acknowledgement

This research project has been challenging, rewarding and frustrating at times, every emotion has been felt throughout this research. Having said that it would be my pleasure to extend my gratitude to my supervisors for giving me the opportunity to undertake this masters, in particular I'd like to thank Dr Aniello Palma whom I had the absolute privilege to work with and got to know personally over the course of the year. Would like to thank him for being incredibly reassuring, encouraging and has helped me acquire genuinely important skills that will help me in my future career as a chemist and all-round scientist.

As well as my supervisors I would like to also sincerely thank my lab colleagues, Ashton Stone, Chloe Skingle, James Lockhart, Athina Fotopoulou and Matthew Hockley for all being incredibly supportive and giving me their time, they made this research project sail much more smoothly and I couldn't have achieved the results without their help too.

Finally, I would like to thank my beautiful partner Anusha Khan, my mum and dad Dawn and Duncan Marsh and all my friends and family back home that I've been able to confide in throughout the year.

Declaration

I hereby declare that except where specific reference is made to the work of others, the contents of this dissertation are original and have not been submitted in whole or in part for consideration for any other degree or qualification in this, or any other university. This dissertation is my own work and contains nothing which is the outcome of work done in collaboration with others, except as specified in the text and Acknowledgements. This dissertation contains fewer than 15,000 words in length, exclusive of tables, footnotes, bibliography, and appendices.

Abbreviations

PP II – Polyproline two

PP I – Polyproline one

K – potassium

Ga – gallium

L – ligand

Re - Reynolds number

Ca - Capillary number

We - Weber number

Bo - Bond number

PDMS - Polydimethylsiloxane

CB[8] – Cucurbituril

SPPS – Solid-phase peptide synthesis

Fmoc-Proline-OH - (2-(9H-fluoren-9-yl)acetyl)-L-proline

PP6, Polyproline six – 2-(((3R,5S)-1-(((2S,4R)-1-(((2S,4R)-1-acetyl-4-(carboxymethoxy)pyrrolidine-2-carbonyl)-L-prolyl)-4-(carboxymethoxy)pyrrolidine-2-carbonyl)-L-prolyl)-5-((S)-2-carbamoylpyrrolidine-1-carbonyl)pyrrolidin-3-yl)oxy)acetic acid

PBS – phosphate buffer solution

ZnCl₂ – Zinc chloride

Zn(OAc)₂ – Zinc acetate

TsOH.H₂O - p-Toluenesulfonic acid monohydrate

Cbz.Cl - Benzyl chloroformate

NaHCO₃ - Sodium bicarbonate

NaH – Sodium hydride

THF – Tetrahydrofuran

Pd/C – Palladium on carbon

Fmoc.Cl - Fluorenylmethyloxycarbonyl chloride

NMR – nuclear magnetic resonance

IR – infra-red spectroscopy

LCMS – liquid chromatography-mass spectrometry

HPLC – High-performance liquid chromatography

TLC – Thin layer chromatography

α D – alpha D value

DCM – Dichloromethane

MeOH – Methanol

SEM – scanning electron microscopic

AFM – Atomic force microscopy

DLS – dynamic light scattering

CD – Circular dichroism

DMF – Dimethylformamide

pyBop - benzotriazol-1-yl-oxytripyrrolidinophosphonium hexafluorophosphate

DIPEA - N,N-Diisopropylethylamine

Ac₂O - Acetic anhydride

TFA - Trifluoroacetic acid

DTT – Dithiothreitol

TIPS – triisopropylsilyl

DMSO-D - dimethyl sulfoxide-Deuterated

D₂O - Heavy water or deuterated water

EDTA - Ethylenediaminetetraacetic acid

Ppm – parts per million

Contents

| | |
|--|----|
| Abstract | 1 |
| 1. Introduction..... | 2 |
| 1.1 PP II (Polyproline II) overview and why are we using it? | 2 |
| 1.2 Supramolecular chemistry and desired biological applications | 3 |
| 1.3 Polypeptide self-assembling supramolecular network | 4 |
| 1.4 Microfluidics overview and droplet generation | 5 |
| 1.4.1 Microdroplet dimensionless values. | 6 |
| 1.5 3D printing, microfluidics and evaluation | 7 |
| 1.6 Transdisciplinary research | 8 |
| 2. Results and discussion..... | 10 |
| 2.1 Organic synthesis | 10 |
| 2.1.1 Functionalised proline Organic synthetic pathway. Discussion and analytical results | 11 |
| 2.1.2 SPPS Hexamer PP6 design. Discussion and analytical results | 15 |
| 2.1.3 PP II to PP I in Propanol | 18 |
| 2.1.4 Proof of concept, PP6 and zinc joining in bulk solution. Discussion and analytical results. | 19 |
| 2.2 Microfluidics..... | 23 |
| 2.2.1 Design and manufacture of Microfluidic chips | 24 |
| 2.2.2 Issue of leakage, design of inputs and outputs | 28 |
| 2.2.4 Microdroplets generation. Water and oil/surfactant | 32 |
| 2.2.5 Microdroplets generation. Propanol and oil/surfactant | 35 |
| 2.2.6 Microdroplet stabilisation. | 36 |
| 3. Conclusion..... | 39 |
| 4. Future work..... | 40 |
| 5. Experimental..... | 41 |
| 5.1 Organic synthesis | 41 |
| 5.1.1 Synthetic pathway synthesis | 41 |
| 5.1.2 PP II design SPPS | 47 |
| 5.2 Microfluidics microdroplet | 48 |
| 5.2.1 AutoCAD software, Microfluidic chip dimensions | 50 |
| 5.2.2 Chip manufacturing process | 51 |
| 6. References | 54 |
| 7. Appendix..... | 60 |

Abstract

Supramolecular chemistry and microfluidics are both scientific fields in recent decades that have seen a convergence in literature interest. Supramolecular chemistry has seen exciting biologically friendly applications such as the delivery of therapeutic substances or supramolecular catalysis both potentially contributing towards the next generation of medicine. Microfluidics has also seen promising applications such as fluid handling, cell biology and droplet generation. The incorporation of both the fields was explored throughout this thesis, more specifically the conjunction of passive droplet generation and the creation of a biologically friendly polypeptide supramolecular network was attempted. We demonstrated in this work that a functionalised polyproline, consisting of a functionalised hexamer, was able to create in aqueous environment a supramolecular network with different morphology according to the condition used. Remarkably we demonstrated that these supramolecular networks are reversible and chemo-responsive. Passive droplet generation using fluorinated chemicals (water/fluorinated oil interface^[AP1]), using two cross junction 3-D printed microfluidic designs was also demonstrated. However, the desired incorporation of microdroplet and supramolecular formation as the aqueous phase decreased in diameter causing self-assembly was examined, but was not achieved due to the instability of microdroplets, however future project work can be conducted to mitigate this issue of instability.

1. Introduction

The overall goal outlined throughout this thesis was to create and characterise a biological friendly supramolecular network by utilising microfluidic passive microdroplet generation. More specifically PP II (polyproline two) was chosen as the biological friendly building block for the network to be created within a microdroplet at the water/oil interface. The chemical nature and topography of the supramolecular network was then to be characterised. Reasons as to why this research was chosen were because of the exciting biological application such as the delivery of therapeutic substances or supramolecular catalysis. Throughout this introduction key concepts will be mentioned in detail, in conjunction with other concepts to help contextualise this thesis.

1.1 PP II (Polyproline II) overview and why are we using it?

The key building block compound that was synthesised to create the desired supramolecular network was polyproline. More specifically in the case of this research PP II, which is a secondary structure. Polyproline has two stable secondary structures PP I (polyproline one) and PP II even in short oligomers (as little as three helices has been demonstrated ⁽¹⁾). The difference between the two structures is that PP I has a more compact/denser structure and has a Cis (at the amide) configuration structure compared to PP II which consists of trans amide configuration, both structures present a helical structure with specific periodicity [PPII has a periodicity of (n+3) referenced at **figure 1**]. There were three main reasons as to why PP II was considered; the first being that PP II is the most commonly occurring proline in aqueous solution which is helped by its trans confirmation that is also favourable within a polar solution (carbonyl group in the trans confirmation will be able to engage intermolecular hydrogen bonding, hence why it is favourable). The second and the most important reason being that PP II has a favourable helical secondary structure, which can be observed at **figure 1**. So structurally it is able to be easily manipulated due to its key property; steric hindrance and as a result of this PP II trans helical structure means that if you were to observe PP II along the helical axis you would see the faces of PP II are 70 to 120 ° apart ⁽²⁾⁽³⁾⁽⁴⁾, preventing the possibility of intramolecular bonding. The third reason is simply that the PP II is a biologically friendly building block to create the supramolecular network, the desired biological applications that this research could entail such as the delivery of therapeutic substances or supramolecular catalysis. Overall PP II helices are the common structure that is preferred in polar aqueous solutions with proline, PP II is a good candidate to structurally manipulate due its unique chemical properties and is a biologically friendly system.

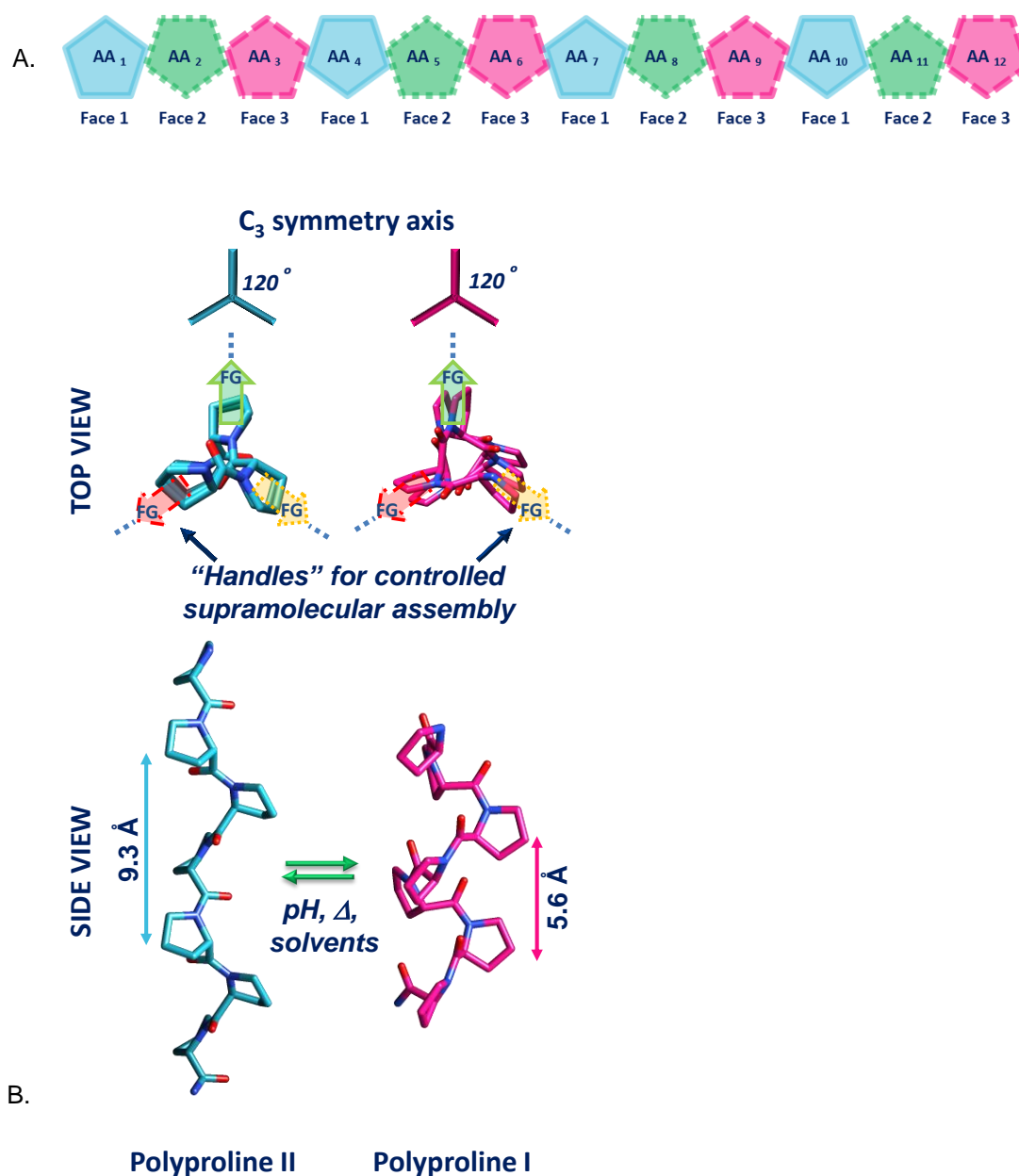


Figure 1: A : Polyproline II with $(n+3)$ periodicity, for example ‘AA₁’ and ‘AA₄’ are equivalent. B : Top and side views of the Polyproline II (all *trans*) and I (all *cis*) helices.

1.2 Supramolecular chemistry and desired biological applications

Supramolecular chemistry is where non-covalent intermolecular interactions of weak and reversible forces such as hydrogen bonding, van der Waals forces and metal-ligand coordination brings compounds together via self-assembly. Supramolecular chemistry is useful for understanding biological processes and creating very large complex materials and molecular architecture ⁽⁵⁾. Jean-Marie Lehn who won the Nobel Prize in Chemistry in 1987 and was the pioneer effectively into this field coined the term ‘supramolecular chemistry’ ⁽⁶⁾ and quoted the definition of supramolecular chemistry is the ‘chemistry of molecular assemblies

and of the intermolecular bond' ⁽⁷⁾, meaning that neighbouring non-covalent compounds will come together as a result of interacting, which strongly reiterates what the supramolecular field is about. Supramolecular architecture assembly understanding could lead to the understanding of biological processes as it mimics those processes, and if you can observe record and understand the supramolecular building process you could possibly understand the fundamental important interactions that occur at the mesoscopic scale and could lead to huge breakthroughs in biological applications such as next-generation medicine also known as personalised medicine. ^[8].

To briefly outline exciting near future biological applications of supramolecular chemistry, which primarily includes delivery of therapeutic substance such as drugs, genes, sensors and supramolecular catalysis (to name a few examples). Delivery of therapeutic substances have seen a surge of interest due to the issue of the prematurely releasing within healthy tissues causing undesired side effects or not reaching the targeted site. This is due to traditional delivery methods not adapting to varying physiological conditions within the body, as well as permeability of crossing certain membranes and dealing with the immune response ⁽⁹⁾. Supramolecular networks are potentially able to adapt to these changing conditions giving a higher degree of accuracy for the release of the substances. Supramolecular catalysis works by bringing parts of coordinate ligands to where the reaction takes place, or by providing extra interactions for the speed up in reaction between catalysts and substrates ⁽¹⁰⁾. In a sense this could be highly effective in speeding up important chemical reactions and present exciting possibilities.

1.3 Polypeptide self-assembling supramolecular network

Polypeptides are biological polymers in which the monomeric units are amino acids linked together via peptide bonds, (the carboxyl group of one amino acid and the amine group of the next amino acid) ⁽¹¹⁾. Formation of self-assembling supramolecular polypeptide networks, as well as characterisation of these networks by utilising TEM (transition electron microscopy) or SEM (scanning electron microscopy) and other analytical techniques has been well documented throughout literature. For example, an α -helical peptide sequence self-assembling into 'objects including nanofibers, nanotubes, and nanosheets' ⁽¹²⁾ or coiled peptide bundles self-assembling into cage structure ⁽¹³⁾, potentially being able to be used within drug delivery, are two recent literature examples. However, one notable example of an article ⁽¹⁴⁾ published in 2019 that was more closely related with the goals of this thesis, used varying polyproline lengths known as a 'oligoprolines'. It was demonstrated to self-assembled with quaterthiophene ($C_{16}H_{10}S_4$) which is a tetramer sulphur-rich aromatic heterocycles. The researchers were able to conclude that although oligoprolines were not able to form a

supramolecular network on their own, they were able with another molecular building block. The network organisation/shape was also able to change depending on the oligoproline length (monolayer, double layer sheets and helical twist structure). This article was able to provide support of the theory that a polyproline design was able to self-assemble with an appropriate building block, which gave credence to the theorised methodology of this thesis. This thesis sets out to accomplish and fill in gaps of knowledge regarding assembly of a polyproline design via generated microdroplets and to characterise this network, which will be discussed more in depth later within this thesis.

1.4 Microfluidics overview and droplet generation

Microfluidics has been given the nickname 'lab on a chip', it is the study of manipulating and analysing fluids through tens to hundreds microlitre scale channels. Microfluidics has offered many advantages over the course of its conception; the first being what was previously mentioned in the context of observable interactions at the micrometre and mesomere scale of fluids, containing the reagents and solvents to interact differently, providing a more in-depth look and better understanding into these interactions ⁽¹⁵⁾. The actual practical advantageous uses of this technique have been documented as; streamlining complex protocols (maintaining conditions), severely reducing cost and amount of solvent used which is not only great financially but also environmentally, being able to accurately control the volume occupied by samples and reagents in which chemical reactions occur, and also provides (as previously mentioned) scalability, but also can analysis batch samples with different solvents with a quick result turnover rate ⁽¹⁶⁾. With all these advantages microfluidics has been a revelation within important cutting-edge fields, particularly within analytical chemistry and biochemistry disciplines ⁽¹⁷⁾.

There are three main methodologies for microfluidics manipulation; 'Open microfluidics', 'Continuous-flow microfluidics' and 'Droplet microfluidics', this section of the introduction will focus on droplet microfluidics as that is the method that will be referenced and used in the methodology sections of this thesis. 'Droplet microfluidics' manipulates surface tension creating droplets. Typically the water (containing the sample) and the oil are pumped from two separate microfluidic channels that eventually join to a single point to create the microdroplets, below at **figure 2** is a complete overview of the commonly use designs and techniques taken from ⁽¹⁸⁾ to help illustrate how microdroplets are created, this offers several advantages over other microfluidic designs and methods; 'each droplet is analogous to the traditional chemist's flask' ⁽¹⁸⁾ which essentially means that each droplet is Compartmentalised meaning they can have different volumes and conditions within each droplet with sample of regents demonstrating different reactions and giving better control of specificity of results (so good

quantitative measurements). Microdroplets also have physical advantages of using fewer reagents or solvent, quick turnover of mixing of reagents and samples, and it's automated and continuous giving higher degrees of precision and accuracy, therefore, giving identical desired volume microdroplets ⁽²⁷⁾⁽²⁸⁾⁽²⁹⁾.

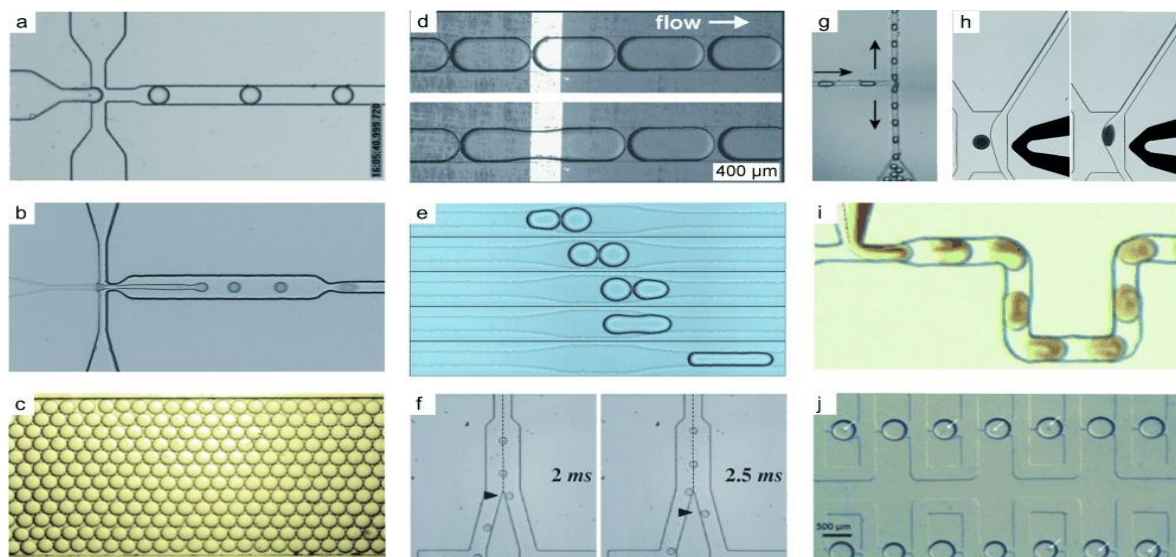


Figure 2: referenced from ⁽¹⁸⁾. A complete overview of common microfluidic designs and methods compiled together [a] droplet formation in a flow-focusing device. [b] Droplet formation from jetting in a flow-focusing device. [c] Delay line/storage area all referenced from ⁽¹⁹⁾. [d] Droplet fusion by electrocoalescence (electrical field) referenced from ⁽²⁰⁾. [e] Passive, channel-geometry-mediated droplet fusion referenced from ⁽²¹⁾. [f] Electrosorting of droplets referenced from ⁽²²⁾. [g] Channel-geometry-mediated droplet splitting referenced from ⁽²³⁾. [h] Electric-field-induced emulsion separation referenced from ⁽²⁴⁾. [i] Mixing the contents of droplets in a winding channel referenced from ⁽²⁵⁾. [j] Droplet storage referenced from ⁽²⁶⁾.

1.4.1 Microdroplet dimensionless values.

Within the context of microdroplet generation the following equations and dimensionless values Re (Reynolds number), Ca (capillary number), We (weber number) and Bo (bond number) are considered throughout the literature ⁽³⁰⁾.

- 'Re' is the inertial force (pressure from the momentum of liquid)/viscous force (the consistency of liquid), essentially low values of Re indicates that there will be a laminar flow, which is where layers of fluids will not mix and at high values of Re (at <4000) turbulent flow which results in fluids following irregular patterns OR mixing ⁽³¹⁾, in the context of microdroplet generation the Re is not completely necessary to consider, but is to overcome laminar flow.
- 'Ca' considers the surface tension from a channel and the viscous force from a solution. Ca is equal to viscous force/interfacial tension ⁽³²⁾, typically in the context of microfluidics the higher the capillary number the more droplets that are formed ⁽³³⁾.

- 'We' is defined as inertial force/interfacial tension, essentially the higher the We number the faster the droplet formation occurs, whereas the lower the value, microdroplet formation is much more difficult ⁽³⁴⁾.
- Finally, 'Bo' which is defined as buoyancy/interfacial tension. The dimensionless value compares gravitational and surface forces. Often values are less than 1. Bo aids in characterisation of microdroplet shape ⁽³⁶⁾.

We proposed a method to produce stable monodispersed microdroplets for creating a supramolecular network. These values were not highly considered in the methodology as the microfluidic dimension and designs were based on previous successful literature, which will be discussed in further detail throughout the results and discussion as well as the experimental, however when considering new microfluidic designs, surface materials, as well as interfaces (e.g. oil and water) these dimensionless values are often considered throughout the literature.

1.5 3D printing, microfluidics and evaluation

To briefly universally outline what 3-D printing is; the main processes are called 'Additive manufacturing (AM), Filament Deposition (FDM), and Stereolithography (SLA) which are a group of fabrication processes, where three-dimensional parts are constructed by adding layers of materials on point, line, or planar surfaces' ⁽³⁷⁾. This means that a 3-D model is designed in a CAD (Computer-Aided Design) file using computer software such as 'AutoCad', which slices (digitally) horizontally across the object. After the AM processes the layers and layers of the chosen material, it creates the physical 3-D model in a 3-D printer ⁽³⁸⁾. With any innovative technology it has presented many advantages such as higher speed of manufacture, a lower cost of manufacture (due to no need for costly tools, moulds and labour). There was also less waste, and because the manufacturing is automated it therefore means a higher degree of the accuracy and precision ⁽³⁹⁾. So as with all these immediate advantageous opportunities presented from 3-D printing, it's natural to assume this technology would transfer into other fields and microfluidics is no exception. An article ⁽⁴⁰⁾ that looked into the 3-D printed microfluidic devices, although there some disadvantages towards using 3-D printing such as 'printer waste' and some 3-D printers have higher rates of accuracy and precision/overall performance (which is varied among different types of printers). Overall the article concluded that it could easily replace traditional 'soft lithography in PDMS' as it did offer more or less all the advantages previously mentioned above, which present exciting applications within the future of chemical and biological uses. Another example that looked into microfluidic design biological application also concluded that it could 'displace soft lithography... 3-D printing does not require extensive, high-density automation and would

allow biomedical scientists to have direct access to the immediate manufacture of microfluidic devices. ⁽⁴¹⁾.

1.6 Transdisciplinary research

As previously highlighted throughout this introduction there has been previous research into the creation of a supramolecular polypeptide networks and even using polyproline designs, however there is yet literature to be conducted for the creation of a polypeptide design network by utilising microfluidics (passive droplet-based in particular). The methodology discussed later within this thesis was heavily inspired by the article ⁽⁴²⁾ published in 2016. The article managed to demonstrate proof of concept, between polymer supramolecular self-assembling network and using microfluidics. It helped demonstrate ditropic and tritropic monomers joined together using the CB[8] (Cucurbituril) compound to join them together (below **figure 3** illustrates this). The self-assembling supramolecular network joined together via droplet microfluidics using the water and oil interface which caused the Supramolecular compound to come together via self-assembly in a microdroplet (spherical-like structure) **figure 4**. Overall the article concluded a crosslinked supramolecular was able to develop at the interface of a droplet and was also responsive to chemical and UV stimuli, however the gap in knowledge within the article was the actual characterisation of the network such as whether the network was a bilayer, monolayer or a honeycomb-like structure. To reiterate this article was an important reference point for the work discussed throughout this thesis, as it demonstrated the use of passive microdroplet generation using microfluidics, creating a self-assembling supramolecular network, and although characterisation of the network was not achieved in that study it demonstrated the methodology was able to be achieved the desired results of this thesis. This study was the initial inspiration behind the goals of the research project that will discussed throughout this thesis. To recap, the overall goals and objectives of this research was create a supramolecular network via droplet microfluidics using a 3-D printed droplet-generating T-junction chip, at a water/oil interface. The aqueous phase containing polyproline and zinc would interact with the oil at the junction and form a microdroplet, and the droplets would then be collected on observation glass. Over time the microdroplet would reduce in diameter (via evaporation) and the reduction in size would allow the polyproline and zinc to come together creating a self-assembly network. The network would finally be characterised using techniques such as DLS (dynamic light scattering) and SEM-EDX (Scanning Electron Microscopy - Energy Dispersive X-Ray Analysis). The possible future implications of this research would be biologically friendly future applications such as drug delivery or supramolecular catalysis.

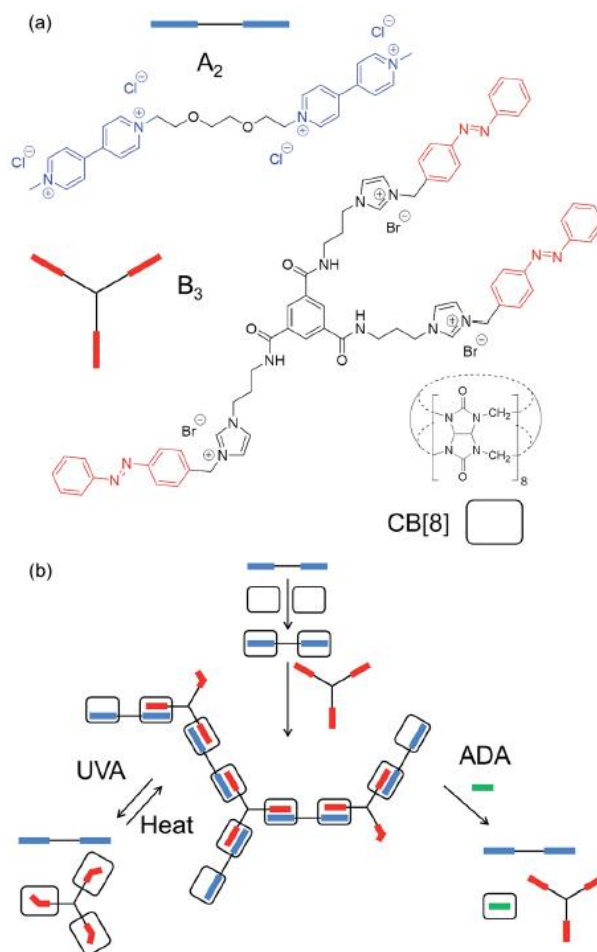


Figure 3: Referenced from ⁽⁴²⁾. '(a) Chemical structures and schematic representations of $CB[8]$, and the ditopic (A_2) and tritopic (B_3) monomers used in this work. (b) Overview of the proposed assembly process' and demonstrating the networks stimuli response of UVA, heat and ADA.

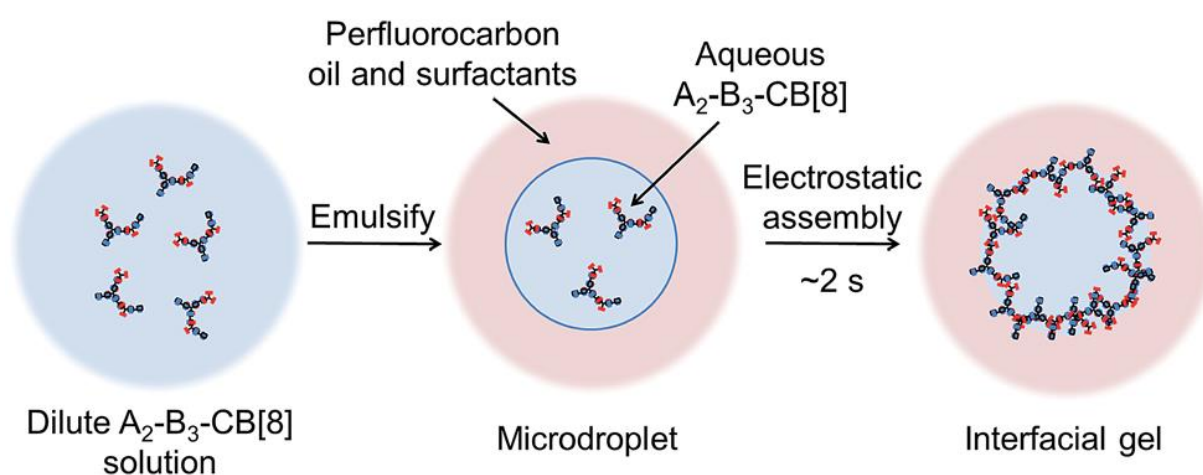


Figure 4: Referenced from ⁽⁴²⁾. Outline of the assembly process from a dilute solution to an interfacial gel. After emulsification and electrostatic attraction, the concentration and density of the polymer rapidly increase as the droplet evaporates, creating the self-assembling supramolecular network.

2. Results and discussion

2.1 Organic synthesis

The overall goal of the organic synthetic side of the research was to synthesis a designed polyproline via SPPS (solid-phase peptide synthesis). More specifically a hexamer design (with intermediates of Fmoc-Proline-OH and a functionalised proline), the name of this design was simply expressed as PP6 (polyproline six), shown below at **figure 5**.

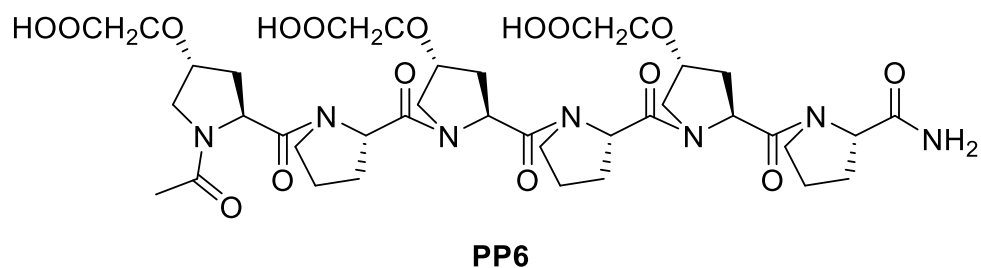


Figure 5: Chemical structure of PP6

The functional group of tert-butyl acetate was chosen as it was able to be cleaved orthogonally to typical condition used during SPPS, leaving behind a COO⁻ group which would enable the metal coordinate zinc to join creating the self-assembly supramolecular network. Position 4 of proline 1,3,5 were functionalised as this position allows the functional group to point into the solvent and therefore engage in supramolecular interactions. Moreover, due to the periodicity of polyprolines, the three non-natural amino acids will be functionalising the three different faces of the polyproline. Polyprolines are known to be very tolerable to functionalities. The focus of this work was solely on PP[^] in its PPII form however, as discussed in paragraph 2.1.3, PP6 does show the typical CD shift expected for a short oligomer like this (peak at 225nm moving in the positive region). The Fmoc-pro line-OH was bought from a chemical manufacturer and the functionalised proline was synthesised, which is mentioned below throughout the results and discussion organic synthesis section as well as the experimental. After a sufficient amount of functionalised proline was synthesised the PP6 was synthesised using SPPS (solid-phase peptide synthesis), starting from a rink amide resin, then adding on the Fmoc-proline-OH and afterwards adding on the synthesised functionalised proline in this pattern was repeated until a six-chain polypeptide was synthesised. Before microfluidics was incorporated the hexamer polyproline was placed within a bulk alkaline solution along with a Zn²⁺ salt solution, (more specially Zn(AcO)₂) which done in order to cause the self-assembly of the supramolecular network via a metal coordinate. The reasons for the choice of Zinc for the metal coordinate were as followed; Zinc is non-toxic within humans and so therefore could be used in biological applications (as previously mentioned for the future application of this research). The other reason being that its one of the metals that can be viewed under NMR,

which would've made it a good candidate in order to help characterise the Supramolecular network

2.1.1 Functionalised proline Organic synthetic pathway. Discussion and analytical results

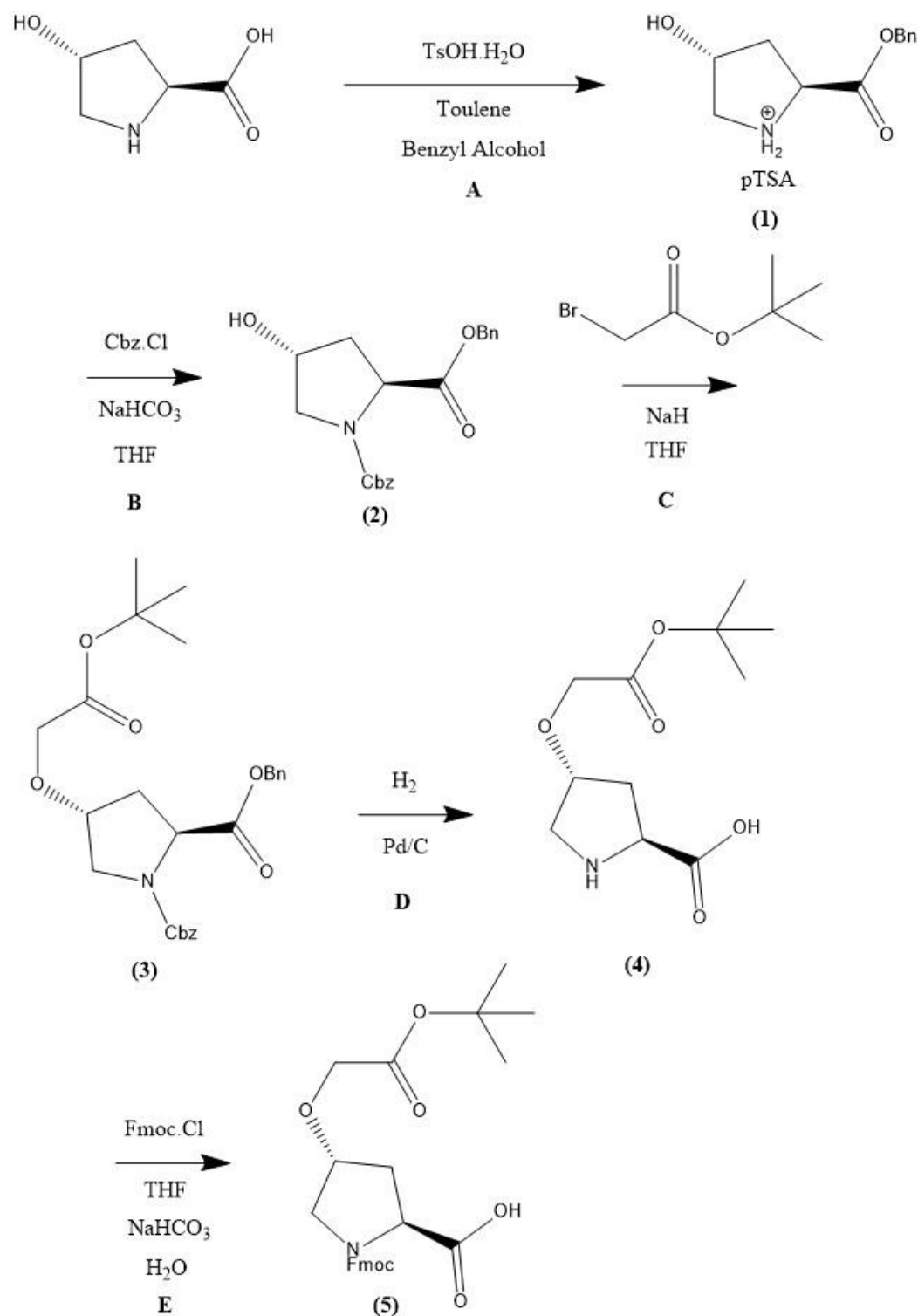


Figure 6: Overview of initial Organic synthetic pathway, to gain the desired functionalised proline and provide the proof of concept. Reaction **A** was the benzylation reaction that

protected the alcohol group of carboxylic acid giving product (1). Reaction B was Cbz protection on the amine group giving product (2). Reaction C was the alkylation of the alcohol group, giving product (3). Reaction D was the hydrogenation to deprotect product (3) giving product (4). Reaction E was the Fmoc protection onto the amine group, giving product (5).

Figure 6 describes the synthetic pathway that was devised in order to gain the functionalised proline, this reaction scheme had to be repeated on several incidents due to overall low yield gained. Each step had the following explanations as to why it was necessary in order to gain the functionalised proline:

- **Reaction A** ⁽⁴³⁾ was a benzylation, in order to protect the OH group of the carboxylic (producing an amine salt). This was done initially at the beginning in order to make later synthesis and purification via gradient chromatography easier. The issue with purification via chromatography using standard silica gel with carboxylic acids or polar compounds, in general, is that partitioning or the separation of the layers is less reliable as the polar compound will interact with the silica C-H bonds and will often remain within the column rather than separate out. Therefore, flushing columns is often required. So, it was decided in order to mitigate this effect a benzylation was carried out. Purification of **product (1)** was achieved via recrystallization and then vacuum dried in an oven. Average yield 80.3% (reaction was performed three times 82%, 78%, 81%).
- **Reaction B** ⁽⁴⁴⁾ was a Cbz protection reaction, which was used to protect the amine group of the proline. This was done for two reasons, the obvious reason being to protect the amine group from reacting with reagents later in the synthetic steps and the other reasons being that at reaction C (alkylation) involves a strong base and Cbz doesn't react with the base and remains stable under the conditions used. Purification of **product (2)** was achieved via gradient column chromatography using 6:4 petroleum ether and ethyl acetate with a Rf value of 0.35. Average yield 79.0% (reaction was repeated twice 75% and 83%)
- **Reaction C** ⁽⁴⁵⁾ was an alkylation reaction, in which a tert butyl acetate was added to the OH group of the proline, this was done in order to function as the point at which metal coordinate would self-assemble, joining the hexamer polyproline to create the supramolecular network. **Product (3)** was purified via gradient column chromatography again using 7:3 petroleum ether and ethyl acetate with a Rf value of 0.35. Average yield 52.0%. (65%, 45%, 46% reaction performed three times)

- **Reaction D** ⁽⁴⁶⁾ was a hydrogenation reaction to simply remove the two protection groups of the benzyl group on the carboxylic acid and the Cbz on the amine group. No purification of **product (4)** was required. Average yield 92.5%. (93 and 92 reaction performed twice).
- **Reaction E** ⁽⁴⁷⁾ finally was the Fmoc protection, to protect the amine group. This was done because the SPPS design of the hexamer involved Fmoc chemistry. which involves the cleavage of Fmoc using a specified mixture of reagents, in order to couple with an amino acid creating the sequence of the polypeptide chain. Purification of **product (5)** was at first tried to be achieved via recrystallization by a small volume of diethyl ether, large volume of petroleum ether, and then placed within the freezer overnight. However, **product (5)** didn't precipitate out into solution, so therefore column chromatography was used (9:1 DCM and methanol, giving a R_f value of 0.4) and then followed by flushing the column with methanol. Average yield 35.0% (37 and 35, 33 reaction performed three times).

Product **(1)**, the benzylation reaction with the starting material of trans-hydroxyl proline, the product was characterised using ¹H NMR, IR and LCMS after the product was purified via recrystallization after being washed diethyl ether, filtered and then washed again with ether and finally dried in a vacuum oven. The ¹H NMR and IR were to confirm the presence of the amine salt p-Toluenesulfonic acid, which can be observed below at **appendix 1** and **2**. The LCMS spectra confirmed the expected molecular mass of the compound being m/z 393.

Product **(2)** was purified via gradient chromatography, dried under high vacuum and analysed with ¹H NMR, IR and LCMS. Initially, ¹H NMR demonstrated that the 1st attempt at purification via column chromatography using the system of 6:4 Petroleum ether to ethyl acetate was somewhat thwarted by an issue regarding the petroleum ether solvent. The petroleum ether solvent purchased was of 'analytical grade', however it gave 'grease' peaks at the lower chemical shift regions, which is what **appendix 3** demonstrates, as well as the ¹H NMR spectra of the 'analytical grade' petroleum ether shown at **appendix 4**. After changing the solvent of petroleum ether to 'Laboratory-grade', this appeared to mitigate the issue, as demonstrated by the ¹H NMR at **appendix 5**. After gradient column purification and the product being dried once again, this gave little to no peaks of 'grease'. The ¹H NMR and IR spectrum were used to confirm the presence of the Cbz protection group which is shown at **appendix 5** and **6**. LCMS was used to confirm the expected molecular mass of m/z 356.

Reaction C presented an issue of creating a diastereomers shown below at **figure 7** This was suspected as when a TLC was taken using the system of 7:3 Petroleum ether:ethyl acetate from the reaction it showing two spots on top of each other with very similar R_f values (0.35).

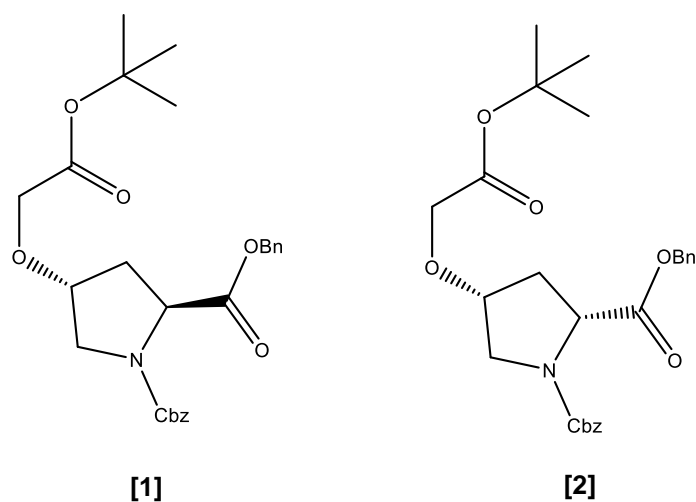


Figure 7: The suspected structures of the diastereoisomers, product **1** being the trans (S) configuration and **2** being Cis (R) configuration.

In order to gain a purified Product (**3**) gradient column chromatography was required. ¹H and ¹³C NMR, IR and LCMS spectra were recorded and then polarimeter were performed after the chromatography column was performed. First the appropriate set of fractions were collected and dried, a polarimeter reading was taken of the two suspected Product **3** fractions that had very similar R_f values of 0.35. Both compounds were dissolved in solution giving a concentration value of 1. One solution gave a reading of -00.32 and the other +00.28 which after the values were times by 100 gave an 'αD' (alpha d) value of -32 and +28. The negative value strongly suggests that a compound is of trans configuration and the positive value strongly suggests Cis. Product (**3**) was highly likely to be the negative αD value set of fractions. Product (**3**) was analysed using ¹H NMR spectra (**appendix 7**), which showed the characteristic peaks of the tert-butyl acetate group at the singlet peak at the 1.47 ppm chemical shift region, indicating the presence of the three CH₃ groups. ¹³C NMR spectra were taken to show the number of carbons present on product (**3**) which is 23 which is the number of peaks present in the ¹³C spectra (**appendix 8**). IR spectra at **appendix 9** the wavelengths help indicate the presence of the functional groups so the tetra butyl acetate, Cbz and the amine salt. Finally, LCMS was used to confirm the molecular mass which was expected to be m/z 470.5.

Product (**4**), ¹H NMR, IR and LCMS spectra was taken, both the ¹H NMR and IR analysis was simply a case of seeing whether the peaks within the aromatic region of both the IR and ¹H

NMR had gone. At **appendix 10** and **appendix 11** indicates the peaks and wavelengths of Cbz and benzyl group within the aromatic regions had gone and therefore the hydrogenation was successful in deprotecting product **(3)**, removing the Cbz and benzyl group. The LCMS was used to confirm the molecular mass which was expected to be m/z 246.3.

Finally, product **(5)** ^1H , ^{13}C NMR, IR, LCMS spectrum and Polarimeter was taken after gradient and flash chromatography and dried under high vacuum. The ^1H NMR and IR spectrum shown at **appendix 12** and **13** simply shown the peaks within the aromatic region indicating that Fmoc had joined and protected the amine group of product **(4)**. 26 carbon atoms are present on product **5** and the number of peaks consolidates with this number at **appendix 14**. LCMS was used to confirm the molecular mass which was suspected to be roughly m/z 468.5. The compound was dissolved and had a concentration of 0.8, The polarimeter reading a negative reading of -00.22 which after being times by 100 and then divided by 0.8 gave an αD value of -27.5 indicating that it was the desired trans optical configuration.

2.1.2 SPPS Hexamer PP6 design. Discussion and analytical results

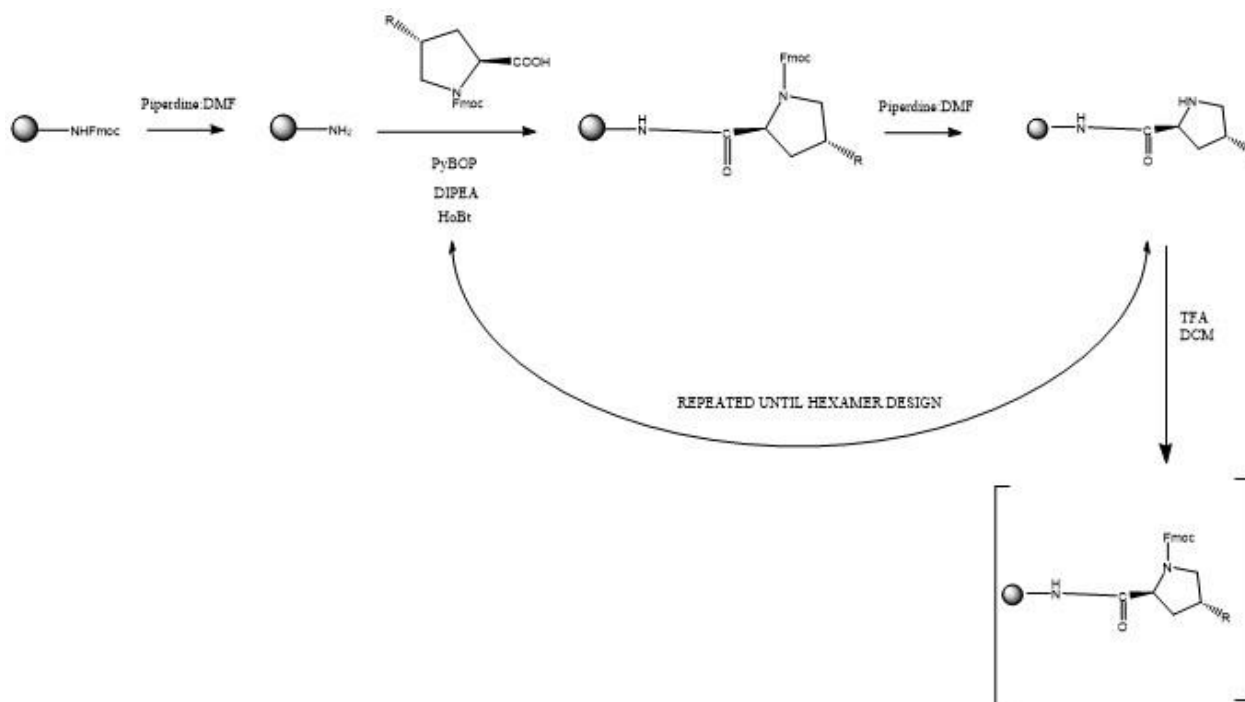
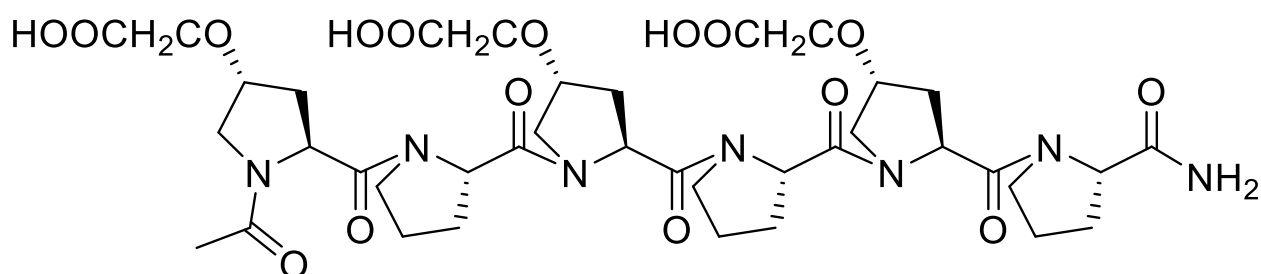


Figure 8: Overview reaction of SPPS synthesising the hexamer PP6 design.

Once enough of **product (5)**, functionalised proline was synthesised, PP6 was then synthesised. The overview of the SPPS reaction is demonstrated at **figure 8**. The methodology procedure of SPPS ⁽⁴⁸⁾ were as followed;

- Rink amide resin beads were deprotected using 8:2 DMF and Pyridine

- The 1st coupling mixture was added consisting of commercially bought Fmoc-Proline-OH, pyBop, HoBt and DIPEA.
- An aliquot of the resin beads was taken and the kaiser test was then employed to check for primary amines if the beads remained colourless then the coupling was successful.
- Capping mixture was added which consisted of 10:2.5:100 Ac₂O, DIPEA and DMF to mop up any remaining free amines
- Once again, an aliquot of the resin beads was taken and the kaiser test was deployed. SO, the first coupling had been completed.
- The deprotection mixture was added again to deprotect the Fmoc-proline, after which the coupling mixture consisting of the synthesised functionalised proline, pyBop, HoBt and DIPEA was added.
- An aliquot of the resin beads was taken, and the chlorophyll test was then deployed, to test for free secondary amines. If the beads were colourless then the coupling was successful.
- The coupling was repeated four more times, with intermediate changing of the proline with the coupling mixture until the desired hexamer PP6 design was achieved. (figure 9 shows the chemical structure of the PP6 design and 3-D top-side and side view of the PP6 design).



PP6

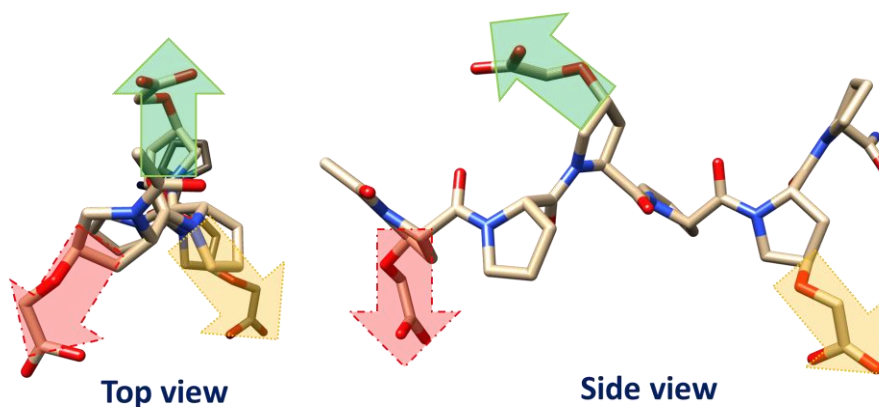


Figure 9: Chemical structure of hexamer PP6. 3-D model of polyproline showing the top-view and side-view. (Model was generated by optimised geometry calculated with MOPAC software at the PM6 level, confirmed as a minimum by frequency analysis).

After the final coupling had been completed the cleavage reaction from the rink resin was then performed ⁽⁴⁸⁾⁽⁴⁹⁾, the cleavage mixture consisting of 88% TFA, 5 % DTT (Dithiothreitol), 5% TIPS (triisopropylsilyl), and 2% water which was added to the resin containing the PP6 design. The cleavage solution was slowly dripped into a cold solvent of diethyl ether, causing the PP6 hexamer to crash out into a white precipitate. The solution with the precipitate was centrifuged and decanted, washed with diethyl ether and decanted again. Finally, the solid was dried under vacuum.

The solid product was comprehensively analysed using ¹H, ¹³C NMR, LCMS, IR spectra and then a CD (circular dichroism) was taken in solution, which is demonstrated at **appendix 15, 16, 17, 18** and **figure 10**. The combination of the spectrum analytical techniques such as the ¹H, ¹³C gave chemical shift peaks helping to demonstrate the structure of the hexamer polyproline design and LCMS helped cement the predicted molecular mass (863 m/z) of the desired polyproline design. The LC retention time spectra was also used to measure the purity, and the spectra showed an asymmetrical peak with a very slight 'shoulder' peak possibly indicating a slight impurity. However, overall the peak purity of the 'main' peak suspected to be PP6 was 92-93%. The type of polyproline that was aimed for in this research was PP II in solution, and the CD spectra was used to confirm this as the data gained was compared to a known database of polyproline II. The polyproline was dissolved in TFE and the CD (**figure 10**) gained matched the known database value of PP II, as well as an IR spectrum (**appendix 19**), was taken whilst the PP6 was in TFE.

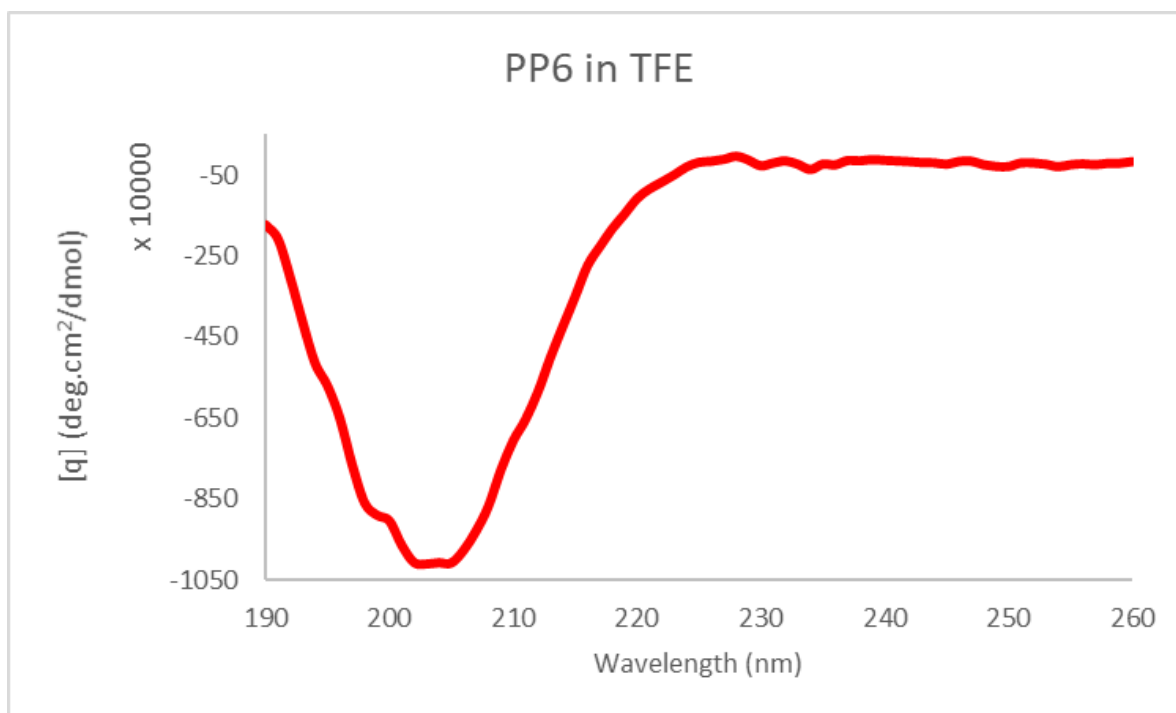


Figure 10: CD spectra of PP6 dissolved in TFE solution, indicating PP II confirmation.

2.1.3 PP II to PP I in Propanol

One of the future desired applications of this project was for biological friendly applications, such as drug delivery. The way in which this was theorised to be achieved was that PP I (which is much more of a compact closed structure of polyproline consisting of cis configuration compared to the PP II) would create the supramolecular network and slowly convert into PP II which is a less compact structure. What this means is that as the PP I would slowly convert into PP II, which would cause a time delay in which the therapeutic substances are being released, thus reaching to the desired targeted areas within the body. In literature it's been documented that apolar solvents such as propanol at low temperatures (5 °C) have influenced changing the conformation of PP II to PP I ⁽⁵⁰⁾. This was replicated in this research, the hexamer PP6 was dissolved in propanol and was left in the fridge over the course of 5 days. After which a CD was taken as well as IR. The CD spectra of PP6 in TFE and propanol is reported below **figure 11**. These spectra were recorded at the same concentration therefore it is clear that there are significant differences between the two species. This would suggest in agreement to the literature ⁽⁵⁰⁾ that a PPII to PPI transition did occur in propanol. However due to time constraints, we only focused on supramolecular networks involving PPII.

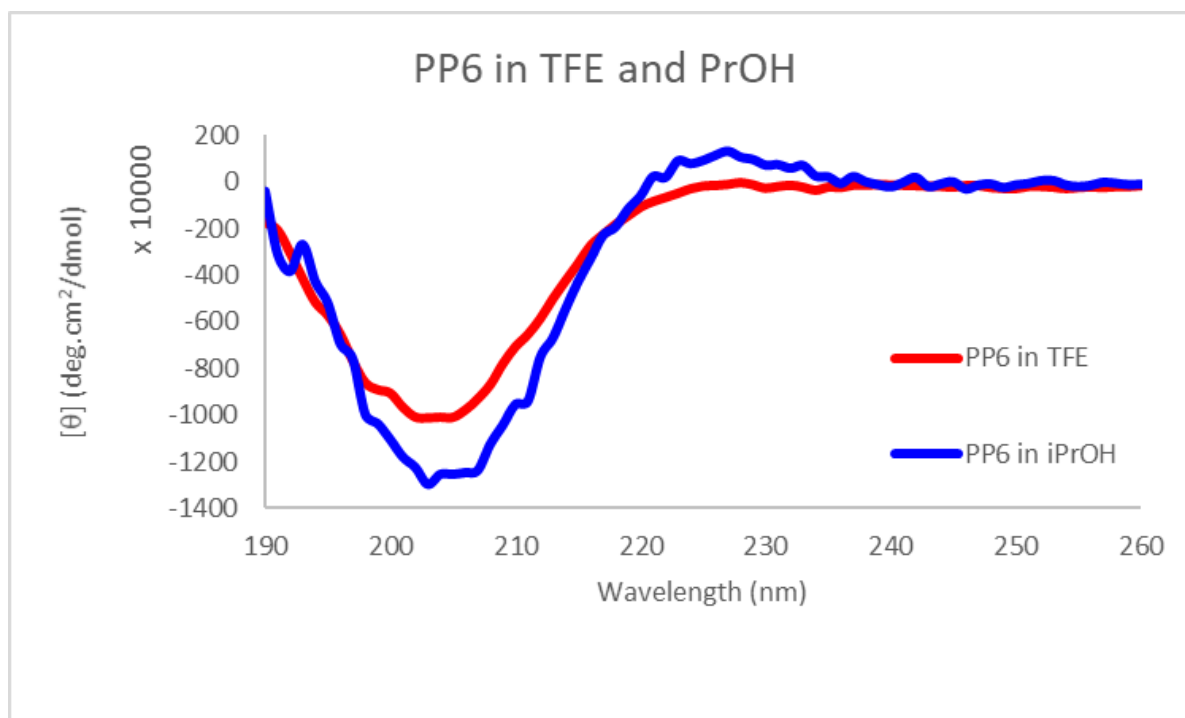


Figure 11: CD spectra overlap of PP6 in TFE indicated by red line and the PP6 in propanol

2.1.4 Proof of concept, PP6 and zinc joining in bulk solution. Discussion and analytical results.

A proof of concept for PP6 in solution to join with a metal coordinate was attempted in order to demonstrate that a supramolecular network could be formed, before the implementation of the microfluidic aspect of the research project. PP6 was dissolved in ultra-pure water with NaOH and D₂O giving a 0.1 M solution. 1 M of Zn(OAc)₂ D₂O solution added intermediately two times. ¹H NMR, DLS and SEM-EDX were taken before the addition of the Zn(OAc)₂ solution and after the two increments of the Zn(OAc)₂ solution. The NMR results (**figure 12, 13, and 14**) were very ambiguous there only slight changes within the 2.0 – 4.0 ppm (parts per million) chemical shift region, but overall the results were not strong enough to suggest any changes had occurred nor had a supramolecular network had been formed.

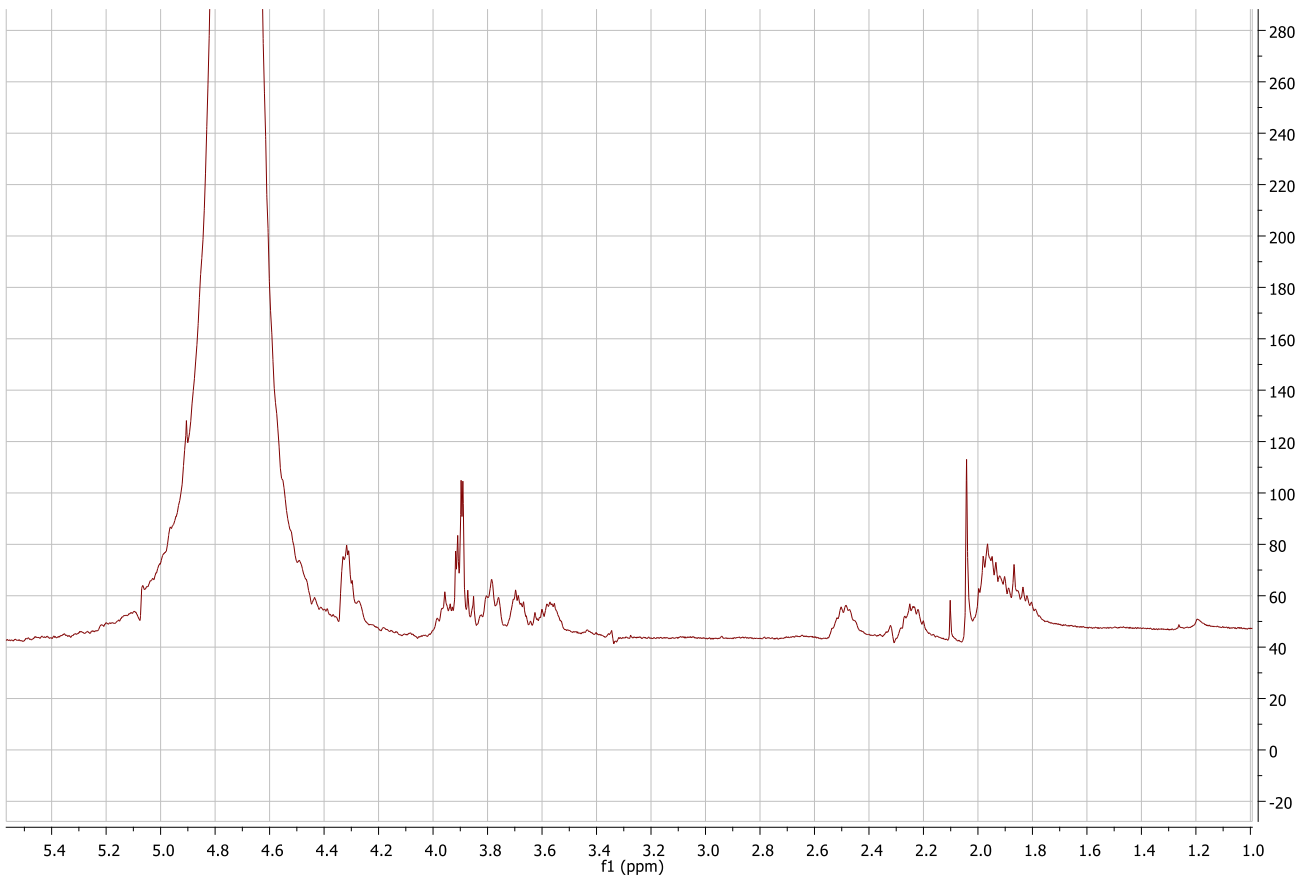


Figure 12: ^1H NMR spectra PP6 in saturated NaOH with D_2O solution.

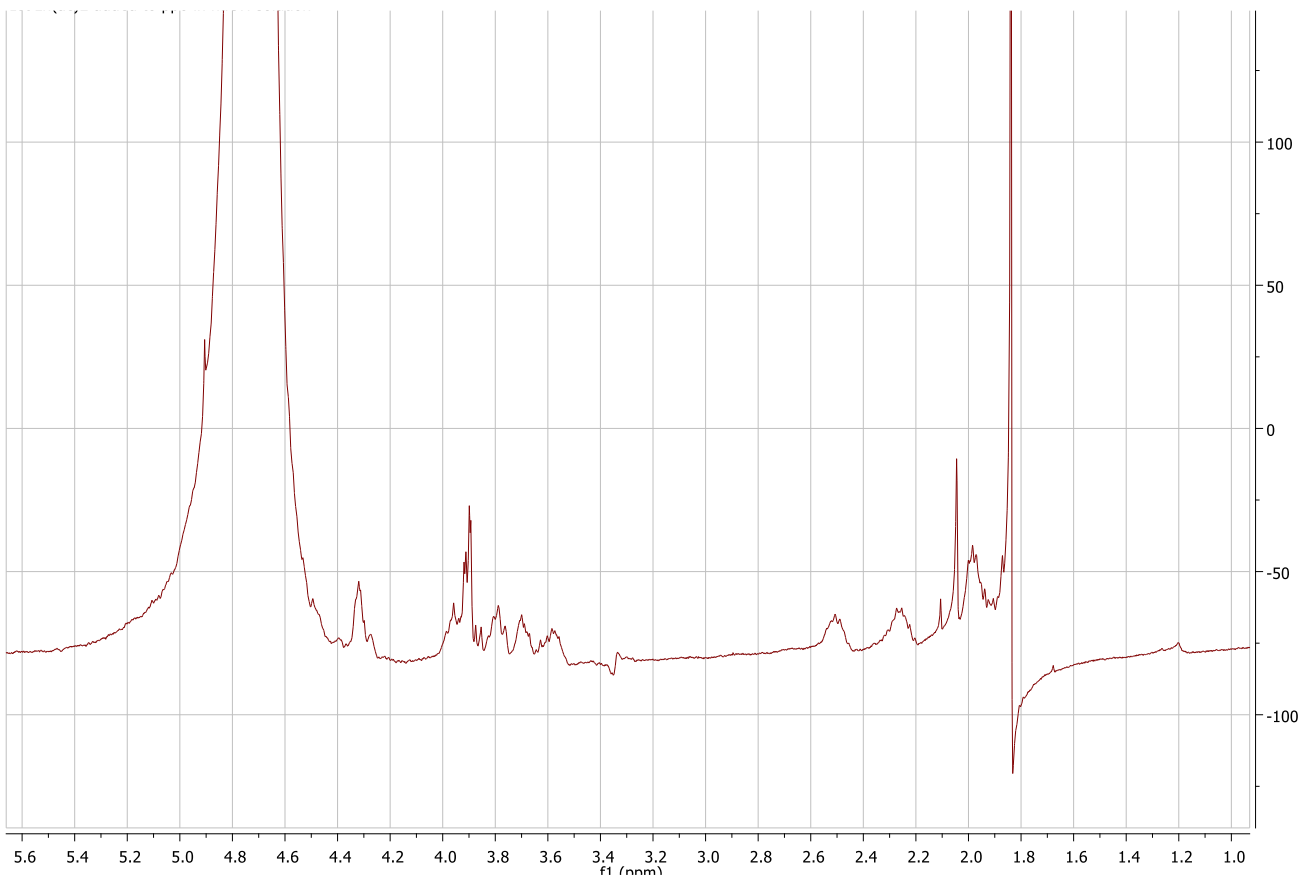


Figure 13: ^1H NMR spectra PP6 1st addition $\text{Zn}(\text{OAc})_2$ D_2O solution

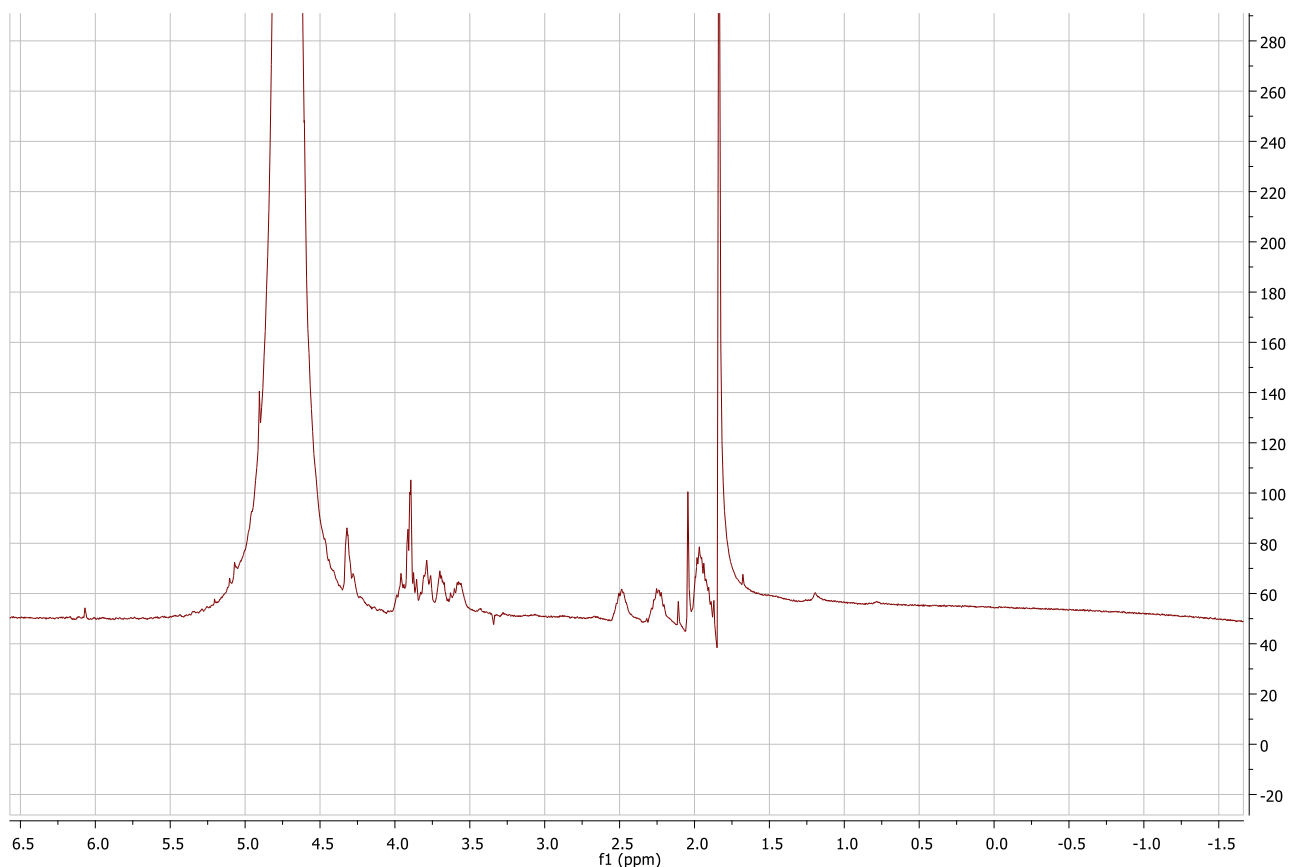


Figure 14: ^1H NMR spectra PP6 2nd addition $\text{Zn}(\text{OAc})_2$ D_2O solution

The combined DLS size distribution data shown at **figure 15** was far more promising demonstrating supramolecular network formation. DLS was used to determine the hydrodynamic diameter of particles, and the supramolecular formation would be indicated as the $\text{Zn}(\text{OAc})_2$ would be added the hydrodynamic size should increase, and this was consistent by the shift increase in diameter on the DLS spectra from the blue lined peak to the dotted red and green lined peaks strongly indicating the supramolecular formation of the $\text{Zn}(\text{OAc})_2$ the PP6. To further cement this data, The dotted purple lined peak at the DLS spectra **figure 15** demonstrated a lowered shift in diameter by the introduction of the chelating agent of EDTA (Ethylenediaminetetraacetic acid), which reacted with zinc to form a complex breaking up the supramolecular network and just leaving the PP6 on its own.

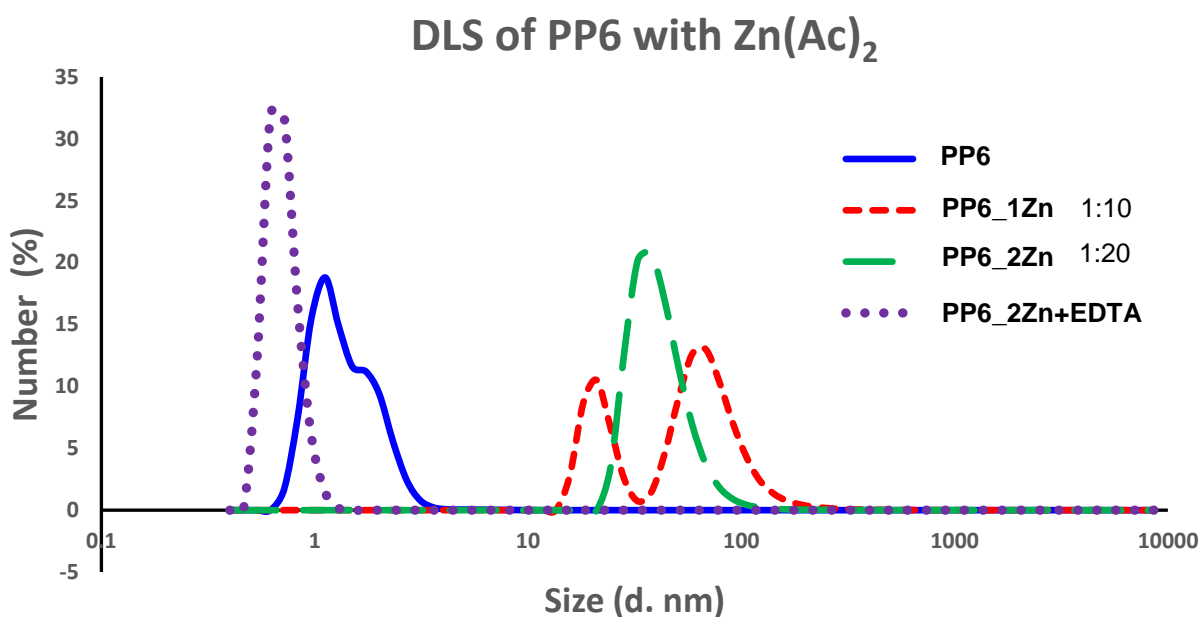


Figure 15: DLS of PP6 (blue line), PP6_1Zn (red dotted line), PP6_2Zn (green dotted line) and PP6_2Zn+EDTA (purple dotted line). DLS helped provide proof PP6 was promoting the formation of a supramolecular polymer with the Zinc coordinate, which is then broken up by a chelating agent dissolved in water.

The SEM-EDX data images also were exciting and helped support the DLS data. Below at **figure 16** shows the topography progression after each addition of Zn(OAc)₂. At **figure 16** (a) is the SEM image and (b) is the EDX. **Figure 16** shows the homogenous distribution of the PP6. At (c) showing the SEM image, (d) and (e) showing the EDX image at **figure 16** shows the pockets of spheres forming after the first equivalent of the Zn(OAc)₂ solution was added. Finally, at (f), (g) and (h) **figure 16** after the second equivalent of Zn(OAc)₂ was added a skin like spherical film had formed, indicating a supramolecular network had been created. Once again helping to support that a self-assembly had occurred between the PP6 and zinc coordinate. This experiment demonstrated the responsive nature of the PP6_Zn1 and PP6_Zn2 supramolecular polymers. Overall both the SEM-EDX and DLS data strongly indicated the formation of the supramolecular network, which in turn helped provide the proof of concept that the formation was possible and supporting the possibility of the microfluidic microdroplet concept of the project.

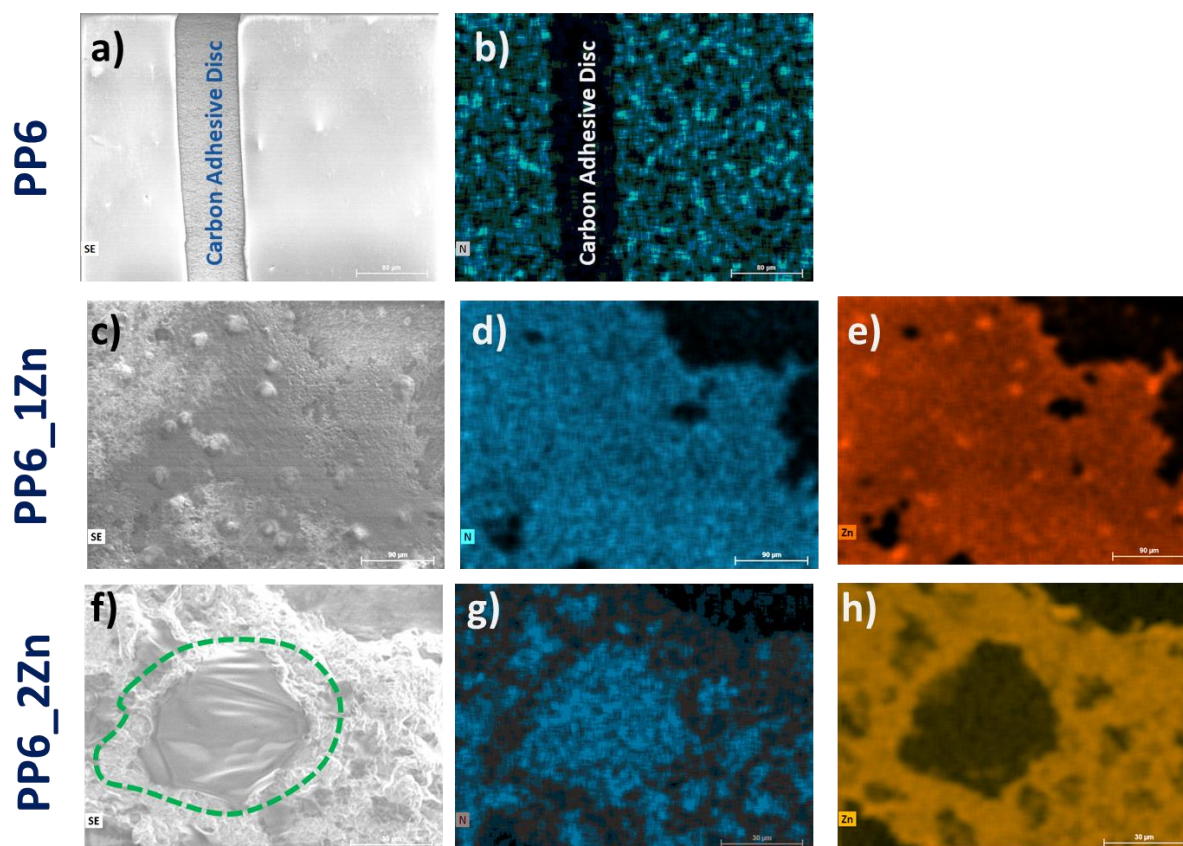


Figure 16: (a) SEM images of the PP6, with the carbon adhesive disc. (b) EDX image of PP6 with blue indicating nitrogen. (c) PP6_1Zn SEM image, pockets of supramolecular spheres being formed. (d) and (e) EDX image both the blue and orange colour indicating the nitrogen with spheres of black formed indicating supramolecular sphere formed. (f) PP6_2Zn SEM image, of supramolecular network forming a skin-like surface, which is highlighted by the green dotted line. (g) and (h) EDX analysis once again demonstrating the outline shape of the supramolecular network formed. (In the skin-like section marked with green dots at (f) Zn is still present, the sample was placed on top of a carbon support and we predicted that the polymer was extremely thin and therefore a very weak signal you see in panel (h)).

2.2 Microfluidics

The second component of this research was the incorporation of microfluidics in order to generate monodisperse microdroplets via emulsion at the aqueous and oil (with surfactant) interface. Therefore, bringing the PP6 and chosen metal together creating the self-assembling supramolecular network. At **figure 17** shows the overview diagram of how the supramolecular network was theorised to be formed. The concept was inspired originally by the reference ⁽⁵⁴⁾ mentioned previously in section 1.8. Throughout this section, the brief overview of the methodology and the chip designs will be discussed as well as the results gained from the manufactured microfluidic chips. The microdroplets formation equations mentioned previously

in section 1.5.1 were not considered throughout the methodology as the dimensions and flowrate were based on the previous literature successful designs.

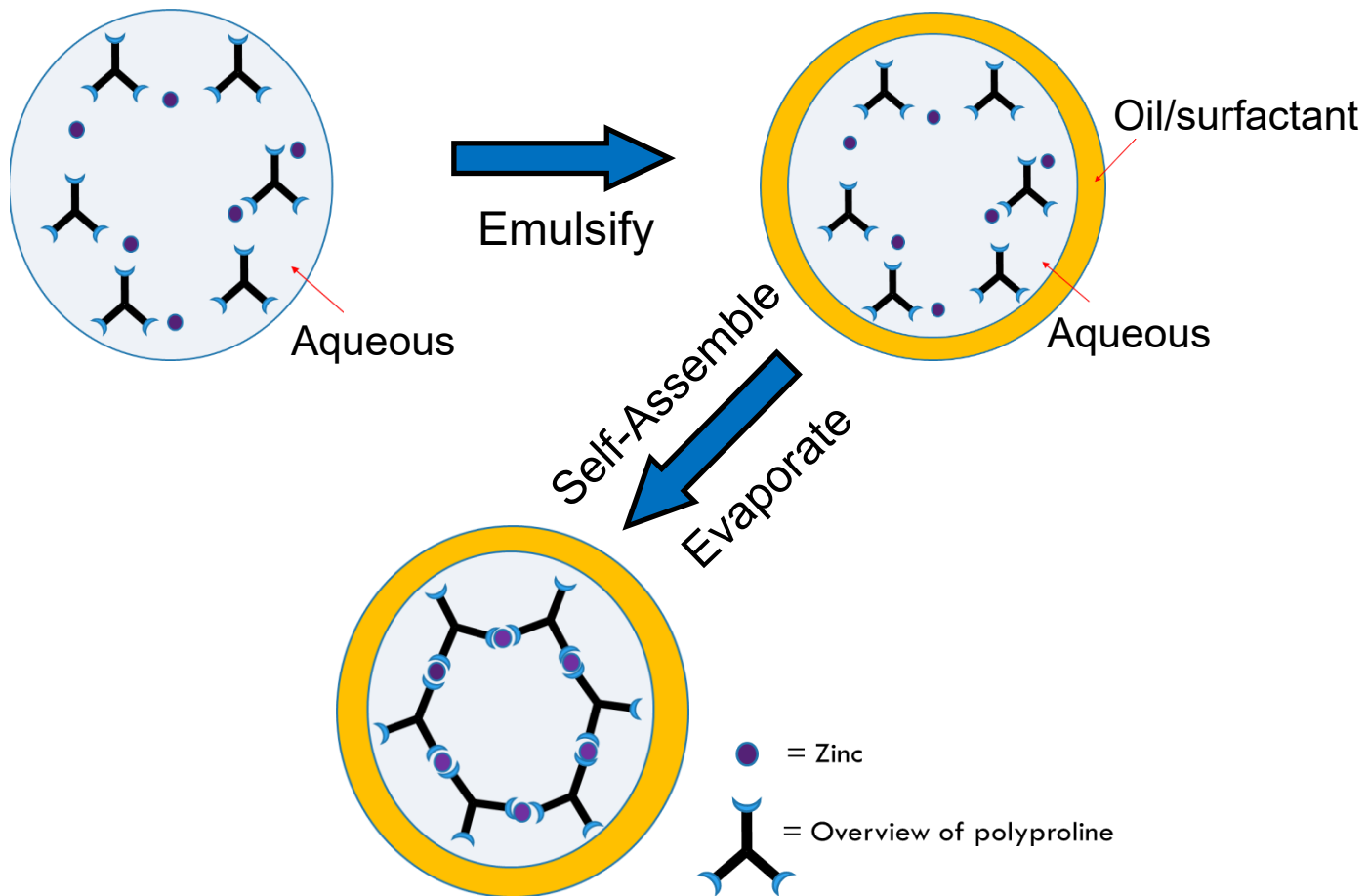


Figure 17: diagram of a representative microscopic image showing microdroplets emulsify and evaporated over time shrinking the diameter of the sphere and creating self-assembling of polyproline with zinc.

2.2.1 Design and manufacture of Microfluidic chips

As mentioned previously in section 1.6, 3-D printing has had become more and more of a popularised technique used within several STEM field industries, due to the increased reliability and accuracy over the last two decades. So, 3-D printing was decided to be utilised in the design and manufacturing of microfluidic chips. Auto-Cad was the 3-D computational software that was used in order to design the microfluidic chips, and three chip designs were considered. Shown at **figure 18** were the rough schematics of the main designs; 'T' junction chip ⁽⁵¹⁾, 'X' junction chip ⁽⁵²⁾, and 'zig-zag' mixing chip ⁽⁵³⁾.

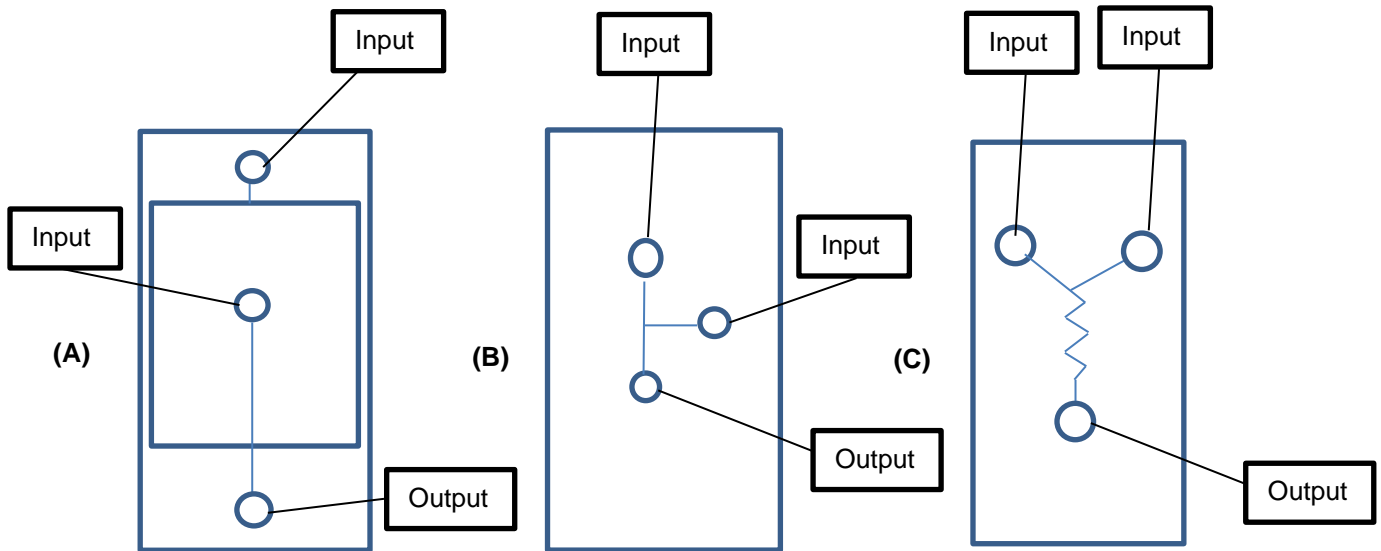


Figure 18: Microfluidic chip schematics. (A) 'X' junction microfluidic chip. (B) 'T' junction microfluidic chip. (C) 'Y' junction 'Zig-zag' microfluidic chip. With each Input and output ports labelled.

The auto CAD designs of the chips were exported to the 3-D printer software known as 'form labs 2 PreForm', after which the designs were printed at 0.025 mm resolution using the 'Form labs 2' 3-D printer. At **figure 19** are the resin chip designs after they have been printed and cured via UV radiation. PDMS and curing agent was then poured on top of the resin chip and left to cure in an oven to create the PDMS mould. After which the PDMS mould casting was plasma cleaned onto a glass surface, (oxidises the surfaces and then an electrode creates free radicals onto the glass and PDMS mould surfaces) after each of the surfaces were gently pressed on top of each other forming a very tight seal. The results of the manufacture of the plasma cleaned microfluidic chips is shown at **figure 20**.

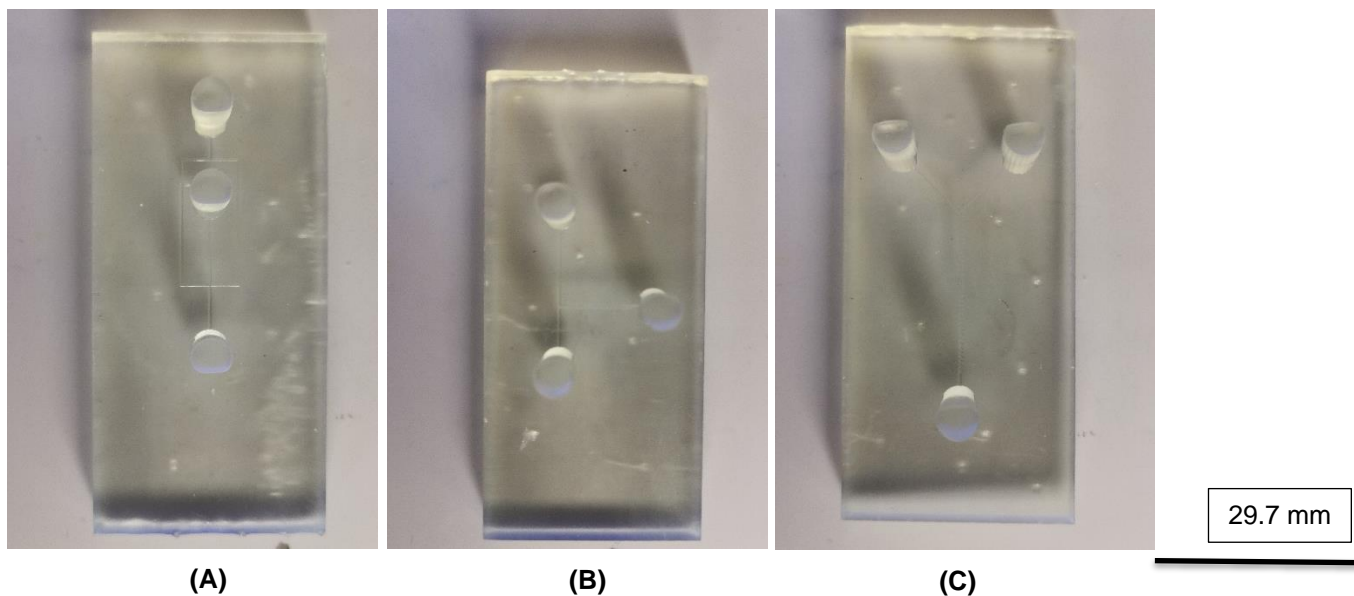


Figure 19: Microfluidic UV cured resin chips. (A) 'X' junction microfluidic chip. (B) 'T' junction microfluidic chip. (C) 'Y' junction 'Zig-zag' microfluidic chip. With scale bar.

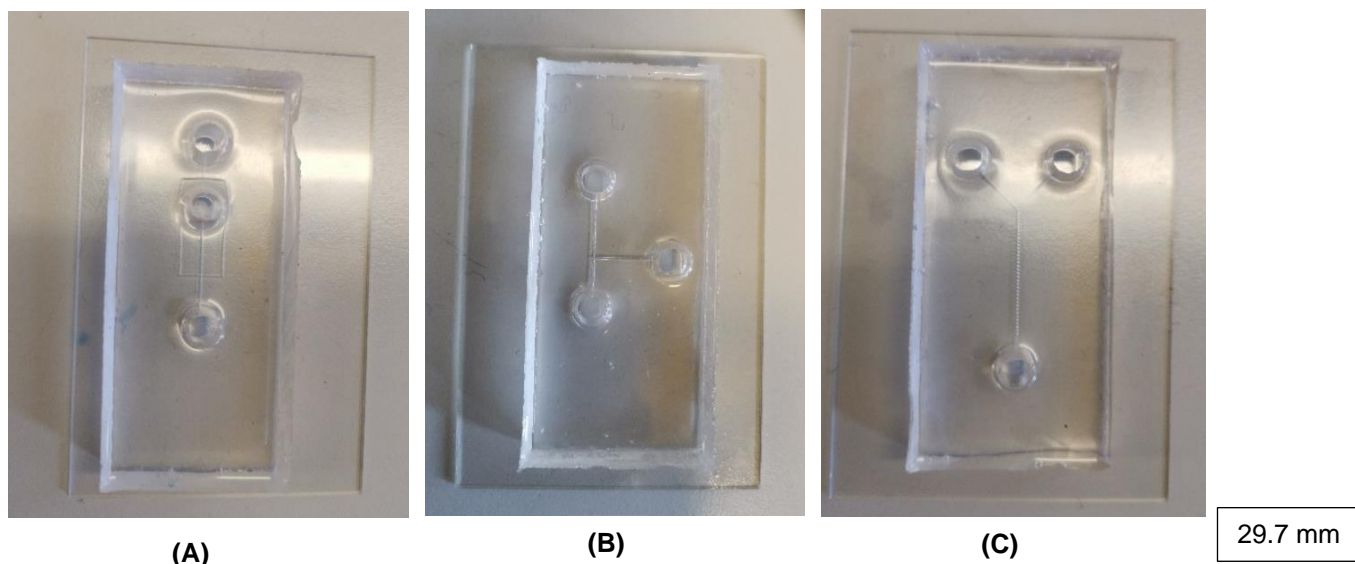


Figure 20: Plasma cleaned microfluidic chip designs on glass slides. (A) 'X' junction microfluidic chip. (B) 'T' junction microfluidic chip. (C) 'Y' junction 'Zig-zag' microfluidic chip. With Scale bar.

The key dimensions of the microfluidic channels were the height of the channels being 0.1 mm (100 micrometres), and the width was 0.2 mm (200 micrometres) and 0.1 mm at the pinch of the junctions of the 'X' and 'T' designs based on literature⁽⁵⁴⁾. Below at **figure 21** shows the microscopic image of the microfluidic channel designs. At (A) and (B) at **figure 21** Both were used for passive cross junction microdroplet manipulation. What this means is that when the aqueous and oil phase (with surfactant) cross met, it created emulsion, and formed microdroplets. The mixing zig-zag design which is shown at **figure 21** (C) was manufactured in order to mix the zinc and PP6 compound on the microfluidic chip itself rather than mixing in a bulk solution, the ideal set-up is shown at **figure 22**. This was done to more accurately mix the zinc and PP6 in order to prevent having a big collocate molecule before getting to the cross junction of the 'X' or 'T' chip, as the idea was that the supramolecular network comes together within the microdroplets in a spherical manner.

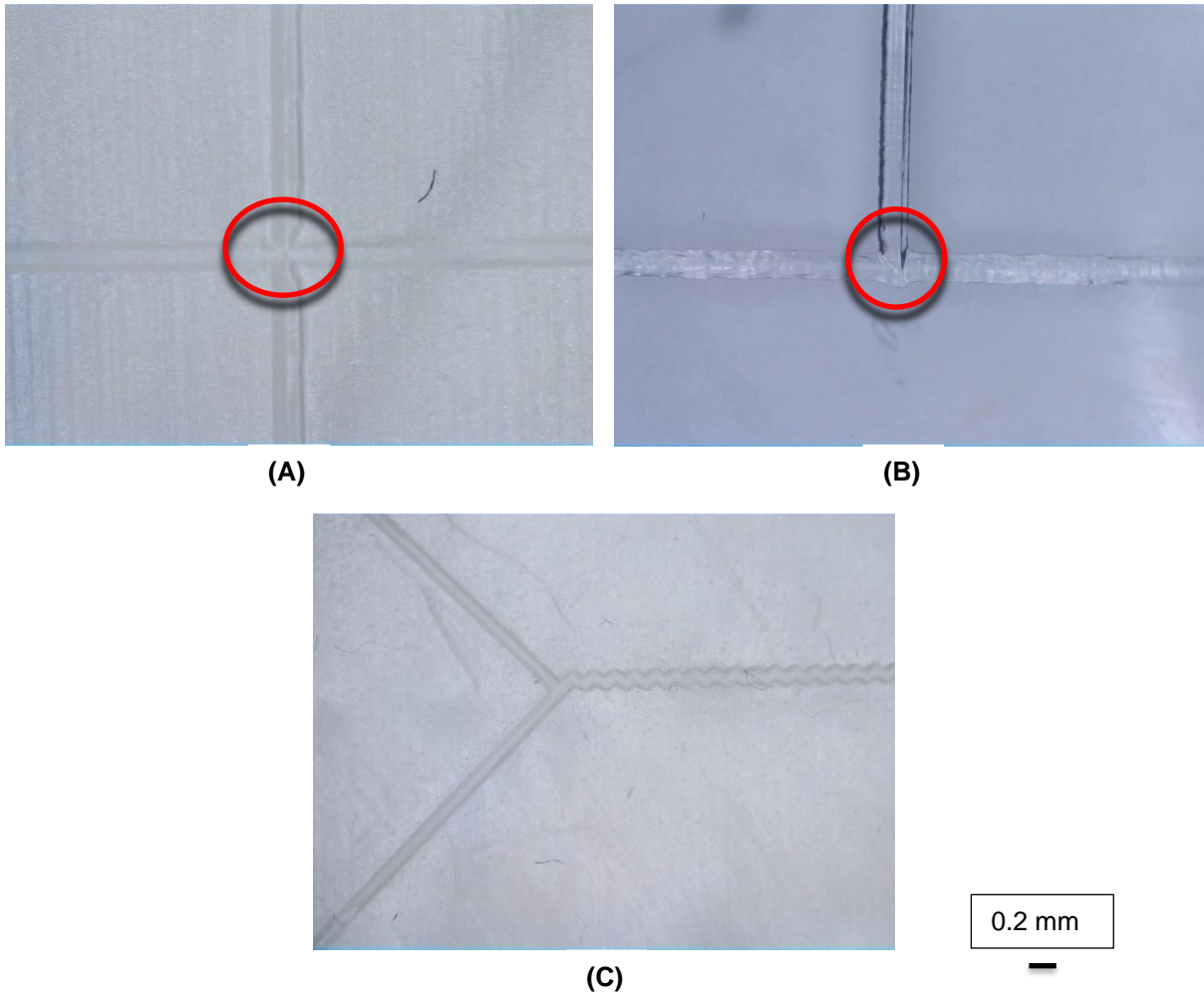


Figure 21: Microscopic image of 'X' junction with a red circle highlighting 'pinch' at (A). 'T' junction with a red circle highlighting 'pinch' at (B). 'Y' junction with 'zig-zag' design at (C). With scale bar.

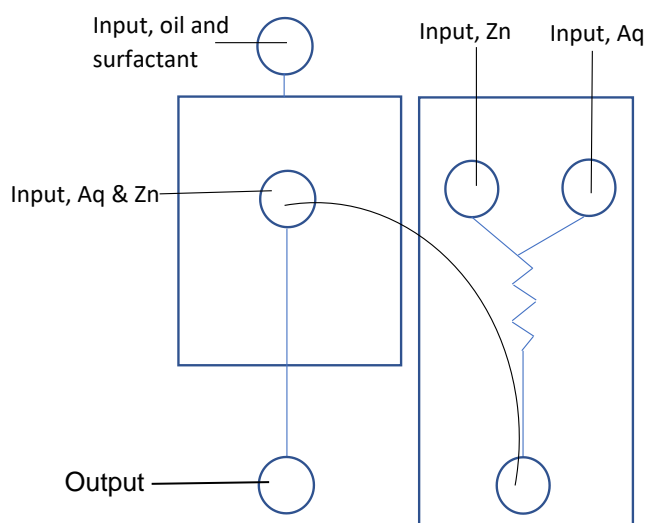


Figure 22: schematics of example ideal set-up. Mixture chip with two inputs of Zinc and aqueous containing PP6 design. The outlet of mixture chip connected to the input of the 'X' junction chip.

2.2.2 Issue of leakage, design of inputs and outputs

The first beta designs of the microfluidic chips of the junction and the mixing designs had different input and output designs. Initially, a wide blue 'adaptor' was inserted directly within the inputs and outputs on top of the glass surface, this was done in order to have a 'plug-and-play' element. This caused huge pressure within the microfluidic chip and caused a big issue of leakage, despite the slow flow-rates of the syringe pump at 1-10 microlitres per minute or 10-100 microlitres per hour, this still caused leakage often in the inputs, an example of this is shown below at **figure 23**. Two main issues would arise as a result of leakage, the first being that only a very small quantity of the aqueous phase would be available, therefore this issue would lose an excessive amount of valuable material. The second being when it came to generating monodisperse microdroplets this would also be an issue, as there is not a constant flow, therefore disrupting the consistency of the spherical microdroplet shapes.

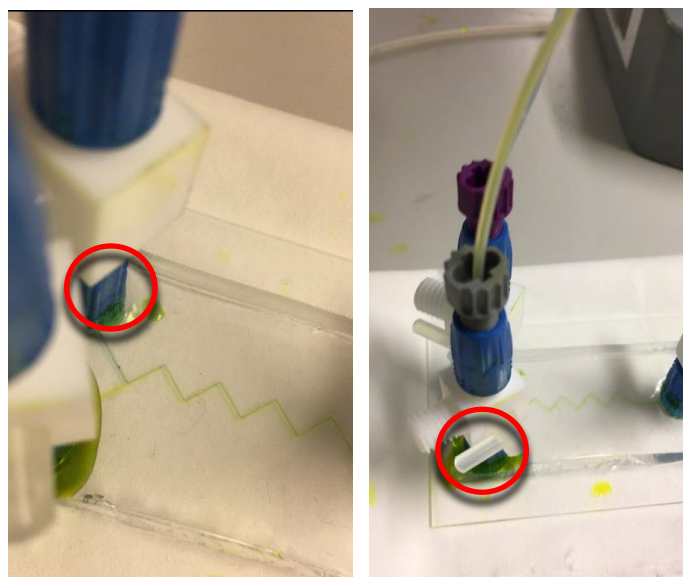


Figure 23: Photos of blue adaptor leakage demonstrated by the red circle.

In order to mitigate this issue of leakage, the blue adaptor as shown above in **figure 23** was replaced, and the inputs and outputs would be designed centred around the 'Omnifit™' screws which are shown below at **figure 24**. These screws were the outlet in which the fluids would exit from the tubing. The screws were significantly smaller in diameter compared to the blue adaptor; therefore, reducing backpressure significantly. The other design iterations that were taken into consideration was the omifit screw would fit tightly within the Inputs and outputs, as well as the omifit screw wouldn't be inserted directly on top of the glass surface but would

rather fit tightly above the glass, also reducing a lot of backpressures as well as leakage. The dimensions of the omifit were considered by designing the bottom half of the inputs and outputs as 3.8 mm at the bottom half and 4.3 mm at the top half in diameter. Below at **figure 25** is the AutoCAD cylinder shape designed input and outlet shape.



Figure 24: microscope image of Front and side view of the omifit screw.

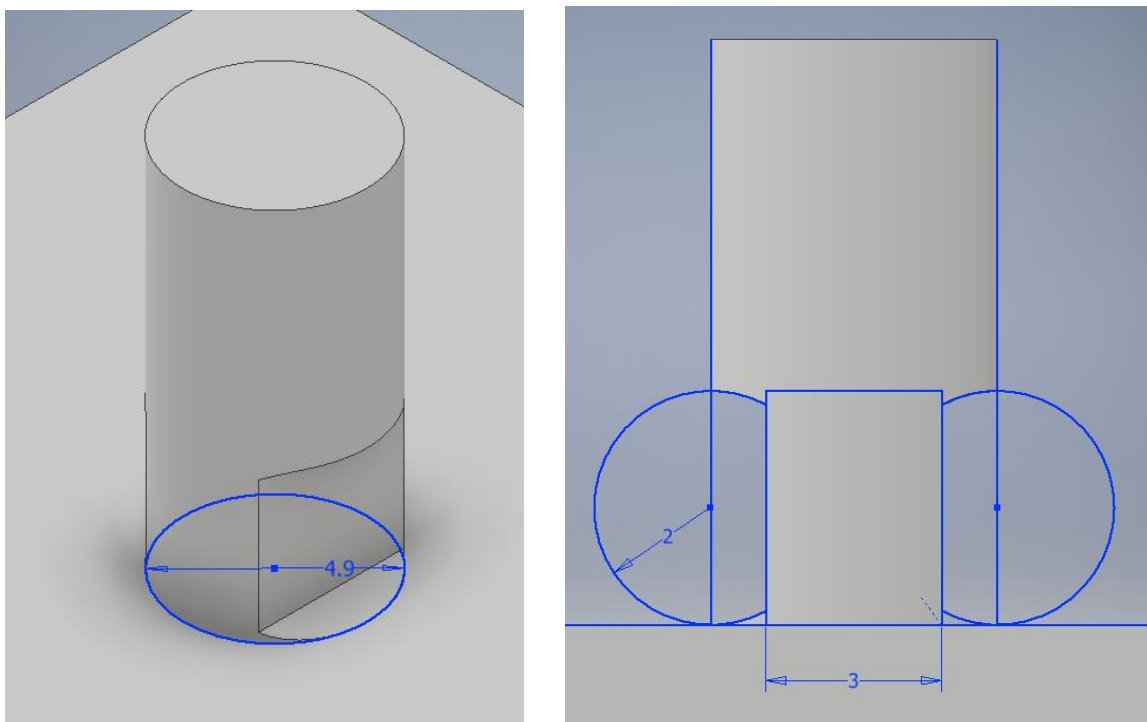


Figure 25: The dimensions of the omifit inputs and outputs. Cylinder shape, the top half having a wider diameter of 4.3 mm and the bottom half being 3.8 mm in diameter.

Overall this reduced leakage significantly, as the tight fit and the omifit placement above the glass at the 4.3 mm diameter (**figure 26**) caused a steady flow when the syringe pumps were turned on. At **figure 27** shows an example of the difference between the inputs and outputs on PDMS casted plasma cleaned chips. However, one issue that was become evident after reusing the manufactured microfluidic chips, after continually re-inserting the omifit screws,

this presented an issue of causing a loosening and widening of the PDMS inputs and outputs, which in turn lessened the tight fit and sometimes caused leakage. Therefore, new microfluidic PDMS plasma cleaned chips had to be manufactured every 5-10 uses.

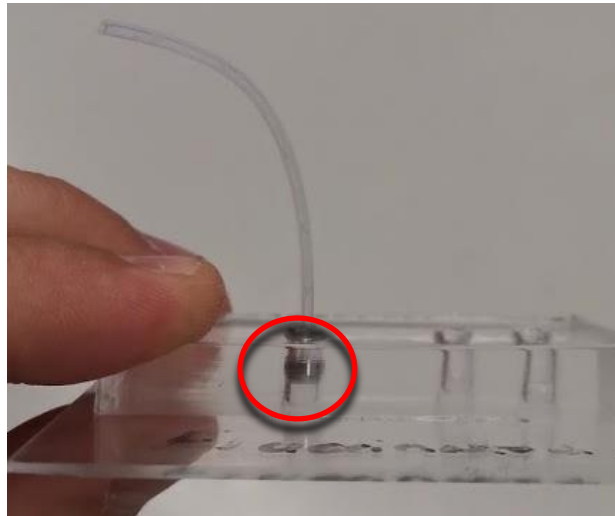


Figure 26: A photo of the omifit inserted in the new designed input and output side-on.

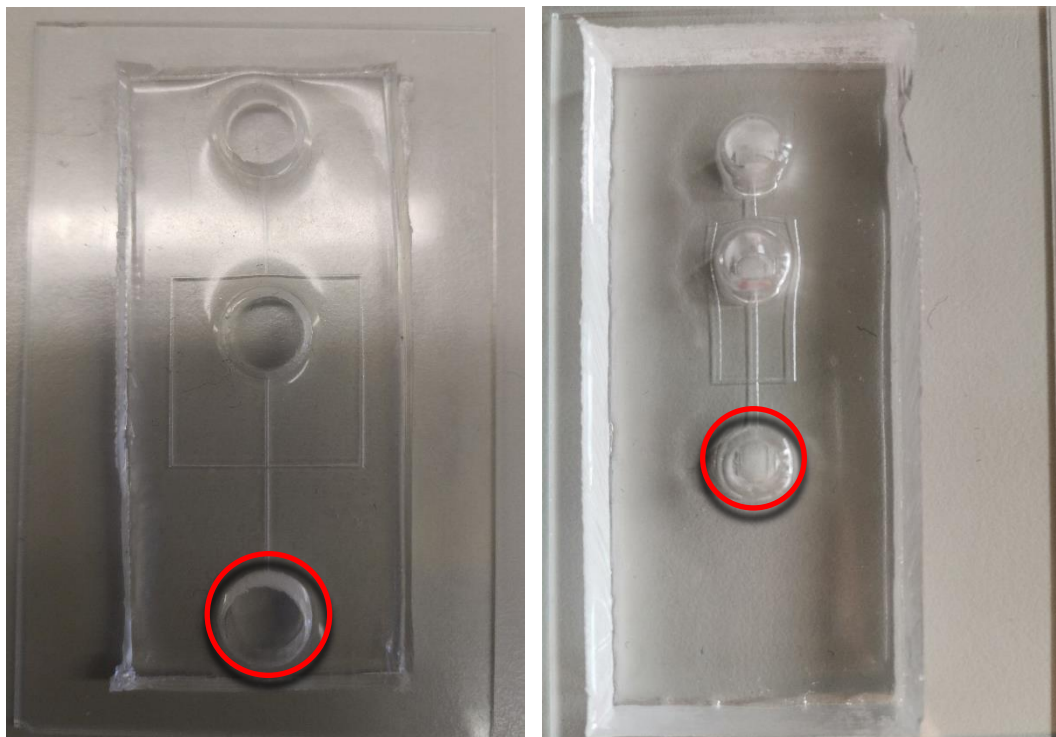


Figure 27: Photo of plasma cleaned beta and final 'X' junction design chips, with redesign before and after of inlets and outlets indicated by the red circle. As well as reduction in overall microfluidic channel length.

2.2.3 Mixing Chip. Discussion and results

As discussed briefly in section 2.2.2, the mixing chip was manufactured in order to mix the zinc solution and the PP6 solution together within the microfluidic channels forming the aqueous phase. The 'zig-zag' design was referenced in literature ⁽⁵³⁾ as one design that has

demonstrated success. The idea behind this design was to have enough surface area and ridges for two different fluids to interact with each other and overcome the laminar flow. The overall dimensions of the mixing chip channels were as followed; 0.1 mm in height and width, between each zigzag 'step' was 0.4 mm distance them, and the overall length of the whole channel was roughly 2 cm. Below at **figure 28** demonstrates these dimensions.

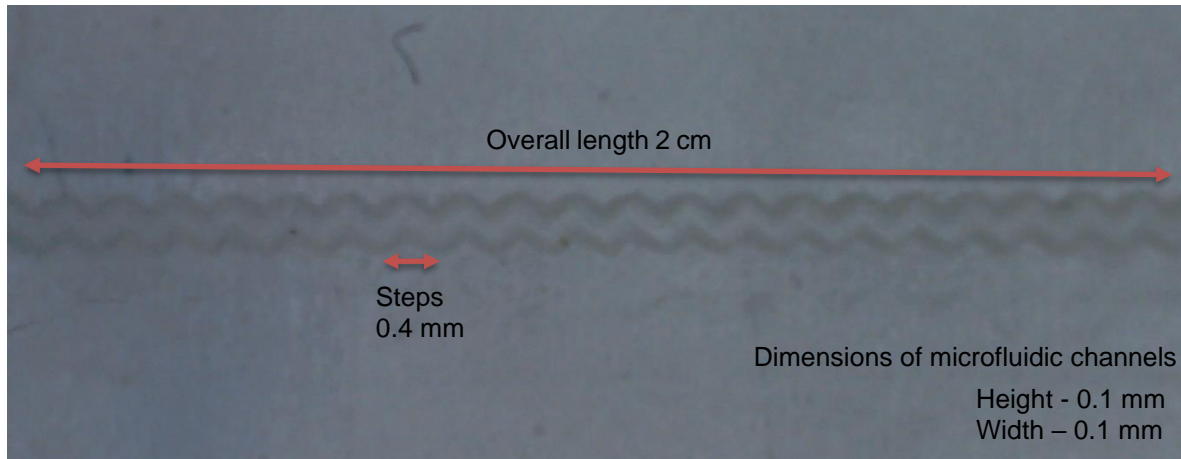


Figure 28: Microscopic image showing dimensions of zig-zag design.

The mixing chip was tested by pumping two separate syringes with two different food colouring of red and blue diluted with ultra-pure water at 10-120 microliters per minute and the results expected where for the colour purple to be observed down the channel as reference in the literature ⁽⁵³⁾. However, this didn't occur and unfortunately the design was unsuccessful in mixing. Instead the microfluidic device produced laminar flow and the two food colouring fluids laid on top of each other (**figure 29**) which was also reported in the literature referenced. Despite the literature the results were not successful. Due to time constraints further optimisation/refinement and further research weren't able to be conducted. Mixing chip was not required for this project but will be used in future work within the final product of this project.

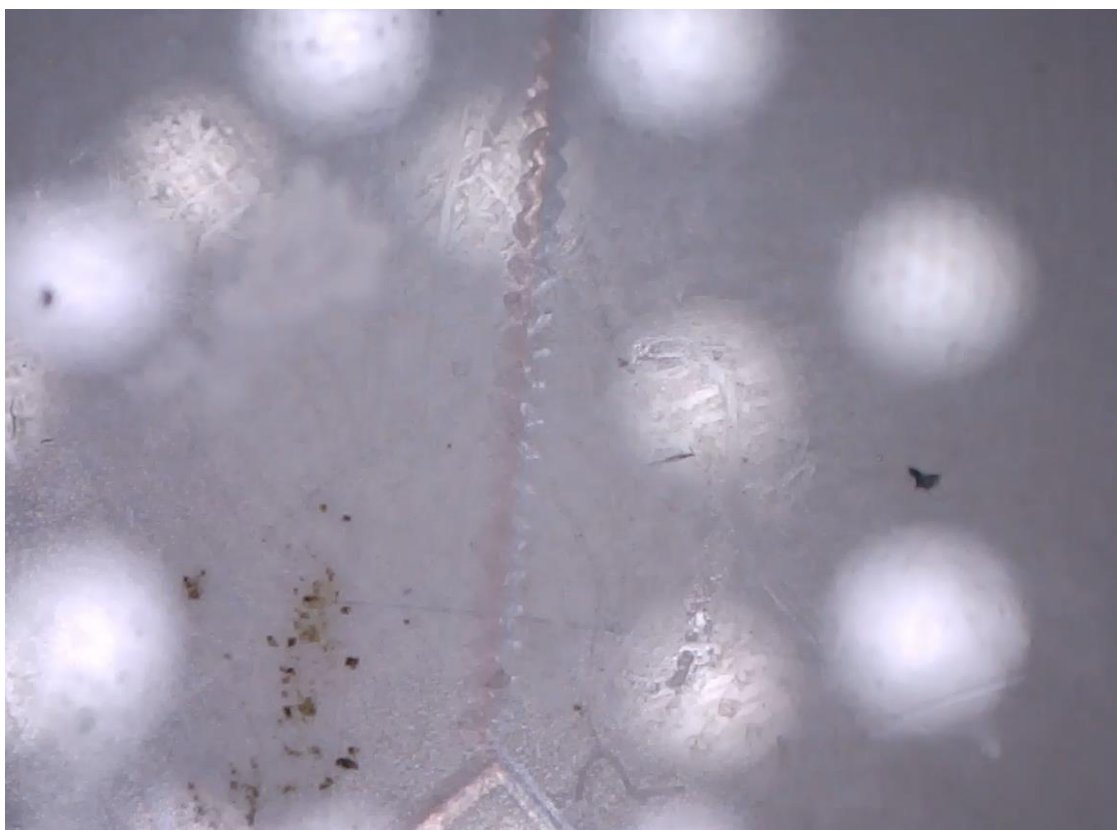
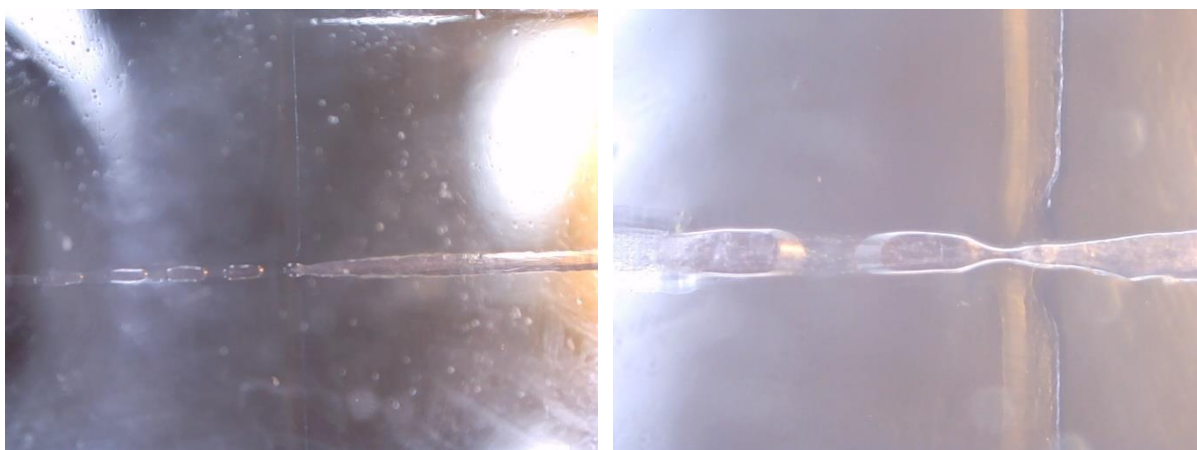


Figure 29: Microscopic image of the 'zigzag' mixing microfluidic the red and blue expressing laminar flow.

2.2.4 Microdroplets generation. Water and oil/surfactant

The 'X' and 'T' junction designs were initially tested with ultra-pure water with red food dye colouring and silicone oil with span 80 (surfactant) to generate microdroplets. Water was pumped at a constant rate at 15 microlitres per minute and the oil with surfactant was pumped at various rates at 30-120 microlitres per minute. The results were successful both the 'X' and 'T' chips both produced microdroplets, which is shown below at **figure 30** and an example of microdroplets being formed at outlets from both the 'X' and 'T' junction is shown at **figure 31**



(A)

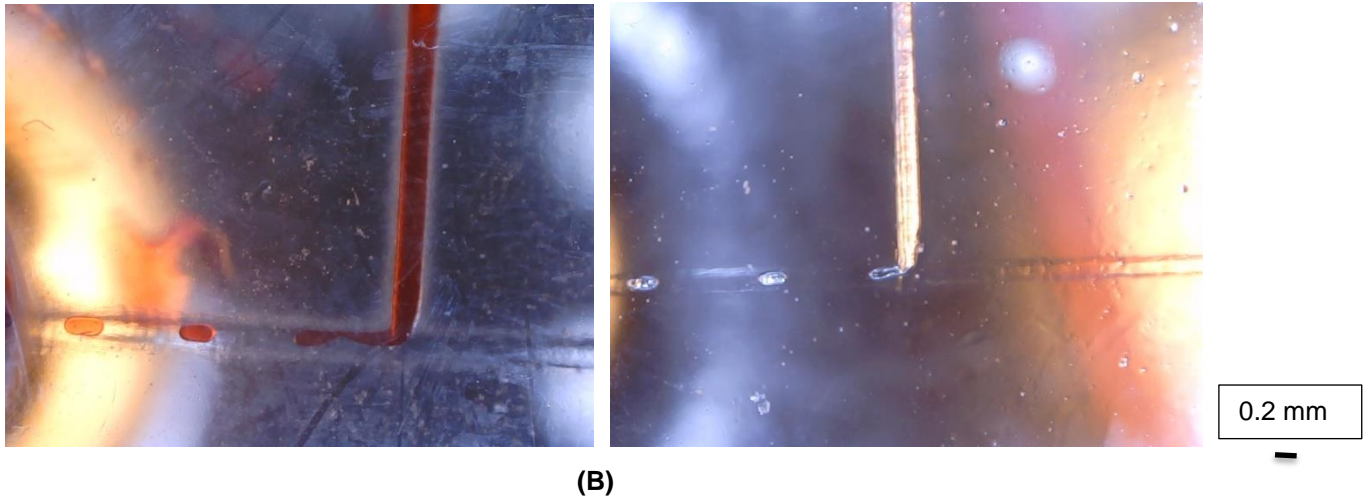


Figure 30: (A) 'X' junction microscopic images taken showing microdroplet generation at the 'pinch' of the junction. (B) T' junction microscopic images showing microdroplet generation at the junction.

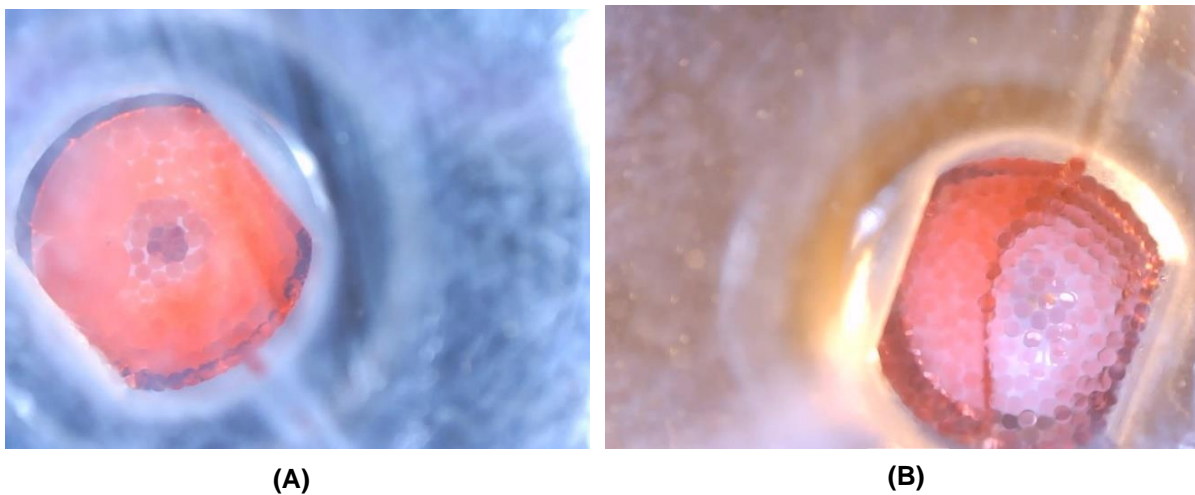


Figure 31: (A) microscopic image of 'T' junction microdroplet accumulation at the outlet. (B) microscopic image of 'X' junction microdroplet accumulation at the outlet.

The microfluidic chips of both the 'X' and 'T' junctions were then tested using fluorinated oil/surfactant, first the channels were fluorinated using fluorinated silane in FC-40 and then was left to cure overnight in the oven at 120° C. ultra-pure water and FC-40 oil with sphere fluidics Pico surf fluorinated surfactant were pumped at the same rates as mentioned previously with the initial tests using the silicone oil, the chips also generated microdroplets using these fluorinated chemicals. The reason why fluorinated oil chemicals were used was because of five reasons, Fluorinated chemicals are biocompatible, commonly organic compounds are insoluble in fluorinated substances, fluorinated chemicals are almost completely inert so therefore are also compatible with many surface material so they don't damage or swell PDMS overtime as well as they have referenced to have high stability with

microdroplet generation ⁽⁵⁵⁾. However, one of the most desired reason is that fluorinated oil/surfactant are denser than water, Droplets on the liquid surface is advantageous as it increases the rate of evaporation. Increased evaporation aids in the formation of the supramolecular network.

Overall the microdroplet generation was able to be achieved by using both the 'X' and 'T' junction, but monodisperse droplets wasn't achieved by the 'X' junction but more accurately by the 'T' junction. Monodisperse droplets were critical in order to provide a more accurate insight into seeing whether the supramolecular network had been formed by having identical sized microdroplets. The microdroplet formed from both chips went up the Omnifit™ in the tubing (example Shown at **figure 32**) and then microdroplets were collected onto glass slides containing fc-40 shown at **figure 33** However, the big issue both microdroplets collected presented was that neither of them remained stable for a long enough period of time, this will be discussed more in detail in section 2.2.7 of this thesis.



Figure 32: Photo of blue microdroplets traveling up the tubing from the outlet of the Omnifit

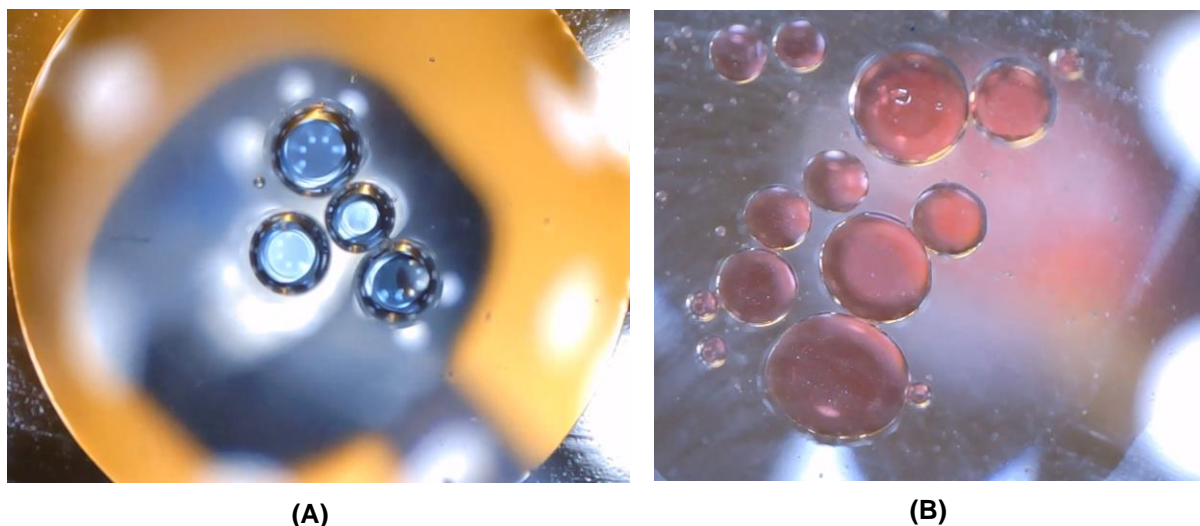


Figure 33: Microscopic image of droplets on a glass slide. (A) microdroplets formed from the 'T' junction chip. (B) microdroplets formed from the 'X' junction chip.

2.2.5 Microdroplets generation. Propanol and oil/surfactant

As mentioned throughout this thesis, one of the future ambitions of this project would be for the supramolecular network to be applied to biological application such as delivery of therapeutic substances, and the method of how this research would impact on that goal would be that an apolar solvent such as propanol at low temperature would convert PP II to PP I. As mentioned, PP I has a more closed compact structure (cis configuration) compared to PP II (trans configuration), overtime the PP I supramolecular network would slowly convert back to the PP II supramolecular network, causing a delay in the release of therapeutic substances. As a proof of concept, the microdroplet generation was attempted with propanol (coloured with red food dye) and fluorinated oil with surfactant with the syringe pump flow rates set at the same rates as previously mentioned at section 2.2.4 of this thesis. Only the 'T' junction chip was used as it generated the most consistently sized microdroplets. The results were not as successful as shown below at **figure 34**. The microdroplets didn't form emulsion at the 'T' junction but instead produced laminar flow and didn't produce microdroplets until at the 'pinch' of the outlet.

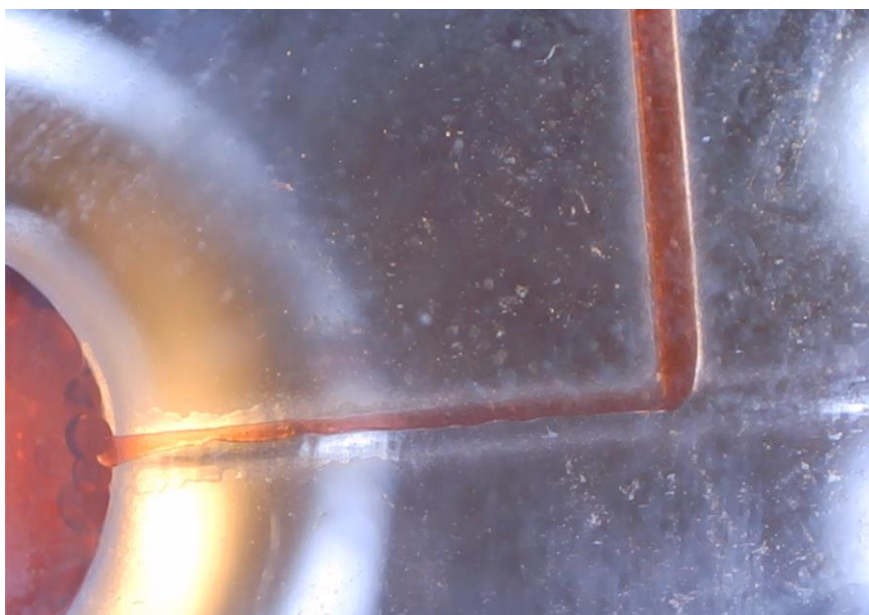


Figure 34: microscopic image of 'T' junction attempt at microdroplet generation with propanol and fluorinated oil with surfactant.

In the context of passive microfluidic microdroplets generation with PDMS casted microfluidic chip, the organics solvent and oil interface is a field that hasn't been researched thoroughly yet. Organic solvent in PDMS has reported issues of swelling and only have been demonstrated in etched silicon plates. There have been methods worked around to introduce organic solvents one example was inserting organic pendants/vesicles inside of aqueous phases ⁽⁵⁶⁾ or there has been success in droplet generation with non-aqueous phases involving 'digital' microfluidics by applying an electric current in the microfluidic channels ⁽⁵⁷⁾. However overall there hasn't been much-demonstrated literature for passive microfluidics, so other methodologies avenues needed to be explored in order to achieve the future ambitions from this thesis.

2.2.6 Microdroplet stabilisation.

Overall the microdroplet droplet generation at the water and oil/surfactant interface using both the 'X' and 'T' junction was successful, but both didn't create stable droplets (typically 10 seconds before they merge which is not the behaviour expected for stabilized droplet). The 'X' junction chip didn't achieve monodisperse droplets, however, the droplets produced were stable for a longer period of time than compared to the 'T' junction chip. The microdroplets formed at the outlets of both designs appeared to remain stable as previously shown at **figure 33** however, the droplets appeared coalesce traversing the Omnifit™ screw fitting and tubing. Although not always, however the droplets would eventually coalesce on the glass slide, an example is shown at **figure 35**.

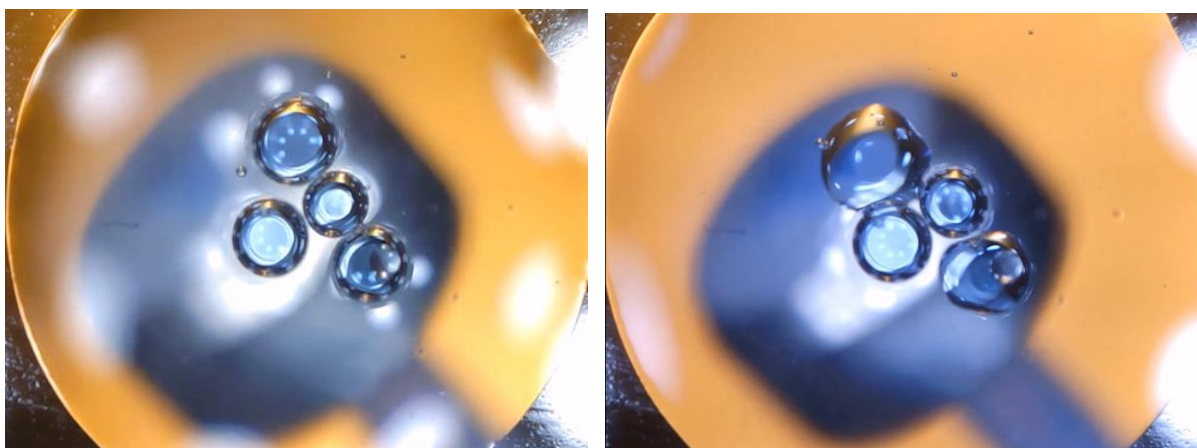


Figure 35: microscopic image of the microdroplets. The microdroplets beginning to coalesce on the right-hand image.

The period of time of microdroplets emulsion wasn't sufficient to be applied to the creation of the supramolecular network. In the ideal conditions, the microdroplets would remain stable and over time the aqueous phase would evaporate, after which an emulsion breaker would be added and observed under the microscope observing an indication of the supramolecular network, this, however, was not the case. There were two suspected design flaws with the 'X' and 'T' junction microfluidic chips, the first being the overall length of the devices to the output was too long, possibly the microdroplets dealing with surface tension from the PDMS over a longer length of time could've disrupted the stability. The second flaw was the omifit fitted in the outlet of the microfluidic devices, the accumulation of the microdroplets forming at the outlet would accumulate until the pressure would push an influx of microdroplets up the omifit into the tubing, as shown previously above in section 2.2.4 at **figure 31**. The pressure acting upon the microdroplets due to the change in volumes using Omnifit™ may have caused coalesce within the tubing before deposition on a glass slide. Two Other suspected issues that failed to create stable droplets were the use of two different mechanical coil-based syringe pumps, which caused very slight delays in either the oil or water phases, so therefore would not maintain a constant flow and would disrupt the consistency of the size of the droplets which may have also perhaps disrupted the stability. The other issue being that according to the manufacturer of the 'pico surf surfactant', the surfactant was optimised to work best within 0.4 mm or less in diameter to create stable droplets, and the Omnifit™ tubing was 2 mm in diameter. So, the two desired redesign of the junction chips if more time was allocated within this research would be to the insert of the tubing directly into the PDMS and to be cured, so no accumulation of the droplets would occur at the outlet and each microdroplet would immediately travel up the tubing reducing the variation of pressure. An overall reduction of the travel time to the pinches of the 'X' and 'T' junctions and towards the outlet. A pressured based system of pumping the phases

would cause significantly less delay and higher consistency in flow rates as well as using tubing that was 0.4 mm in diameter.

3. Conclusion

In summary, for the organic chemistry component of this thesis, it has been demonstrated that a synthetic pathway gained a functionalised proline, which in turn that proline was utilised in SPPS to synthesis PP6. The PP6 was able to dissolve into organic solvent such as TFE, able to dissolve into water (with small 2% addition of methanol) and was able to be dissolve into alkaline water solution (H₂O with NaOH). The analysis of DLS and SEM-EDX helped demonstrated that a supramolecular network was able to be formed within a bulk solution with overall the organic synthesis side of the research was relatively successful (with the synthetic pathway overall yield being an exception to be improved). The ability to form a number of different morphologies using one simple hexamer is remarkable and will be further investigated in the Palma group. For the microfluidic component of this thesis it has been demonstrated that microdroplet generation at the aqueous and oil (with and without surfactant) interface was performed with two different designs ('X' and 'T' junction) manufactured from 3-D printed mould fabrication to PDMS microfluidic device. Although the demonstrated results from this thesis are novel, the final desired result of incorporation of both components to create the supramolecular network was unfortunately superseded by the instability of the microdroplets. The results from the proof of concept for the formation of the supramolecular network in a bulk solution were promising and future analytical data would be desired to be collected using techniques such as AFM (giving the topography of the structure) and neutron scattering (characteristic peak of zinc) to further support supramolecular formation. Overall prioritisation of the redesign of the microfluidic junction chips was required to order to create the desired microdroplet supramolecular network. The results gained from this research was a precursor and able to lay foundations for future work. Only slight increment alterations to this research would result in the desired pursuit of the supramolecular network formation.

4. Future work

There were several aspects of this research that were highly desired to be improved upon for future work such as;

- Optimisation of the synthetic pathway to gaining the final functionalised proline to improve the yield.
- Characterisation of the microdroplets using a measurement operation software.
- To further support the proof of concept using AFM and neutron scattering, as well as trying different zinc derivatives or biologically friendly metal coordinate derivatives.
- Future researching and testing different apolar solvents or methodology to convert the functionalised PP II to PP I for future ambition work mentioned at section 2.2.4.
- Design, Manufacture and test other mixing chip designs, to overcome the laminar flow.

However, the priority future work to be conducted from this thesis was the supramolecular assembly demonstration via microdroplet manipulation which was the end goal when setting out on this thesis, this, however, wasn't able to be achieved. Due to time constraints, the appropriate optimisation of design for the microfluidic junction chips was an issue. The critical redesigns would be the accommodation of the tubing at the outlet rather than the omnifit. overall the constant flow from the omnifits placed in the inlets was sufficient to create the microdroplets, however the omnifits at the outlet not only caused unknown pressures for the influx of droplets to go upwards into the tubing, but it also caused an accumulation to form a 'pool' of microdroplets. Ideally the redesign would involve the direct embedding of the tubing. The direct embedding would allow the droplets to go directly into the tubing rather than accumulate in a pool of droplets and dealing with unknown changing pressures. These future work redesigns as mentioned would ideally increase the stability of the emulsified microdroplets and would allow the demonstration of the microdroplet supramolecular network. Ideally in future work the monodisperse microdroplets would be generated using the fluorinated chemicals, consisting of the FC-40 and 2 % fluorinated surfactant, the droplets would be collected and then left to dry after which the fluorinated emulsion breaker of 1H,1H,2H,2H-Perfluoro-1-octanol would be added to demonstrate the network formation.

5. Experimental

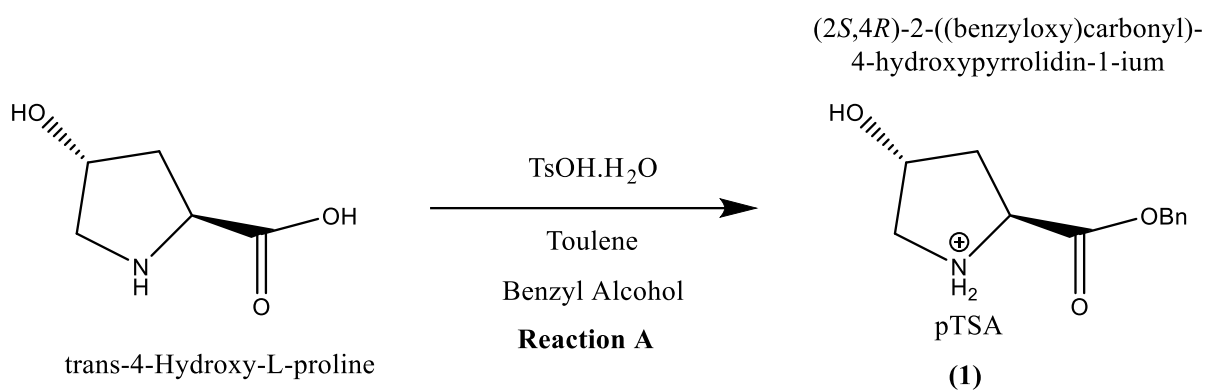
5.1 Organic synthesis

Below is the experimental containing the quantities, equivalences and methodology of the organic synthesis of the synthetic pathway, gaining the functionalised proline and SPPS PP6 design. All the Gradient Flash Column Chromatography was performed on high purity grade silica gel particle size 75-150 μm . All NMR spectra were recorded at room temperature on a Bruker 400 MHz which operated at 100 MHz or 400 MHz for ^1H and ^{13}C analysis. Chemical shifts (δ) units are parts per million (ppm) relative to the deuterated solvent signal (^1H : D_2O , δ 4.79 ppm; CDCl_3D , δ 7.24 ppm), (^{13}C : CDCl_3D δ 77.0). The splitting patterns were characterised as s (singlet), d (doublet), t (triplet), m (multiplet). Liquid chromatography Electrospray ionization mass spectroscopy was performed at low resolution using the UltiMate 3000 from thermo fisher scientific. FTIR (Fourier-transform infrared spectroscopy) with an attenuated total reflectance (ATR) attachment was performed measuring the bonds wavelengths at cm^{-1} . Angle of rotation was measured using a digital polarimeter gaining the αD . Solvent were removed from products using a rotavapor based on a preprogramed database of optimal pressures and temperatures, after which all crudes and purified products were dried under the continuous high vacuum setting of the rotavapor. All deuterated solvents, solvents and reagents for the reactions below described, were purchased commercially from trusted chemical dispensers; fisher scientific, sigma and fluorochem. All chemicals were presumed to be of the highest quality according to the manufacturer.

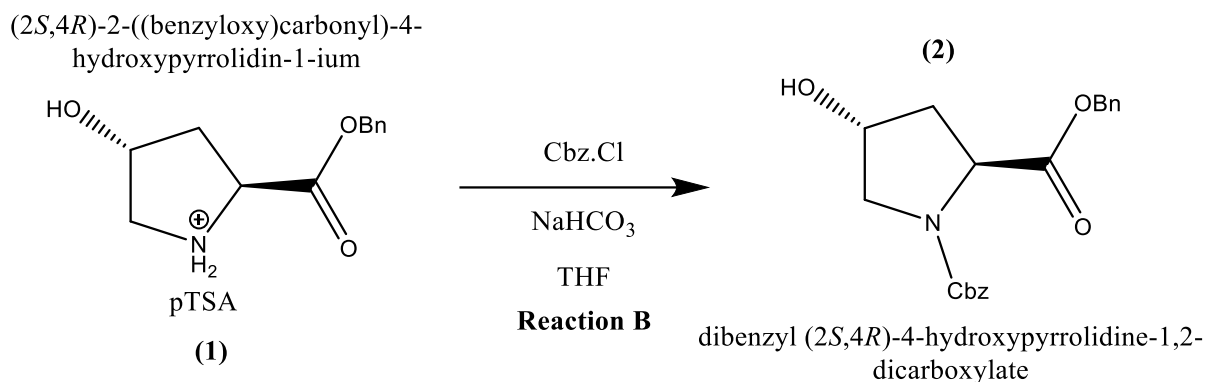
5.1.1 Synthetic pathway synthesis

As prior mentioned in the results and discussions at **section 2.1.1** and at **figure 5** shows the overview, justifications and results of each reaction. Within this section is the quantities, techniques and observations for each reaction for the pathway. This reaction pathway from reaction B onwards was repeated due to the overall low yield gained at the final step, to prevent repetition within this experimental, the reactions described below are represented of typically what the reaction would result in.

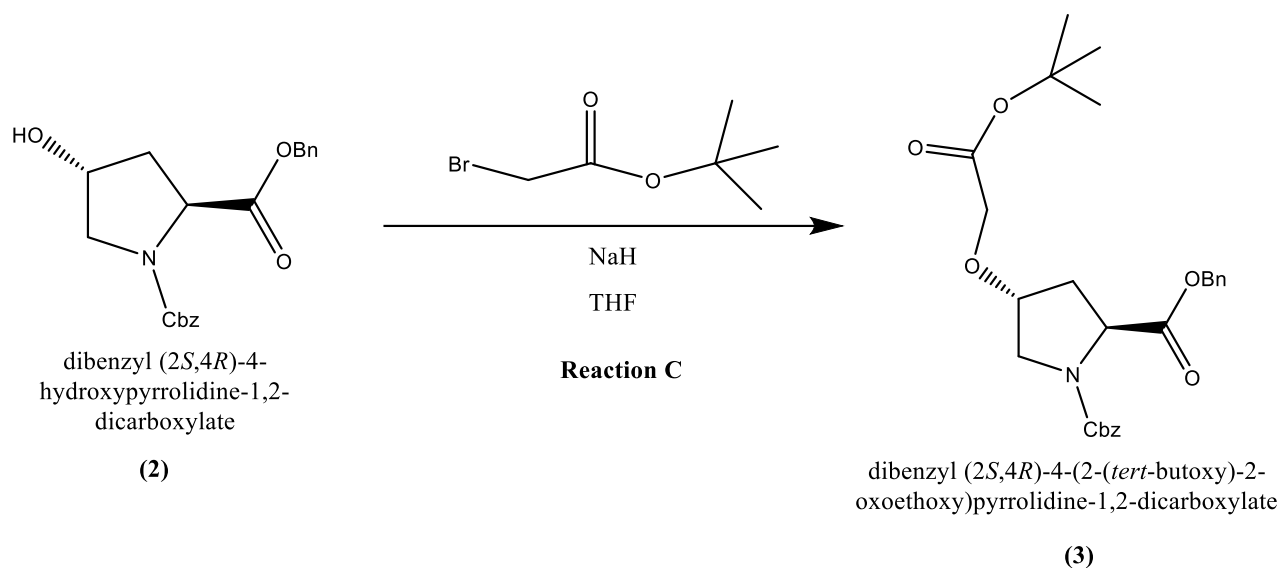
1. *Reaction A*: Reagents **trans-4-Hydroxy-L-proline** (1 eq, 114.4 mmol), **p-Toluenesulfonic acid monohydrate** (1 eq, 114.4 mmol). Solvents **toluene** (134 ml), **benzyl alcohol** (134 ml).



- Weight 15 g of **trans-4-Hydroxy-L-proline** and made up a solution of 134 ml **toluene** and 134 ml **benzyl alcohol**. Weight 21.8 g of **p-Toluenesulfonic acid monohydrate** and added to starting material solution. Mixed and placed under reflux at 125°C for 20 hours, also using a dean stark trap to remove the water. After 20 hours the reaction is cooled down to room temperature and the product is crystallised using cold **diethyl ether** (800 ml). After 30 minutes the oil becomes a white precipitate. Solid is collected via filtration and washed with **ether** (250 ml) and dried in a vacuum oven overnight. 36 g of solid white powder was gained product **(1)** **(2S,4R)-2-((benzyloxy)carbonyl)-4-hydroxypyrrolidin-1-ium)** Yield 80%. This was the purified product and was carried forward onwards to the next reaction.
 - **NMR spectroscopy:** ^1H NMR (CDCl_3): δ (ppm) 2.35 (m, 3H), 2.5 (m, 1H), 5.2 (d, 1H)
7.1-7.7 (d and m, aromatic H).
 - **Mass spectrometry:** ESI-MS(m/z): $[\text{M}-\text{H}]^+$ calcd.for $\text{C}_{12}\text{H}_{16}\text{NO}_3^+\text{C}_7\text{H}_8\text{O}_3^-$, 393.1;found, 393.45
 - **IR spectroscopy:** FT-IR (ATR) v: 592, 893, 1093, 1193, 1294, 1494, 1595, 2297 cm^{-1} .
2. **Reaction B:** Reagents **product (1) (dibenzyl (2S,4R)-4-hydroxypyrrolidine-1,2-dicarboxylate)** (1 eq, 12.7 mmol) **Benzyl chloroformate** (1.18 equivalent, 15.012 mmol). Solvents **sodium bicarbonate** (64 ml), **Tetrahydrofuran** (64 ml).

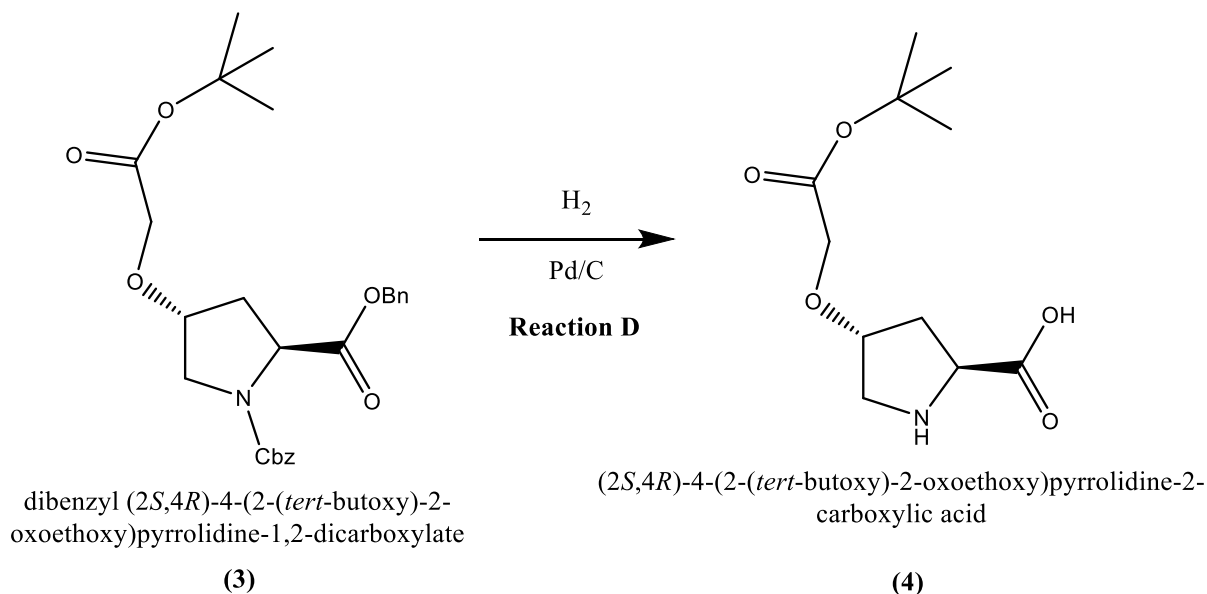


- Weighted 5 g of **product (1) ((2*S*,4*R*)-2-((benzyloxy)carbonyl)-4-hydroxypyrrolidin-1-ium)**, added 64 ml of **tetrahydrofuran** and 64 ml of **sodium bicarbonate** stirred for 10 minutes at room temperature and stirred at 0 °C. Add 2.17 ml **Benzyl chloroformate** to the solution and left to stir for 1 hour. the reaction was quenched with 3 M HCl at 0 °C, check pH to acidic. Reaction was extracted with DCM and wash with brine. Dry solution with MgSO₄ till the solution became clear. Filter and dried in the rotavap until a yellowish oil formed. The compound was purified by silica gel column chromatography using hexane/EtOAc 6:4 using a gradient system. 4.5 g of **product (2) (dibenzyl (2*S*,4*R*)-4-hydroxypyrrolidine-1,2-dicarboxylate)**. Yield 95%
 - **NMR spectroscopy:** ¹H NMR (CDCl₃D): δ(ppm) 7.5 (m, aromatic H), 5.3-5.0 (m, 1H), 3.5 (m, 1H), 2.3 (m, 1H).
 - **Mass spectroscopy:** Mass spectrometry:ESI-MS(m/z):[M-H]⁺+calcd.forC₂₀H₂₂NO₅, 356.4;found, 356.1.
 - **IR spectroscopy:** FT-IR (ATR) v: 592, 692-792, 993, 1093, 1193, 1394, 1595-1695 cm⁻¹.
3. *Reaction C:* Reagents **Product (2) (dibenzyl (2*S*,4*R*)-4-hydroxypyrrolidine-1,2-dicarboxylate)** (1 eq, 2.81 mmol), **60% NaH** (1.5 eq, 4.215 mmol), **tetrabutylammonium iodide** (0.1 eq, 0.281 mmol), **tert butyl bromoacetate** (4 eq, 11.24 mmol). Solvent **DRY THF** (15.2 ml).



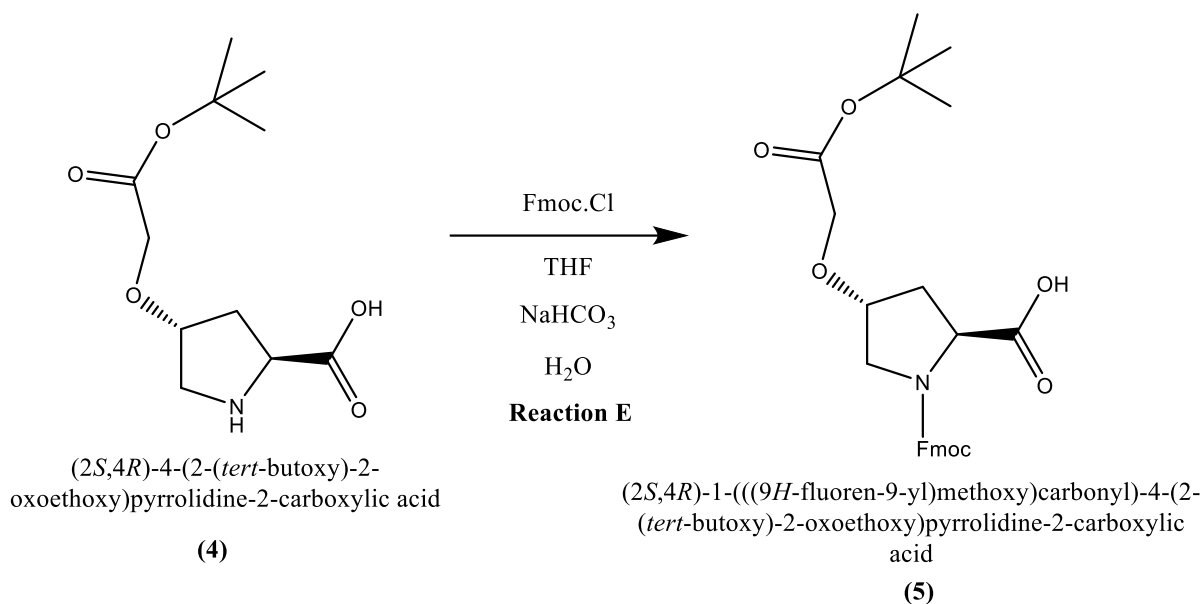
- Under an inert atmosphere, 10.6 ml of **DRY THF** and 0.1686 g **NaH** was added to 1 g of **Product (2) (dibenzyl (2S,4R)-4-hydroxypyrrolidine-1,2-dicarboxylate)** making a solution. 1.8 ml of **tert butyl bromoacetate**, 0.103 g of **tetrabutylammonium iodide** and 3 ml **THF** was added to the solution dropwise. The reaction is left overnight at room temperature. NH_4Cl is added to the reaction mixture and after which the reaction was extracted with **EtOAc**, **brine** was used to wash, and the solution was dried with MgSO_4 . The solution was filtered and dried in the rotavap giving a yellowish oil. Crude was chromatographed using hexane/EtOAc 6:4 using a gradient system. 1.0 g of **product (3) (dibenzyl (2S,4R)-4-(2-(tert-butoxy)-2-oxoethoxy)pyrrolidine-1,2-dicarboxylate)**. Yield 67%.
- **NMR spectroscopy:** ^1H NMR (CDCl_3): δ (ppm) 7.5 (m, aromatic H), 5.3-5.0 (m, 1H), 3.5 (m, 1H), 2.3 (m, 1H), 1.4 (s, 9H).
- **NMR spectroscopy:** ^{13}C NMR (CDCl_3): δ (ppm) 28, 36, 37, 52, 58, 70, 77, 81, 128, 136, 155, 169, 173.
- **Mass spectroscopy:** Mass spectrometry:ESI-MS(m/z): $[\text{M}-\text{H}]^+$ +calcd.for $\text{C}_{26}\text{H}_{32}\text{NO}_7$, 470.5;found, 470.1.
- **IR spectroscopy:** FT-IR (ATR) v: 592, 692, 792, 893, 993-1093, 1193-1394, 1494, 1795 cm^{-1} .
- **Polarimeter:** α_D : -32

4. **Reaction D:** Reagents **Pd/C 10%** (eq 10%). **Product (3) (dibenzyl (2S,4R)-4-(2-(tert-butoxy)-2-oxoethoxy)pyrrolidine-1,2-dicarboxylate)** (1 eq, 2.278 mmol). Solvents **MeOH, EtOAc**.



- 1 g of **product (3) (dibenzyl (2S,4R)-4-(2-(tert-butoxy)-2-oxoethoxy)pyrrolidine-1,2-dicarboxylate)** was dissolved in **MeOH**, 0.120 g **Pd/C** was dissolved in **EtOAc** and was added to the reaction mixture. The reaction vessel was evacuated by an aspirator and thoroughly purged with **N₂ (g)** to give inert atmosphere. **H₂ (g)** was added to vessel and mixture was stirred for 24 hours at room temperature. The mixture was filtered through and washed with **MeOH**. The solution is dried in the rotavap giving a reddish-brown sticky substance. 0.440 g of **product (4) [(2S,4R)-4-(2-(tert-butoxy)-2-oxoethoxy)pyrrolidine-2-carboxylic acid]** was gained. Yield 84%.
- **NMR spectroscopy:** ¹H NMR (CDCl₃D): δ(ppm) 5.1 (s, 1H), 4.2 (m, 2H), 3.8 (m, 1H), 1.4 (s, 9H).
- **Mass spectroscopy:** ESI-MS(m/z):[M-H]⁺calcd.forC₁₁H₁₉NO₅, 246.3;found, 246.2.
- **IR spectroscopy:** FT-IR (ATR) v: 592, 692, 792, 893, 993-1093, 1193-1394, 1494, 1795, 2999 cm⁻¹.

5. **Reaction E:** Reagents **Product (4) [(2S,4R)-4-(2-(tert-butoxy)-2-oxoethoxy)pyrrolidine-2-carboxylic acid]** (1 eq, 1.921 mmol), **Fluorenylmethyloxycarbonyl chloride** (1 eq, 1.921 mmol), **NaHCO₃** (2.1 eq, 4.0341 mmol). Solvent **THF** (7 ml), **distilled H₂O** (3.5 ml).



- 0.4406 g **Product (4) [(2*S*,4*R*)-4-(2-(*tert*-butoxy)-2-oxoethoxy)pyrrolidine-2-carboxylic acid]** was dissolved in 3.5 ml of distilled H₂O with 0.33 g NaHCO₃ at 0°C. 0.496 g **Fluorenylmethoxycarbonyl chloride** was dissolved to 7 ml of **THF**, this solution was added dropwise slowly to the reaction mixture. At 0 °C the reaction mixture was stirred for 1 hr and then left overnight at room temperature. The reaction was cooled again and quenched with 0.1 M of HCl. The reaction was worked up; extracted with DCM, washed with brine, dried and filtered with MgSO₄. The solution was dried in the rotavap. Yellowish oil was purified via recrystallisation. The solution was left in the freezer over 2 days, the compound still didn't crash out fully, so the solution was removed using a rotavapor evaporator and then was purified via gradient chromatography with 9:1 DCM:MeOH, followed by a flushing the column with MeOH. The solvent was removed using a rotavap and then placed under high vacuum via a schlenk line overnight giving a yellowish oil. 110 mg of **product (5) [(2*S*,4*R*)-1-(((9*H*-fluoren-9-yl)methoxy)carbonyl)-4-(2-(*tert*-butoxy)-2-oxoethoxy)pyrrolidine-2-carboxylic acid]** was gained. Yield 40%
- **NMR spectroscopy:** ¹H NMR (CDCl₃D): δ(ppm) 8-7.5 (s,s,d aromatic H) 5.1 (s, 1H), 4.2 (m, 2H), 3.8 (m, 1H), 1.4 (s, 9H).
- **NMR spectroscopy:** ¹³C NMR (CDCl₃D): δ(ppm) 176, 170, 164, 144, 141, 132, 131, 128, 127, 126, 120, 82, 78, 68, 66, 58, 52, 48, 38, 37, 36, 31, 28, 26, 24.
- **Mass spectroscopy:** ESI-MS(m/z):[M-H]⁺+calcd.forC₂₆H₃₀NO₇, 468.5;found, 468.1
- **IR spectroscopy:** FT-IR (ATR) v: 592, 692, 792, 893, 993-1093, 1193-1394, 1494, 1695 cm⁻¹.
- **Polarimeter:** α_D: -27.5

5.1.2 PP II design SPPS

The following experimental was conducted in order to the hexamer PP6 design. SPPS methodology was conducted in a peptide synthesis vessel, and once again all reagents and solvents were purchased from the various trusted chemical manufactures mentioned previously:

- Reagents: **product (5)** (2 eq), **rink amide resin** (1 eq, 0.0824 mmol), **Fmoc-Proline-OH** (3 eq, 0.25 mmol) 0.13 g **pyBop** (3 eq, 0.25 mmol) **HoBt** 0.03 g (3 eq, 0.25 mmol) and **0.06 g** DIPEA (6 eq, 0.5 mmol) **DTT**, **TIPS** . Solvents: **DMF**, **DCM**, **TFA**, **piperidine**, **Ac₂O**, **DIPEA** and **DMF**.

1. 0.103 g **Rink amide resin** beads (1 eq, 0.0824 mmol) was placed inside a peptide reaction vessel and dissolved in DCM till the beads swell up and left 40 minutes. DCM was pushed through with the compressed air and DMF was added and pushed out with compressed air 3x washing the swollen beads.
2. The rink amide resin beads are deprotected using 8:2 DMF and pyridine solution and left to react for 10 minutes. The solution is pushed with compressed air and washed with DMF 3 x. 8:2 **DMF** and **pyridine** solution is added and left to spin for a further 10 minutes. The solution was pushed out with compressed air and washed with DMF 3x.
3. The 1st coupling mixture was made up consisting of 0.09 g **Fmoc-Proline-OH** 0.13 g **pyBop**, **HoBt** 0.03 g and **0.06 g** DIPEA along with a minimum amount of DMF and was sonicated. This coupling mixture was added to the beads and was left for 2 hours. The solution was pushed out with compressed air and was washed with DMF 3x. An aliquot of the resin beads was taken and the Kaiser test was then added to beads, to see if successful.
4. For the first coupling, a Capping mixture of 3 ml was added then which consisted of 10:2.5:100 **Ac₂O**, **DIPEA** and **DMF** and left for to spin 1 hour. The solution was pushed out with compressed air and washed with DMF 3 x. An aliquot of the resin beads was taken and the kaiser test was deployed.
5. For the 2nd coupling, the same deprotection mixture and procedure was followed as the 1st coupling. The 2nd coupling mixture consisting of 0.1 g **product 5** (2 eq) 0.13 g **pyBop**, 0.03 g **HoBt** and 0.06 g **DIPEA** and a minimum amount of **DMF** was added and solution was sonicated. Coupling mixture was added and left to mix for 2hrs. The solution was pushed out with compressed air and washed with

DMF and DCM 3 x. An aliquot of the resin beads was taken, and the chlorophyll test performed.

6. This pattern of coupling mixture was repeated four more times, with intermediate changing the proline with the coupling mixture
 7. On final 6th coupling, the same capping mixture was added as mentioned in the first coupling. The Kaiser test was then added to the aliquot of beads.
 8. After the final coupling was successful the cleavage cocktail which consisted of 1.32 ml **TFA** (88 %), 0.075 ml **DTT** (5 %), 0.075 ml **TIPS** (5 %) and 0.03 ml water (2 %) was added to the resin and left to mix for 30 minutes. The peptide reaction vessel tap was opened and allowing the solution to drip slowly into 15 ml of cold diethyl ether causing the solution to 'crash out' forming a white precipitate.
 9. The solution containing the white precipitate was placed into a 'falcon tube' in which the solution was centrifuged. The solution of diethyl ether was decanted, and 15 ml of diethyl ether was added to the falcon tube, centrifuged, sonicated and decanted off. This was repeated four times. Overall 44 mg of off-white solid consisting of the final product was gained.
- **NMR spectroscopy:** ¹H NMR (D₂O): δ(ppm) 2-2.5 (m,m,m 20 H), 3.4-4.4 (m,m 12H), 4.5-4.9 (m, s 18H).
 - **NMR spectroscopy:** ¹³C NMR (D₂O): δ(ppm) 47-48.
 - **Mass spectroscopy:** ESI-MS(m/z):[M-H]⁺calcd.for C₃₈H₅₃N₇O₁₆, 864.33; found 864.34.
 - **IR spectroscopy:** FT-IR (ATR) v: 792, 993, 1093, 1193, 1294, 1595, 1795 cm⁻¹.

5.2 Microfluidics microdroplet

Below at **figure 36** is a photo example from two different angles of the general setup when preparing for the microfluidic methodology. The setup consisted of two glass syringes, containing the different phases. One containing the water or aqueous phase and the other being the oil with 2% surfactant (silicone oil with Span 80 OR FC-40 with 'sphere fluidic Pico-surf' surfactant). Each syringe was placed on two different syringe pumps; 'Harvard apparatus 22' and 'Pfizer world precision instrument'. One pump was set to a constant rate pumping the water or aqueous phase usually at rates of 15 microlitres per minute (this rate was sometimes modified very slightly to be higher or lower but remained relatively within this range). The other pump set at variable rates of 30-120 microlitres per minute pumping oil with 2% surfactant. The phases were pumped into 'Saint-Gobain Tygon' 1.6 mm internal diameter tubing which was attached via the omifit at the inputs into the junction PDMS cast microfluidic chips. At the outlet there was an omifit with the tubing inserted and attached to a clamp hanging over a

watch glass. The watch glass was balanced on the lenses of the 'MAOZUA' USB microscope which observed microdroplets on the windows 10 camera software app to capture and record.

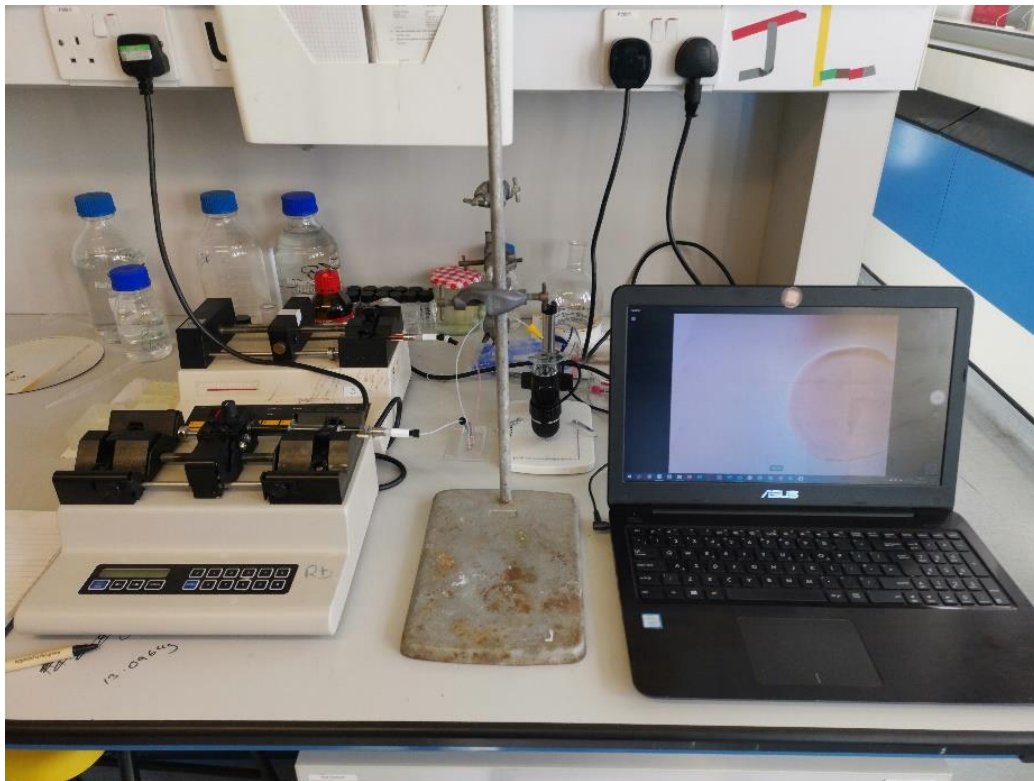


Figure 36: Two photo example of set-up; two syringe pumps with tubing and omifit attached to the inputs of the microfluidic chip, with omifit screw tubing inserted in outlet and held with

clamp hanging above watch glass. The watch glass is observed using USB microscope on window's camera app.

5.2.1 AutoCAD software, Microfluidic chip dimensions

The following experimental is the AutoCAD dimensions of the microdroplet generating successful 'T' and 'X' junctions' chips. As mentioned in section 2.2.6 and 2.2.4 of this thesis, the outlet sizes and overall length of the chips would be reduced in future work, however, the principle of the main dimensions of the 3-D printed chips was able to produce microdroplets. 'X' junction below at **figure 37** shows the length of the channels as well as the AutoCAD dimensions at the 'X' junction pinch with the measurements. 'T' junction below at **figure 38** shows the length of the channels as well as the AutoCAD dimensions at the 'T' junction pinch with the measurements.

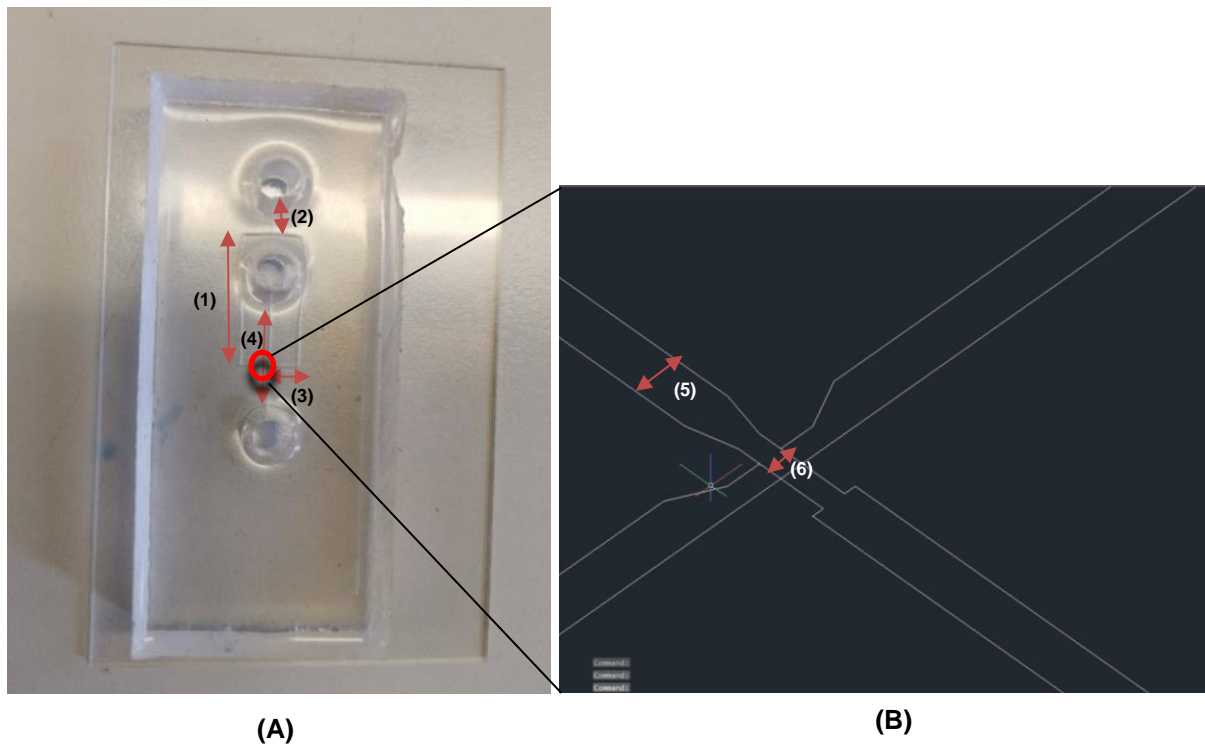


Figure 37: (A) Photo showing of the 'X' junction chip PDMS mould plasma cleaned lengths of channel indicated by the red arrows; (1) 15.8 mm, (2) 3 mm, (3) 3.6 mm, (4) 19.8 mm. (B) screenshot of the AutoCAD schematics of the 'pinch' of the 'X' junction diameter of the channels indicated by the red arrows; (5) 0.2 mm (6) 0.1 mm.

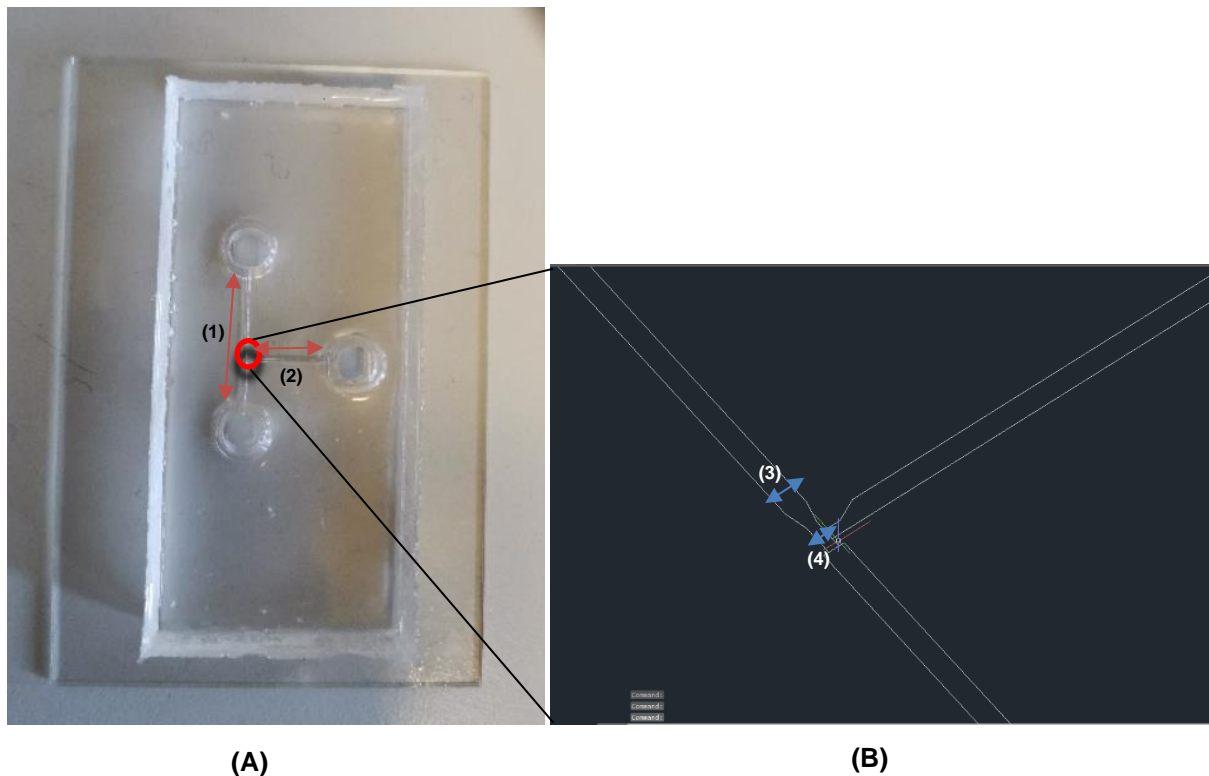


Figure 38: (A) Photo showing of the 'T' junction chip PDMS mould plasma cleaned channel indicated by the red arrows; (1) 19.6 mm (2) 12.3 mm. (B) screenshot of the AutoCAD schematics of the 'pinch' of the 'T' junction diameter of the channels indicated by the red arrows; (3) 0.2 mm (4) 0.1 mm.

5.2.2 Chip manufacturing process

Within this section the general outline from conception to creation of the microfluidic chips is described;

1. AutoCAD microfluidic design was exported to the form labs 2 3-D printer software known as 'PreForm'.
2. PreForm preps the exported AutoCad designs, the resolution was set to 0.025 mm and the file is sent to the 'lab forms 2' printer and is printed.
3. The 3-D printed Clear Resin chip was cleaned in isopropanol and cured in the UV radiation chamber for 60 minutes.
4. A mixture of 9:1 of 9 ml PDMS (Sylgard 184 silicone elastomer base) and 1 ml hardening agent (184 silicone elastomer curing agent) is mixed thoroughly together and then placed inside a vacuum chamber until the bubbles of the mixture had gone.
5. The clear resin chips were placed inside a 3-D printed container shown at **figure 39** which was tailored towards the size of the chips enabling a 'tight' fit.
6. The chips are slotted inside the resin container and the 10 ml mixture of PDMS was poured evenly over the microfluidic chip, for example, demonstrated at

figure 40 and was left In oven at 70-85 °C for 4-6 hours or overnight, (95-110 °C was possible to ensure much faster curing however the higher temperature caused slight bending to the resin chips).

7. The PDMS mould of the chip was then gently cut out around the edges and pushed out from the bottom of the resin container.



Figure 39: Photo of 3-D printed chip container, with hole at the bottom in order for more ease to push the PDMS cast mould out.

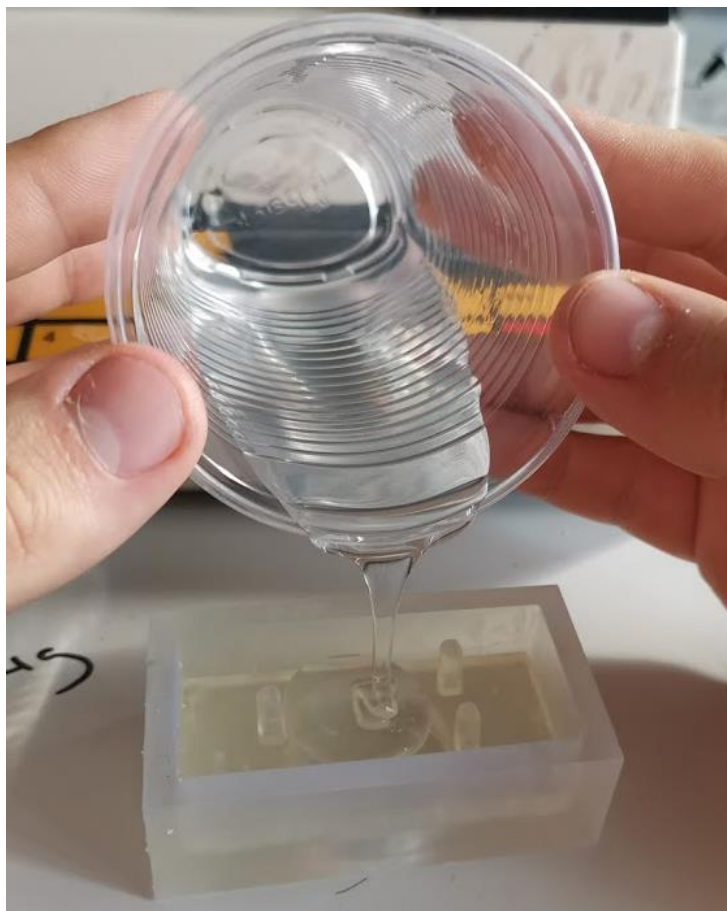


Figure 40: Photo PDMS with hardening agent poured over resin microfluidic chip.

After the PDMS cast has been created, the next step was plasma cleaning onto a glass surface. The 'Electronic diener Zepto plasma surface technology' plasma cleaner was available in this research and the method was as followed;

8. The glass slide and PDMS mould were kept as clean as possible and free from dust.
9. Both surfaces were placed topside in the plasma cleaner and placed under vacuum for 1 minute making the pressure half a bar inside.
10. The oxygen supply was introduced into the plasma cleaner via the gas mainline for 1 minute increasing the pressure to 1 bar.
11. The generator of the plasma cleaner was switch on for 1 minute applying electrons and free radicals to the surfaces.
12. Finally, the plasma cleaner was ventilated and the glass slide and PDMS mould were taken out, and the PDMS cast mould surface microfluidic channel imprinted surface was pressed gently onto the glass slide forming a tight seal. Example of the final manufactured product has been referenced repeatedly throughout this thesis.

Fluorinated microfluidic chips were also manufactured in order to generate microdroplets using FC-40 with 2 % sphere fluidic picosurf fluorinated surfactant. The same method was repeated with the one extra addition at the end of the process which was after the PDMS cast mould were plasma cleaned onto the glass surface FC-40 with 0.5 % 1H,1H,2H,2H-perfluorooctyltriethoxysilane was immediately injected into the microfluidic channels using a syringe and left to cure overnight in an oven at 60 °C.

6. References

- (1) T. Jin, Y. Ito, X. Luan, S. Dangaria, C. Walker, M. Allen, A. Kulkarni, C. Gibson, R. Braatz, X. Liao and T. Diekwisch, *PLoS Biology*, 2009, 7, e1000262.
- (2) P. Kumar and M. Bansal, *J. Struct. Biol.*, 2016, 196, 414–425.
- (3) M. V. Cubellis, F. Cailleux, T. L. Blundell and S. C. Lovell, *Proteins Struct. Funct. Genet.* 2005, 58, 880–892.
- (4) A. A. Adzhubei, M. J. E. Sternberg and A. A. Makarov, *J. Mol. Biol.*, 2013, 425, 2100–2132.
- (5) Zheng, X., Zhang, Y., Cao, N., Li, X., Zhang, S., Du, R., Wang, H., Ye, Z., Wang, Y., Cao, F., Li, H., Hong, X., Sue, A., Yang, C., Liu, W., Li, H., Hermann, J., Alfè, D., Tkatchenko, A., Shi, C., Zhang, X., Yu, C., Yao, Y., Zhang, W., Zhou, C., Li, X., Gong, Z., Jia, C., Lin, Y., Gu, C., He, G., Zhong, Y., Yang, J., Guo, X., V, R., Avakyan, N., Sleiman, H., Mittermaier, A., Packwood, D., Hitosugi, T., Zhang, T., Zhou, L., Guo, X., Cai, L., Sun, Q., Cai, K., Lipke, M., Liu, Z., Nelson, J., Cheng, T., Shi, Y., Cheng, C., Shen, D., Han, J., Vemuri, S., Feng, Y., Stern, C., III, W., Wasielewski, M., Stoddart, J., Song, B., Kandapal, S., Gu, J., Zhang, K., Reese, A., Ying, Y., Wang, L., Wang, H., Li, Y., Wang, M., Lu, S., Hao, X., Li, X., Xu, B., Li, X., Wang, H., Qian, X., Wang, K., Su, M., Haoyang, W., Jiang, X., Brzozowski, R., Wang, M., Gao, X., Li, Y., Xu, B., Eswara, P., Hao, X., Gong, W., Hou, J., Cai, J., Li, X., Yamashina, M., Kusaba, S., Akita, M., Kikuchi, T., Yoshizawa, M., Jiao, J., Li, Z., Qiao, Z., Li, X., Liu, Y., Dong, J. and Jiang, J. (2019). *Supramolecular Chemistry*. [online] Nature.com. Available at: <https://www.nature.com/collections/wypqwypccc>
- (6) NobelPrize.org. (2019). *The Nobel Prize in Chemistry 1987*. [online] Available at: <https://www.nobelprize.org/prizes/chemistry/1987/lehn/biographical/>
- (7) QuoteTab. (2019). *Jean-Marie Lehn Quotations at QuoteTab*. [online] Available at: <https://www.quotetab.com/quotes/by-jean-marie-lehn>
- (8) Atkins, W. (2002). *Supramolecular Design for Biological Applications* Edited by Nobuhiko Yui (Japan Advanced Institute of Science and Technology, Ishikawa). CRC

Title of current Chapter (in this example Appendix)

Press: Boca Raton. 2002. xiv + 410 pp. ISBN 0-8493-0965-4. *Journal of the American Chemical Society*, 124(47), pp.14280-14280.

- (9) Webber, M. and Langer, R. (2017). Drug delivery by supramolecular design. *Chemical Society Reviews*, 46(21), pp.6600-6620.
- (10) P. Ballester, P. van Leeuwen and A. Vidal-Ferran, Reference Module in Chemistry, Molecular Sciences and Chemical Engineering, 2015.
- (11) Biology-online.org. (2019). *Polypeptide - Biology-Online Dictionary | Biology-Online Dictionary*. [online] Available at: <https://www.biology-online.org/dictionary/Polypeptide>
- (12) E. Magnotti, S. Hughes, R. Dillard, S. Wang, L. Hough, A. Karumbamkandathil, T. Lian, J. Wall, X. Zuo, E. Wright and V. Conticello, *Journal of the American Chemical Society*, 2016, 138, 16274-16282.
- (13) J. Fletcher, R. Harniman, F. Barnes, A. Boyle, A. Collins, J. Mantell, T. Sharp, M. Antognozzi, P. Booth, N. Linden, M. Miles, R. Sessions, P. Verkade and D. Woolfson, *Science*, 2013, 340, 595-599.
- (14) N. Ochs, U. Lewandowska, W. Zajaczkowski, S. Corra, S. Reger, A. Herdlitschka, S. Schmid, W. Pisula, K. Müllen, P. Bäuerle and H. Wennemers, *Chemical Science*, 2019, 10, 5391-5396
- (15) Ho, C., Ng, S., Li, K. and Yoon, Y. (2015). 3D printed microfluidics for biological applications. *Lab on a Chip*, 15(18), pp.3627-3637.
- (16) Elveflow. (2019). *Microfluidics? A general overview*. [online] Available at: <https://www.elveflow.com/microfluidic-tutorials/microfluidic-reviews-and-tutorials/microfluidics/>
- (17) Ohno, K., Tachikawa, K. and Manz, A. (2008). Microfluidics: Applications for analytical purposes in chemistry and biochemistry. *ELECTROPHORESIS*, 29(22), pp.4443-4453.

Title of current Chapter (in this example Appendix)

- (18) Theberge, A., Courtois, F., Schaerli, Y., Fischlechner, M., Abell, C., Hollfelder, F. and Huck, W. (2010). Microdroplets in Microfluidics: An Evolving Platform for Discoveries in Chemistry and Biology. *Angewandte Chemie International Edition*, 49(34), pp.5846-5868.
- (19) C. Holtze, A. C. Rowat, J. J. Agresti, J. B. Hutchison, F. E. Angile, C. H. J. Schmitz, S. Koster, H. Duan, K. J. Humphry, R. A. Scanga, J. S. Johnson, D. Pisignano, D. A. Weitz, *Lab Chip* 2008, **8**, 1632
- (20) C. Priest, S. Herminghaus, R. Seemann, *Appl. Phys. Lett.* 2006, **89**, 134101.
- (21) N. Bremond, A. R. Thiam, J. Bibette, *Phys. Rev. Lett.* 2008, **100**, 024501.
- (22) K. Ahn, C. Kerbage, T. P. Hunt, R. M. Westervelt, D. R. Link, D. A. Weitz, *Appl. Phys. Lett.* 2006, **88**, 024104
- (23) D. R. Link, S. L. Anna, D. A. Weitz, H. A. Stone, *Phys. Rev. Lett.* 2004, **92**, 054503
- (24) L. M. Fidalgo, G. Whyte, D. Bratton, C. F. Kaminski, C. Abell, W. T. S. Huck, *Angew. Chem.* 2008, **120**, 2072;
- (25) H. Song, M. R. Bringer, J. D. Tice, C. J. Gerdtts, R. F. Ismagilov, *Appl. Phys. Lett.* 2003, **83**, 4664.
- (26) W. W. Shi, J. H. Qin, N. N. Ye, B. C. Lin, *Lab Chip* 2008, **8**, 1432.
- (27) H. Song, R. F. Ismagilov, *J. Am. Chem. Soc.* 2003, **125**, 14613
- (28) H. Song, J. D. Tice, R. F. Ismagilov, *Angew. Chem.* 2003, **115**, 792;
- (29) J. D. Tice, H. Song, A. D. Lyon, R. F. Ismagilov, *Langmuir* 2003, **19**, 9127
- (30) P. Zhu and L. Wang, *Lab on a Chip*, 2017, **17**, 34-75.
- (31) Nuclear Power, 2019.

Title of current Chapter (in this example Appendix)

- (32) B. Rapp, *Microfluidics: Modelling, Mechanics and Mathematics*, 2017, 243-263.
- (33) C. Marculescu, B. Tincu, A. Avram, T. Burinaru and M. Avram, *Energy Procedia*, 2016, 85, 339-349.
- (34) *Encyclopedia of Microfluidics and Nanofluidics*, 2185-2185.
- (35) H. Gu, M. Duits and F. Mugele, *International Journal of Molecular Sciences*, 2011, 12, 2572-2597.
- (36) C. Baroud, F. Gallaire and R. Dangla, *Lab on a Chip*, 2010, 10, 2032.
- (37) Hassanin, H. and Jiang, K. (2015). Net Shape Manufacture of Freestanding Ceramic Micro-components through Soft Lithography. *Micromanufacturing Engineering and Technology*, pp.239-256.
- (38) Printers, D., Printers, I. and Us, C. (2019). *What is 3D printing? How does a 3D printer work? Learn 3D printing*. [online] 3D Printing. Available at: <https://3dprinting.com/what-is-3d-printing/>
- (39) Berman, B. (2013). 3D printing: the new industrial revolution. *IEEE Engineering Management Review*, 41(4), pp.72-80.
- (40) Waheed, S., Cabot, J., Macdonald, N., Lewis, T., Guijt, R., Paull, B. and Breadmore, M. (2016). 3D printed microfluidic devices: enablers and barriers. *Lab on a Chip*, 16(11), pp.1993-2013.
- (41) Ho, C., Ng, S., Li, K. and Yoon, Y. (2015). 3D printed microfluidics for biological applications. *Lab on a Chip*, 15(18), pp.3627-3637.
- (42) Groombridge, A., Palma, A., Parker, R., Abell, C. and Scherman, O. (2017). Aqueous interfacial gels assembled from small molecule supramolecular polymers. *Chemical Science*, 8(2), pp.1350-1355.
- (43) C. R. Ley, N. R. Beattie, S. Dannoon, M. Regan, H. Vanbrocklin and C. E. Berkman, *Bioorg. Med. Chem. Lett.*, 2015, 25, 2536–2539.

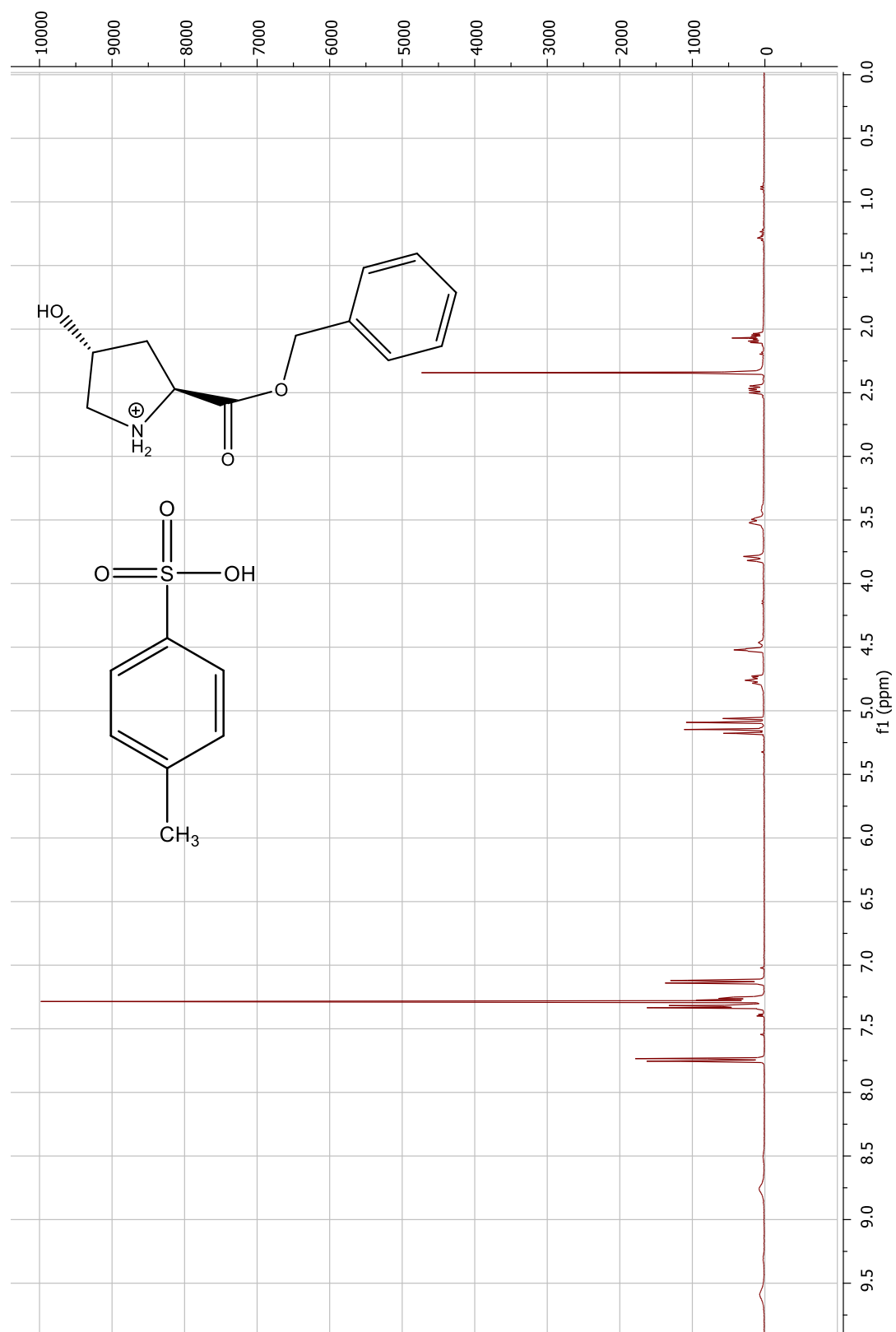
Title of current Chapter (in this example Appendix)

- (44) M. Iwashita, K. Makide, T. Nonomura, Y. Misumi, Y. Otani and M. Ishida, 2009, 5837–5863.
- (45) WO 2018/020358 A1
- (46) F. Zanardi, P. Burreddu, G. Rassu, L. Auzzas, L. Battistini, C. Curti, A. Sartori, G. Nicastro, G. Menchi, N. Cini, O. A. Bottonocetti, O. S. Raspanti and G. Casiraghi, 2008, 5, 1771–1782.
- (47) J. Pícha, M. Buděšínský, K. Macháčková, M. Collinsová and J. Jiráček, *Journal of Peptide Science*, 2017, 23, 202-214.
- (48) J. M. Palomo, *RSC Adv.*, 2014, 4, 32658–32672.
- (49) C. Guy and G. Fields, *Solid-Phase Peptide Synthesis*, 1997, 67-83.
- (50) J. Horng, *Protein Science*, 2006, 15, 74-83.
- (51) Z. Wang, N. Martin, D. Hini, B. Mills and K. Kim, *3D Printing and Additive Manufacturing*, 2017, 4, 156-164.
- (52) E. Piccin, D. Ferraro, P. Sartori, E. Chiarello, M. Pierno and G. Mistura, *Sensors and Actuators B: Chemical*, 2014, 196, 525-531.
- (53) V. Mengeaud, J. Josserand and H. Girault, *Analytical Chemistry*, 2002, 74, 4279-4286.
- (54) J. Baret, *Lab Chip*, 2012, 12, 422-433.
- (55) T. Tran, F. Lan, C. Thompson and A. Abate, *Journal of Physics D: Applied Physics*, 2013, 46, 114004.
- (56) Z. Cygan, J. Cabral, K. Beers and E. Amis, *Langmuir*, 2005, 21, 3629-3634.

Title of current Chapter (in this example Appendix)

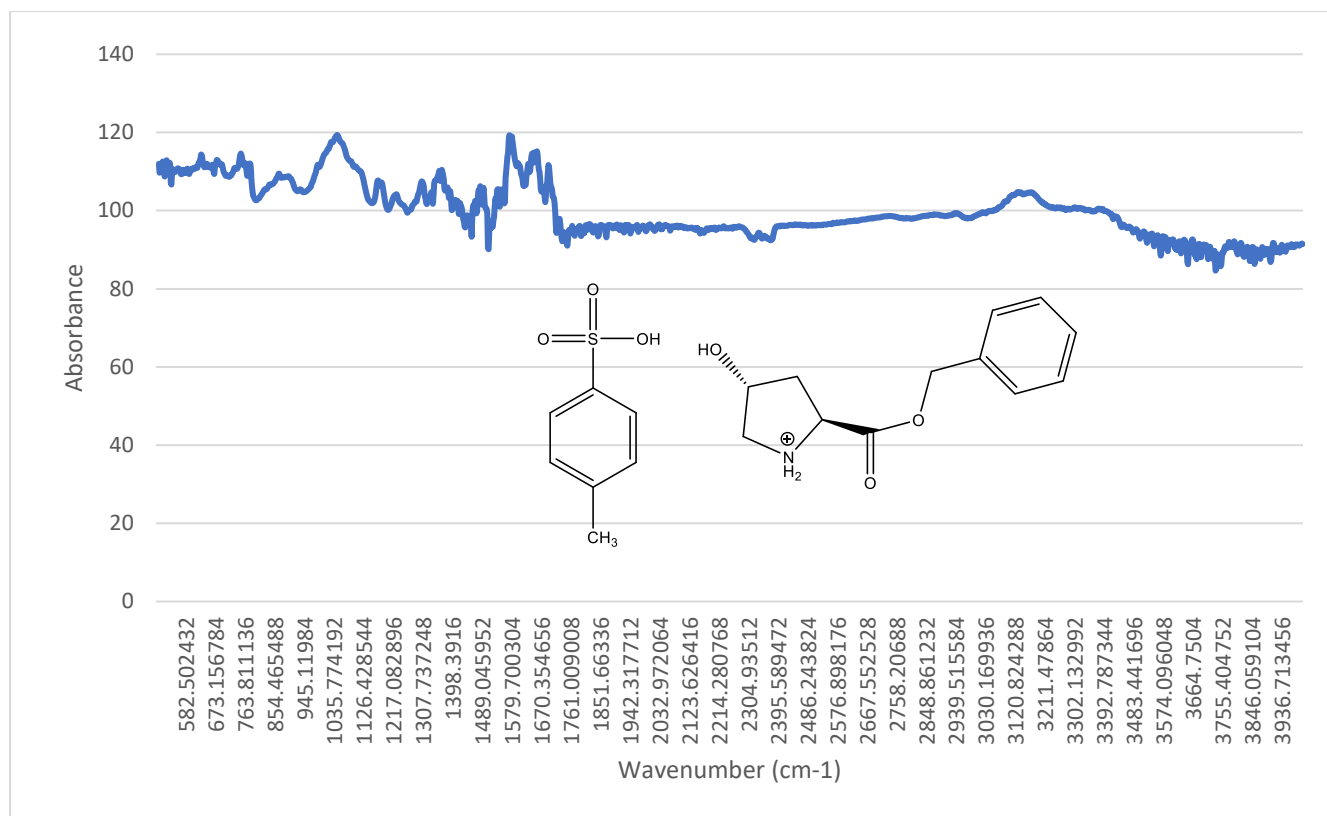
- (57) D. Chatterjee, B. Hetayothin, A. Wheeler, D. King and R. Garrell, Lab on a Chip, 2006, 6, 199.

7. Appendix

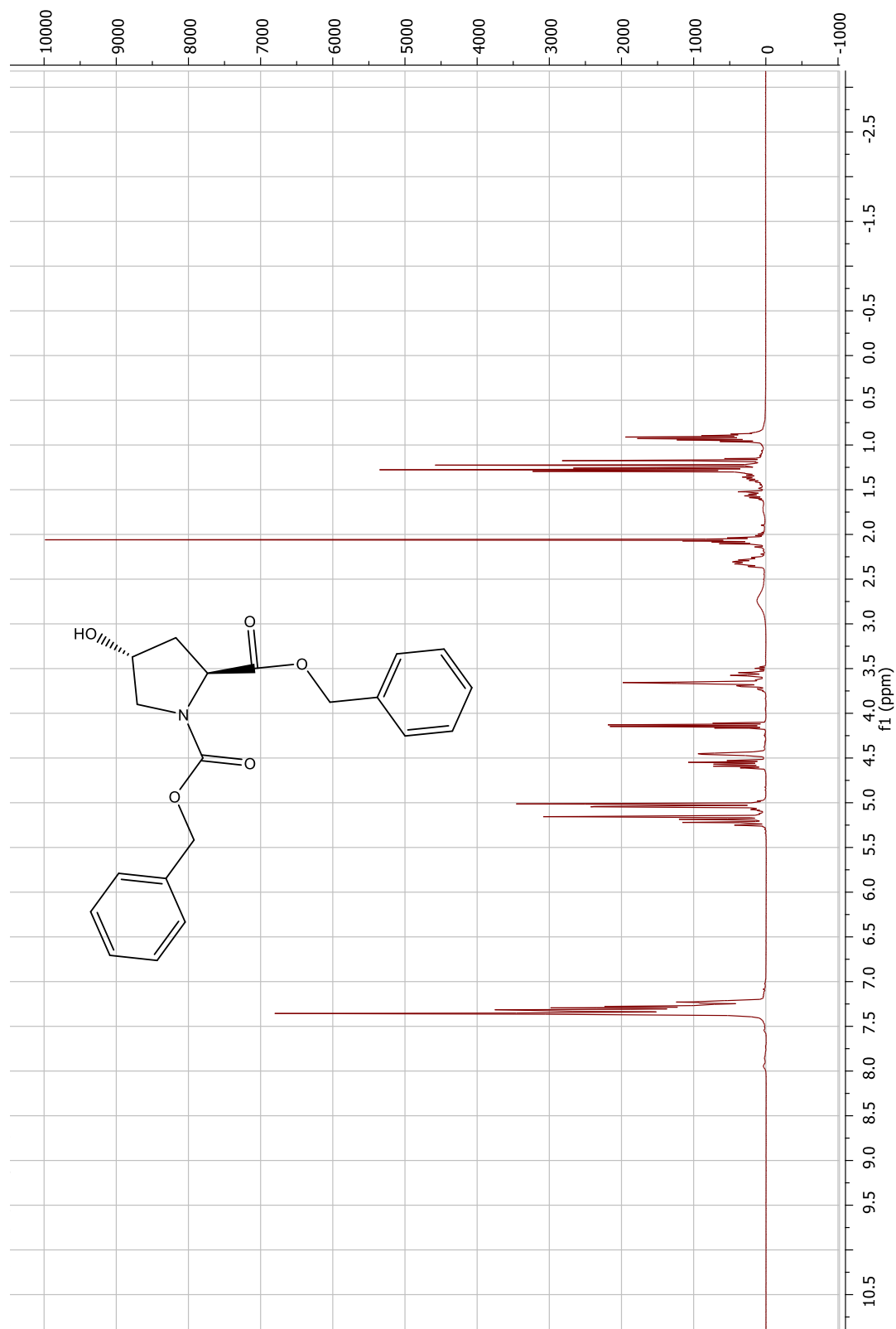


Appendix 1: ¹H NMR spectra product (1). Chemical structure of proline with benzyl attached and TsOH.

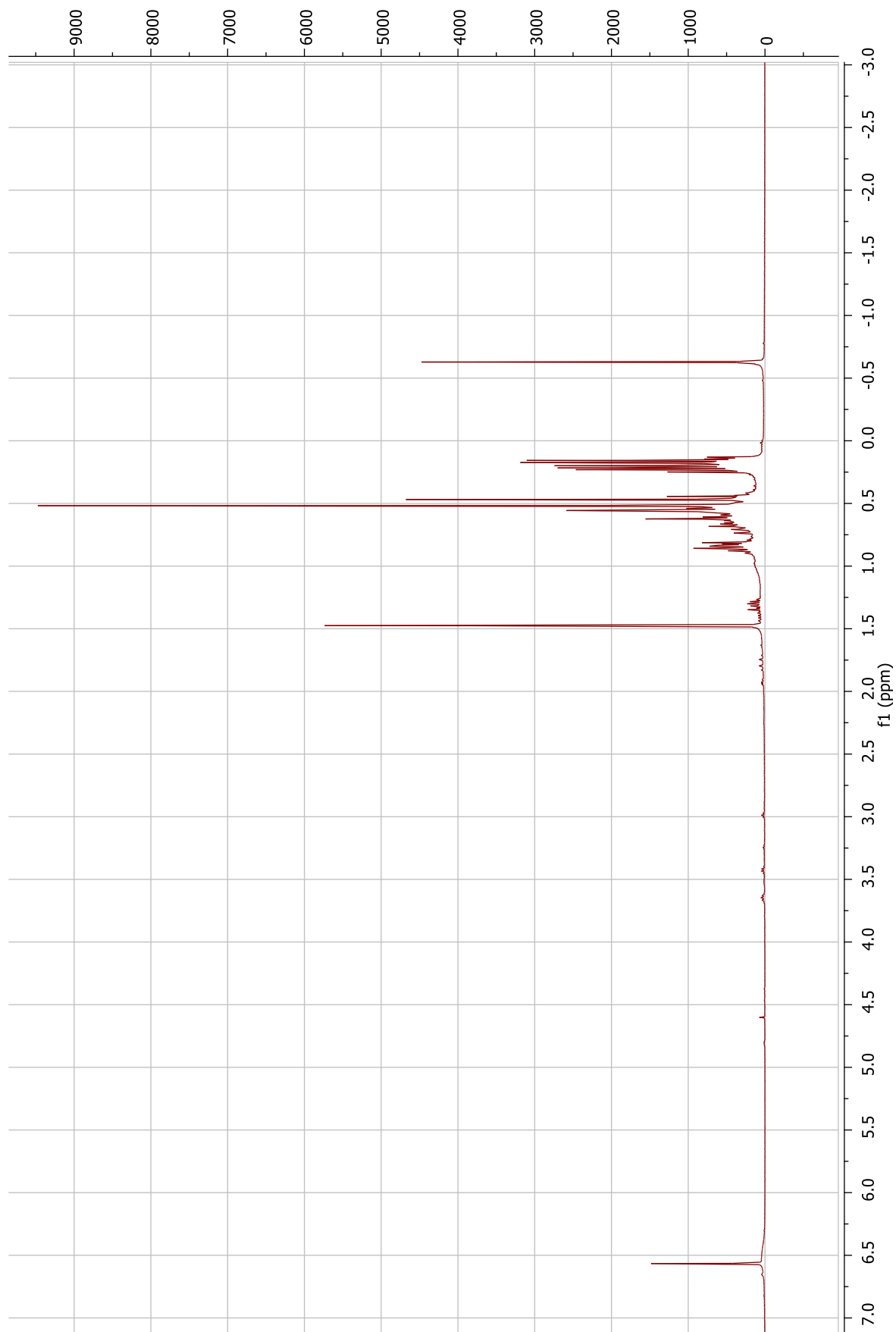
Title of current Chapter (in this example Appendix)



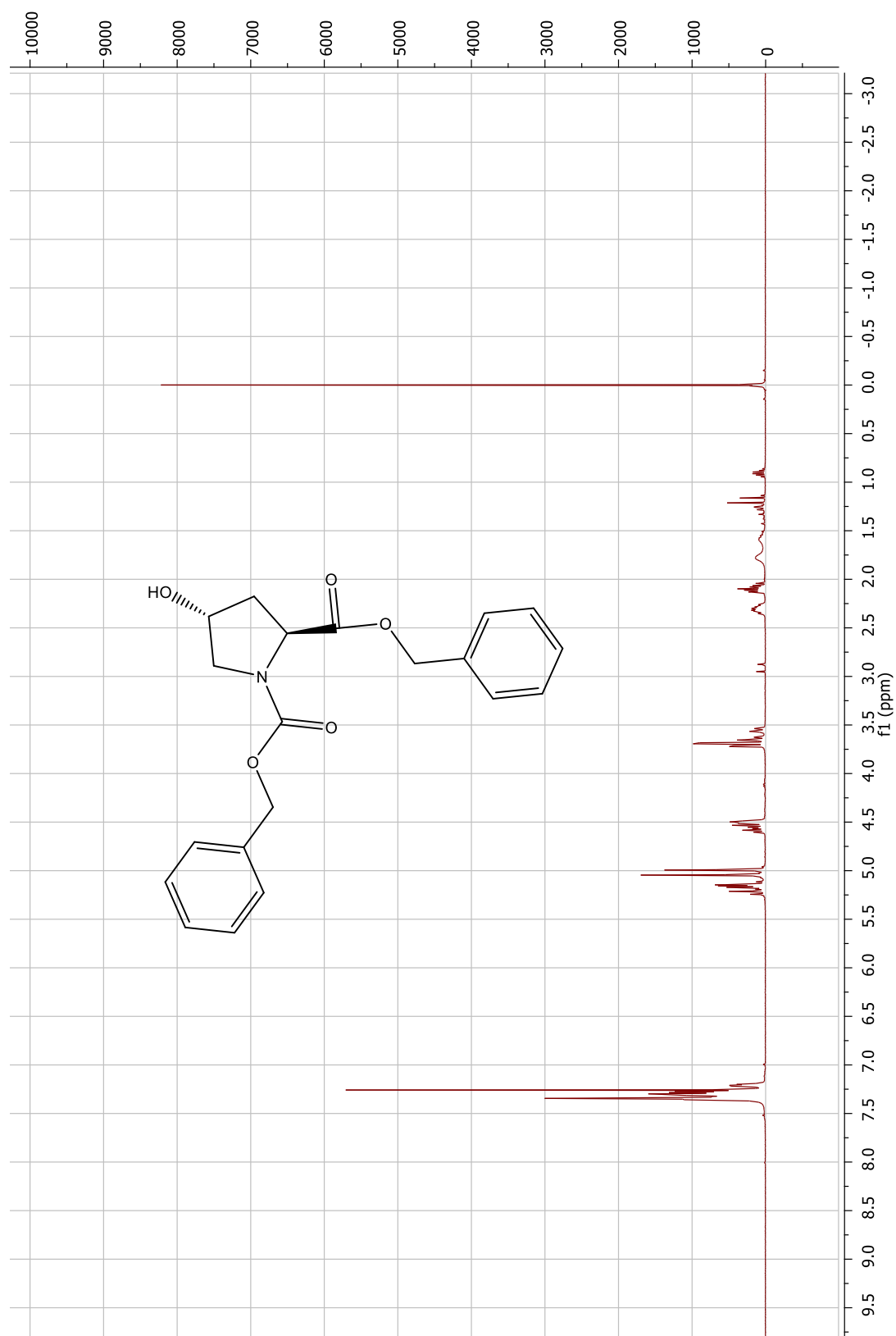
Appendix 2: IR spectra of product (1), text file data convert to excel graph. Chemical structure of proline with benzyl attached and TsOH.



Appendix 3: Chemical structure of proline with benzyl and Cbz group attached to the proline. NMR spectra of product (2) after Flash purification with the 'Analytical grade' petroleum ether solvent system along with ethyl acetate, showing significant 'grease' peaks in the lower chemical shift region.

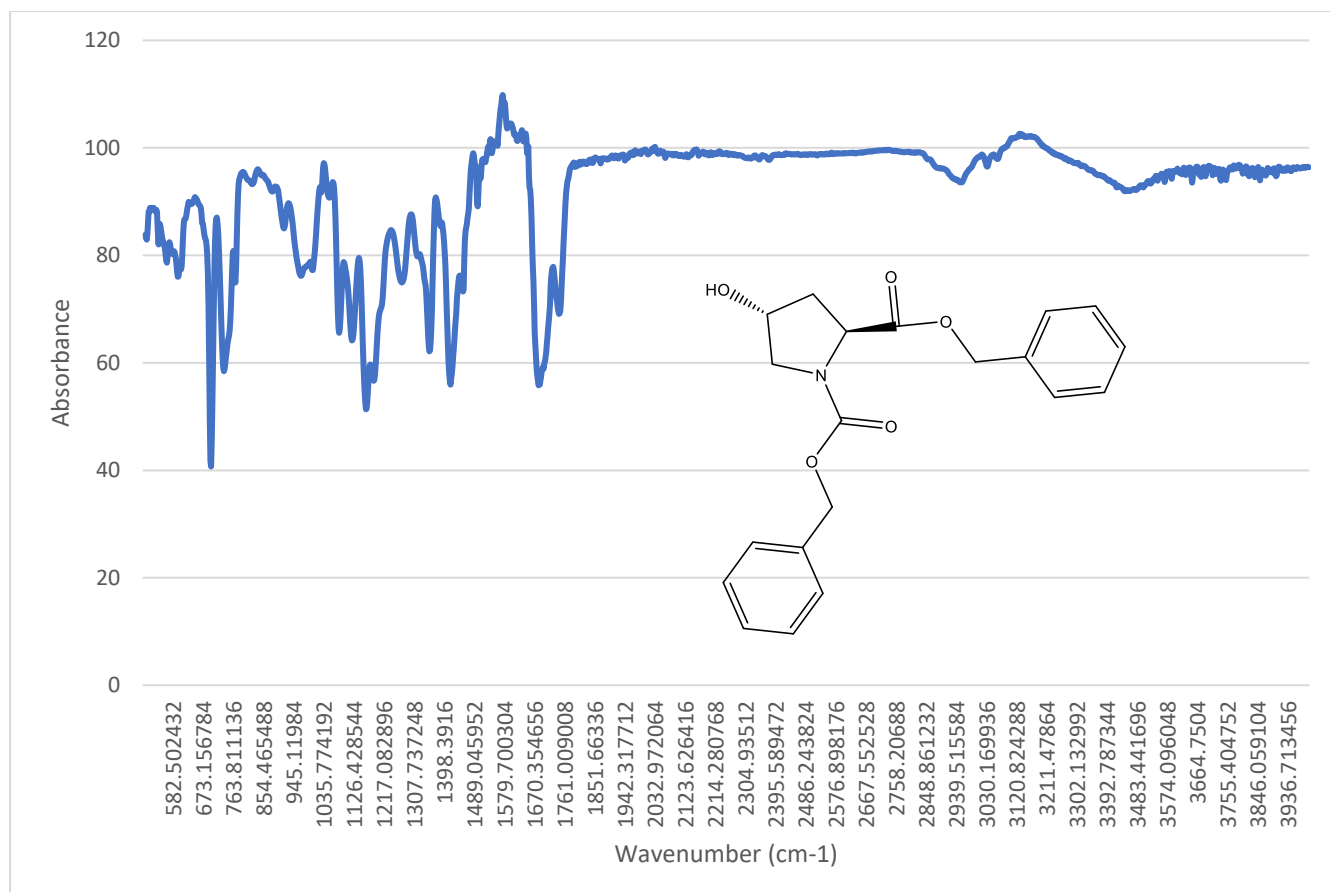


Appendix 4: ¹H NMR of 'analytical grade' petroleum ether, showing the 'grease' peaks

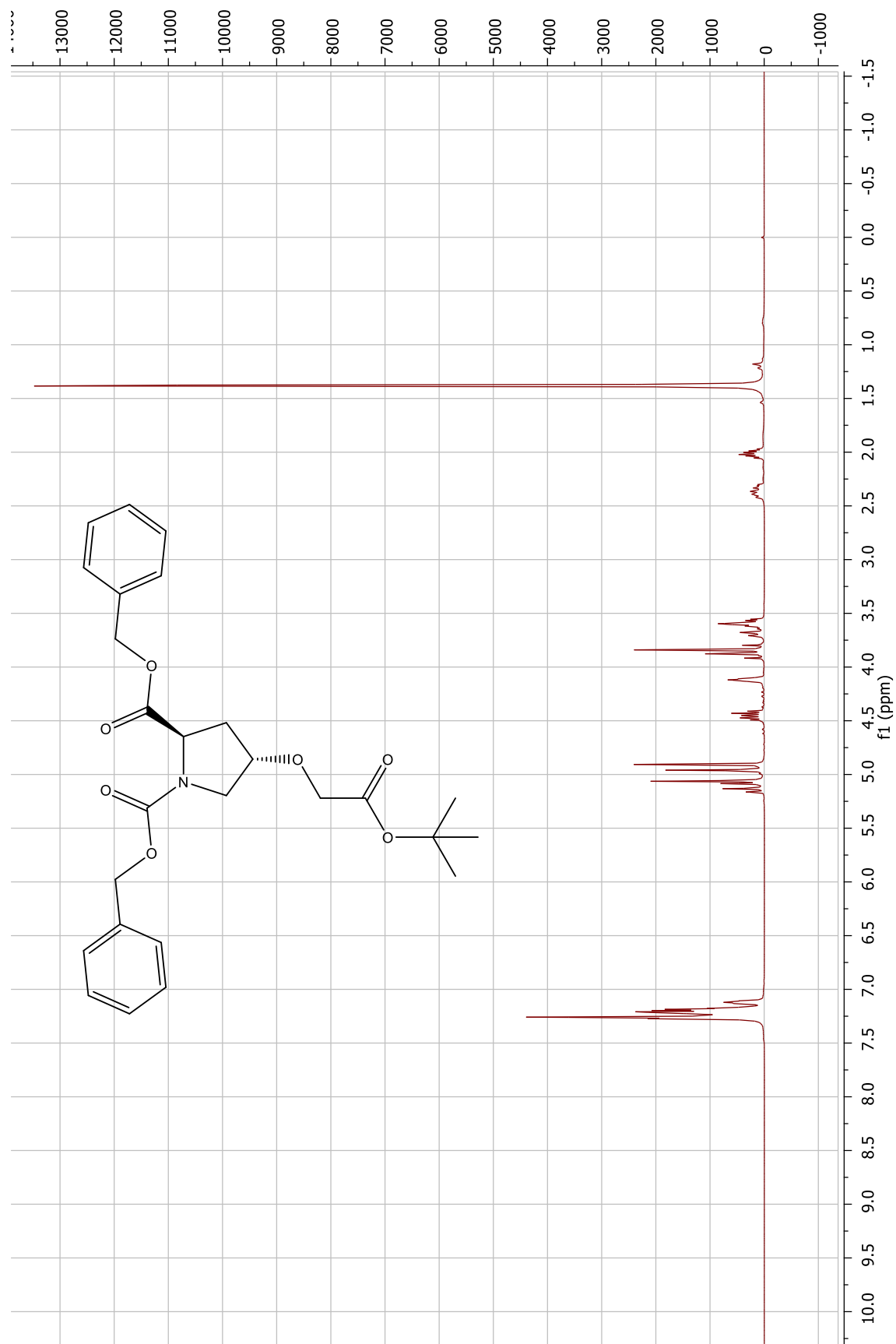


Appendix 5: NMR spectra of product (2) Chemical structure of proline with benzyl and Cbz group attached to the proline. after column purification with the 'laboratory grade' petroleum ether solvent system along with ethyl acetate, showing a big reduction of the 'grease' peaks in the lower chemical shift region.

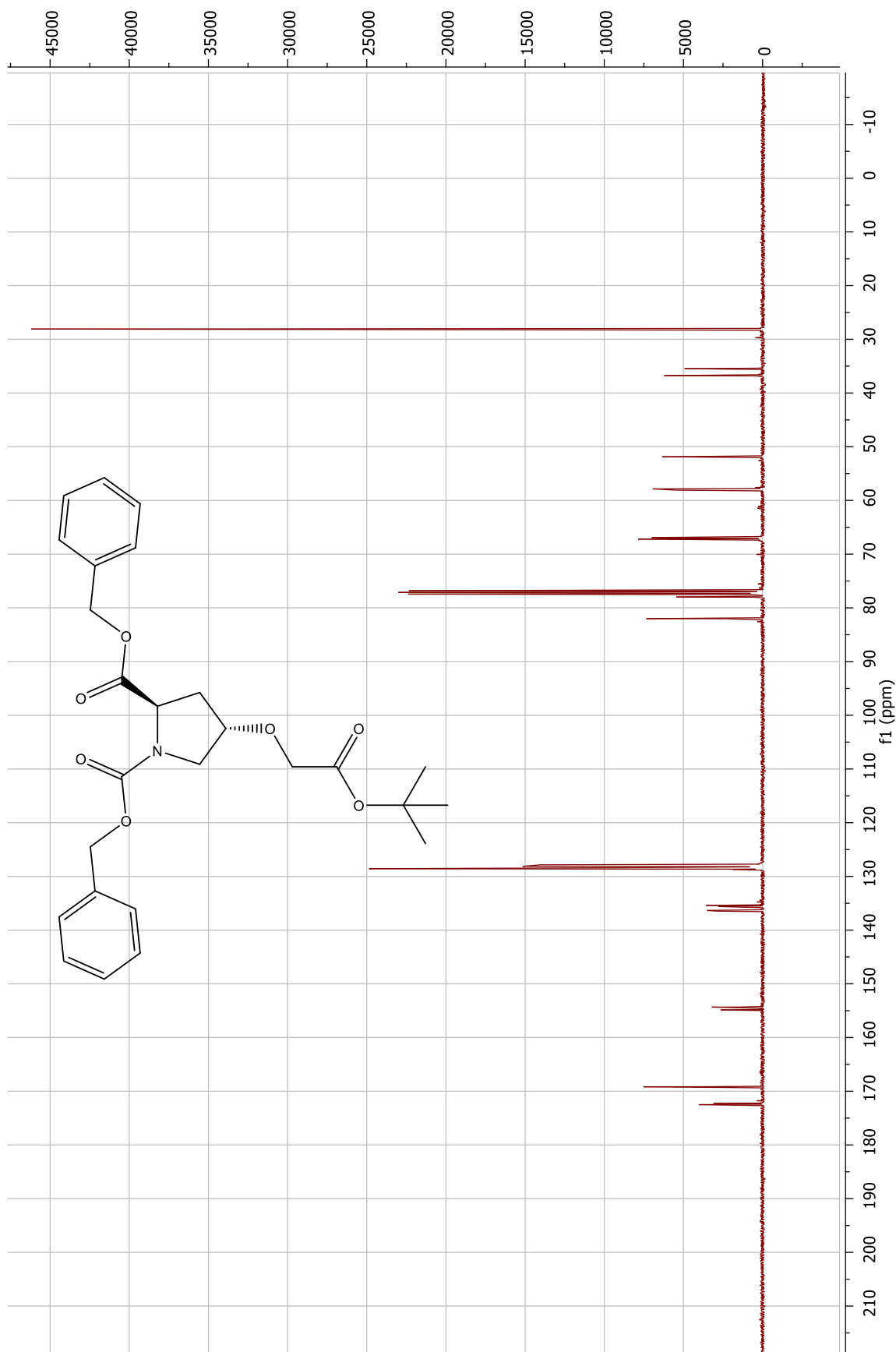
Title of current Chapter (in this example Appendix)



Appendix 6: IR spectra of product (2) text file data convert to excel graph. Chemical structure of proline with benzyl and Cbz group attached to the proline.

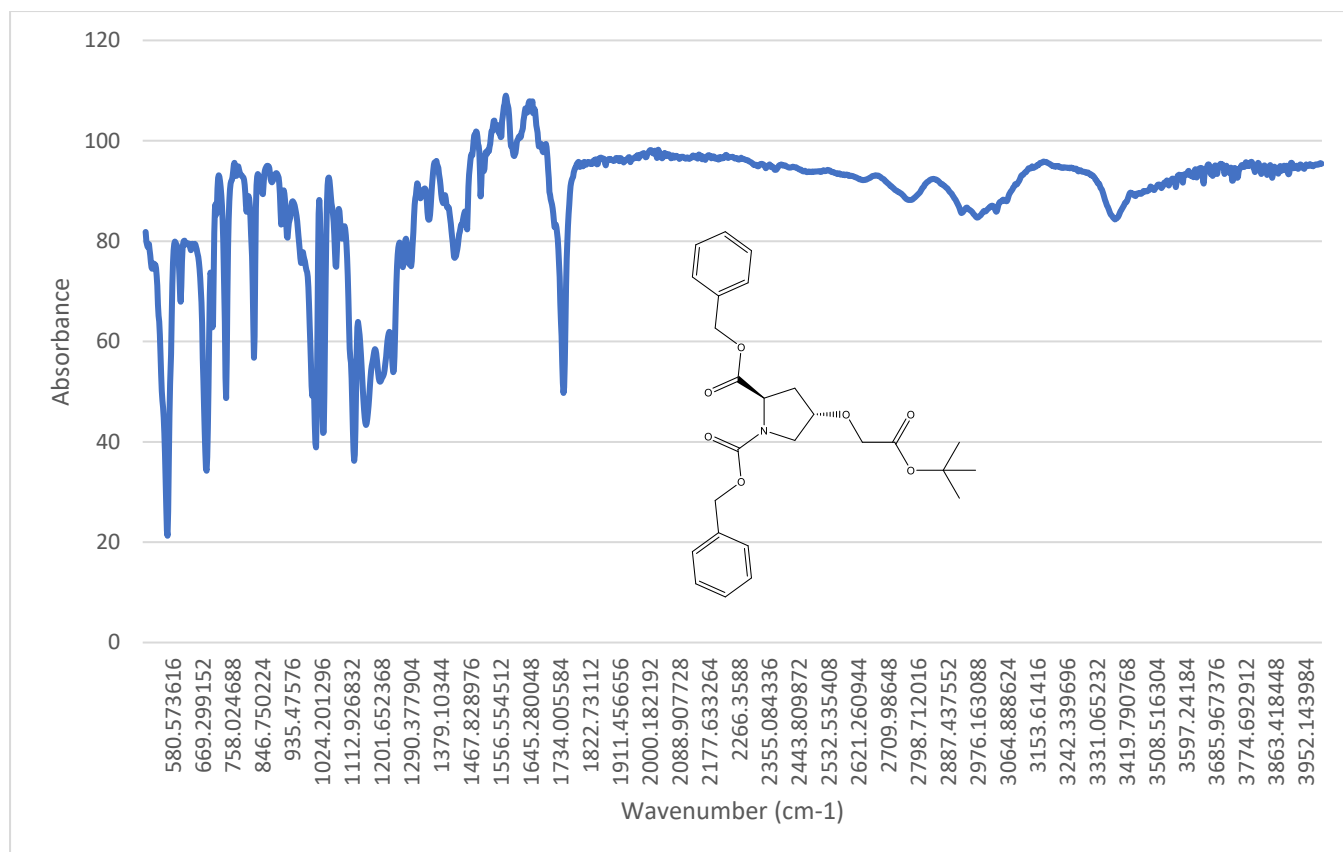


Appendix 7: ¹H NMR of product (3). Chemical structure of proline with benzyl, Cbz and tert-butyl acetate group attached to the proline

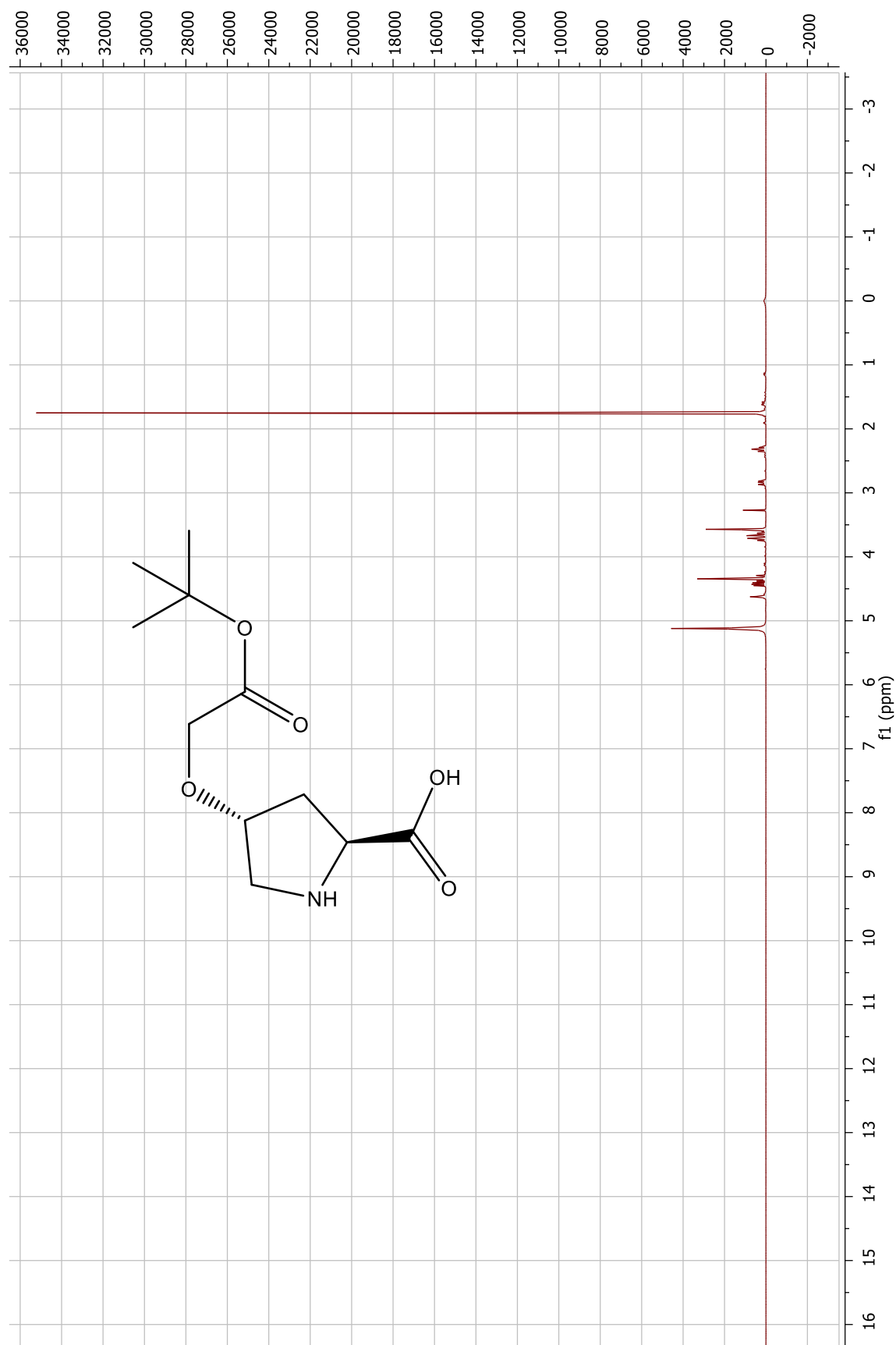


Appendix 8: Chemical structure of proline with benzyl, Cbz and tert-butyl acetate group attached to the proline. ¹³C NMR spectra of product (3).

Title of current Chapter (in this example Appendix)

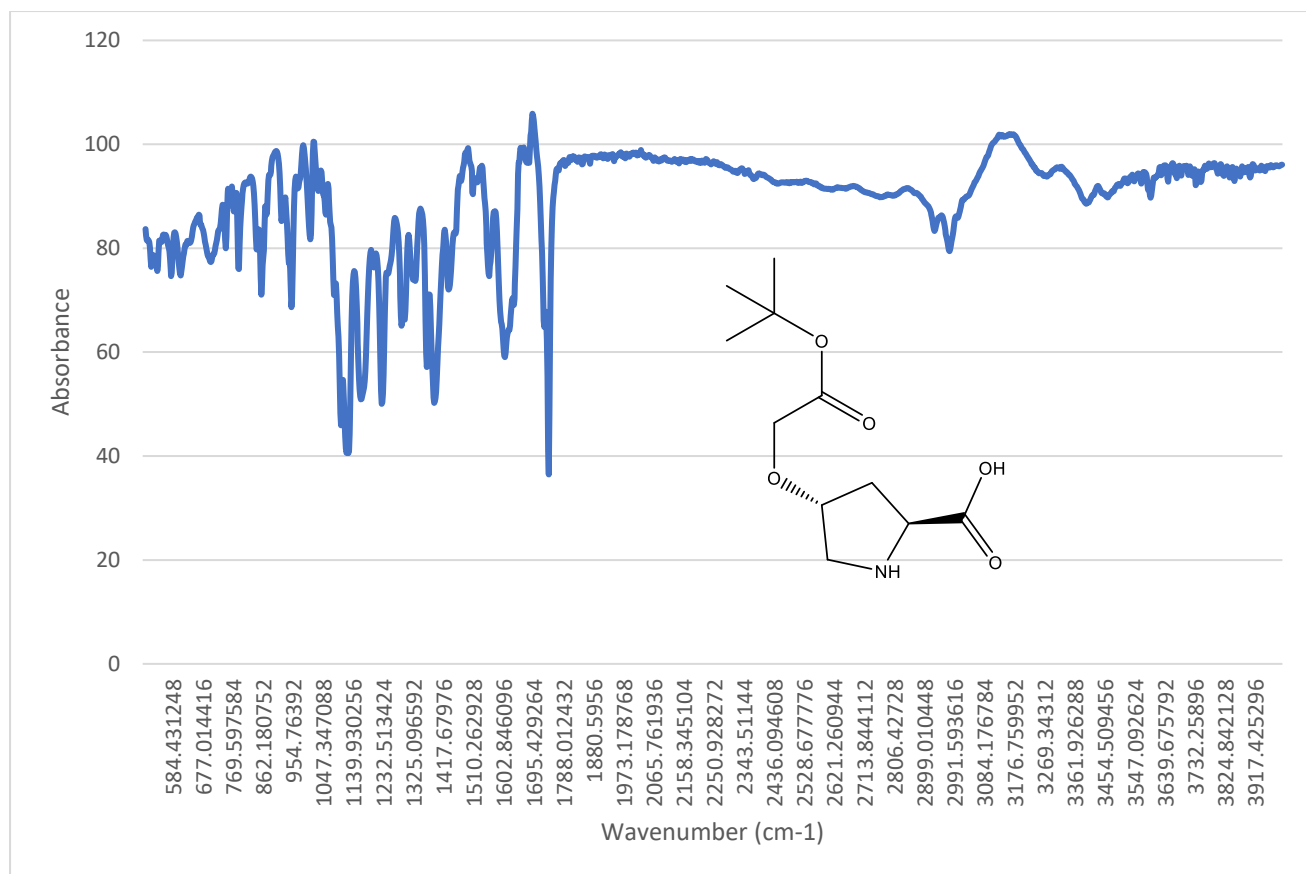


Appendix 9: IR spectra of product (3) text file data convert to excel graph. Chemical structure of proline with benzyl, Cbz and tert-butyl acetate group attached to the proline.

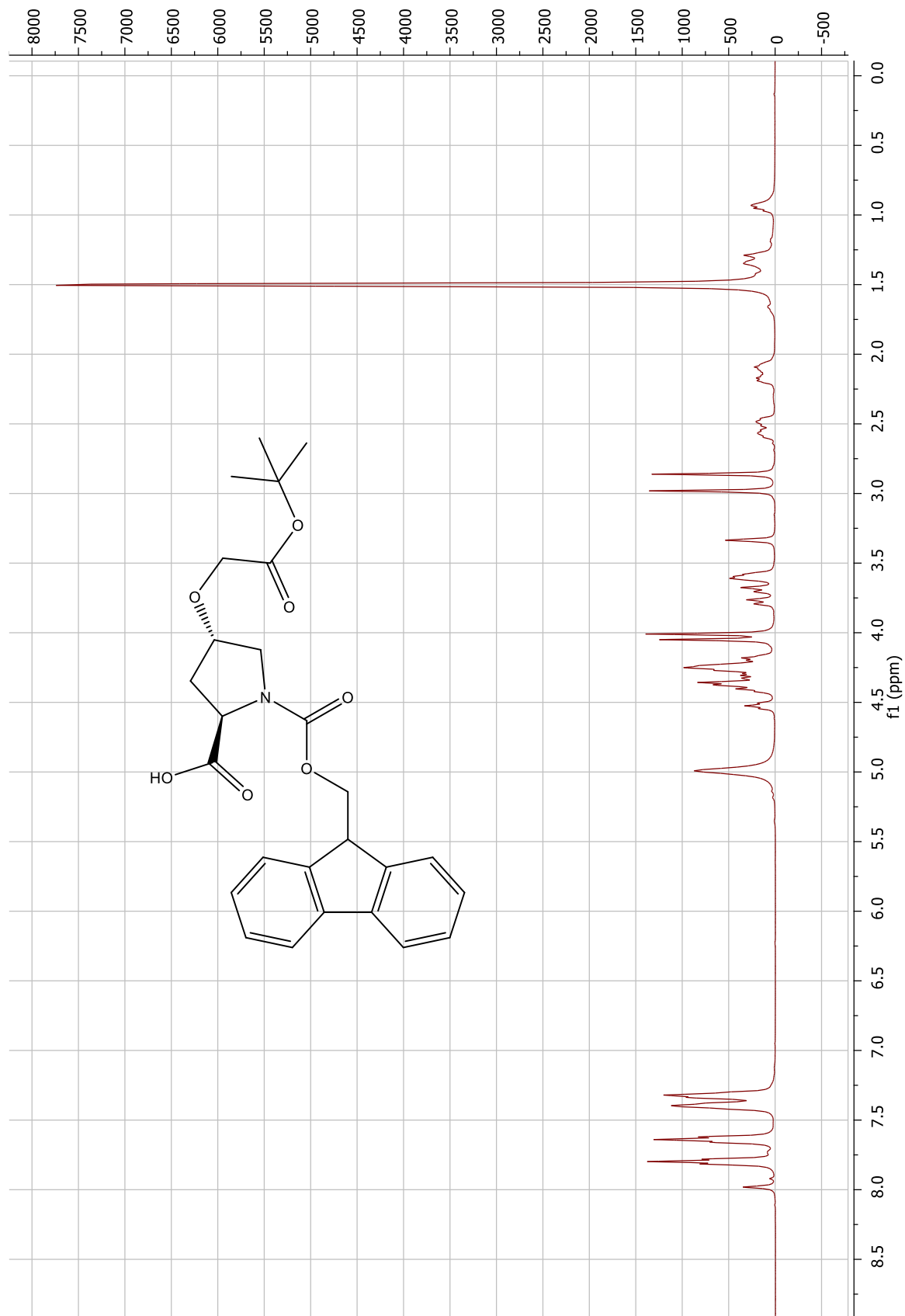


Appendix 10: ^1H NMR spectra of product (4). Chemical structure of proline with tert-butyl acetate group.

Title of current Chapter (in this example Appendix)

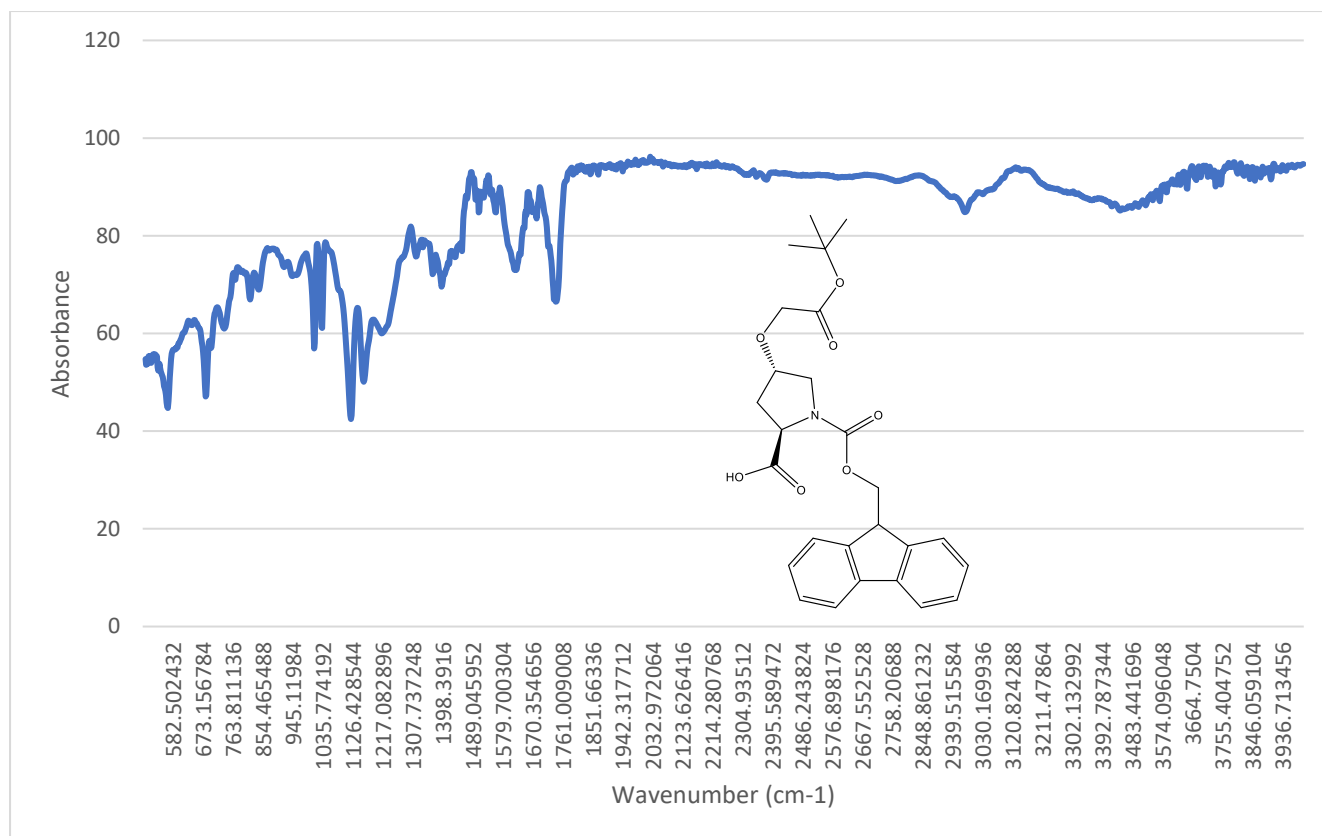


Appendix 11: IR spectra of product (4) text file data convert to excel graph. Chemical structure of proline with tert-butyl acetate group.

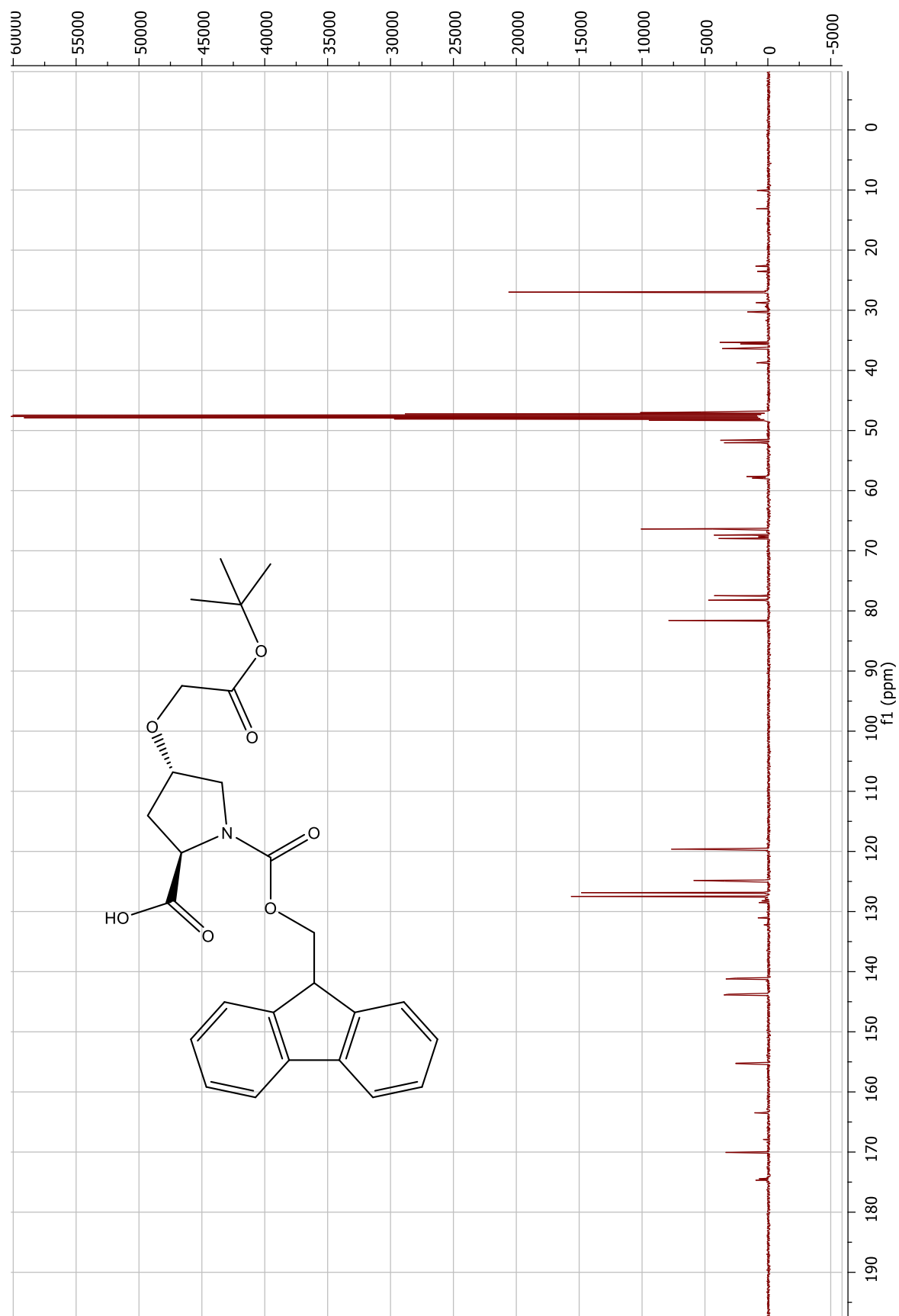


Appendix 12: ¹H NMR spectra of product (5). Chemical structure of proline with tert-butyl acetate group and Fmoc.

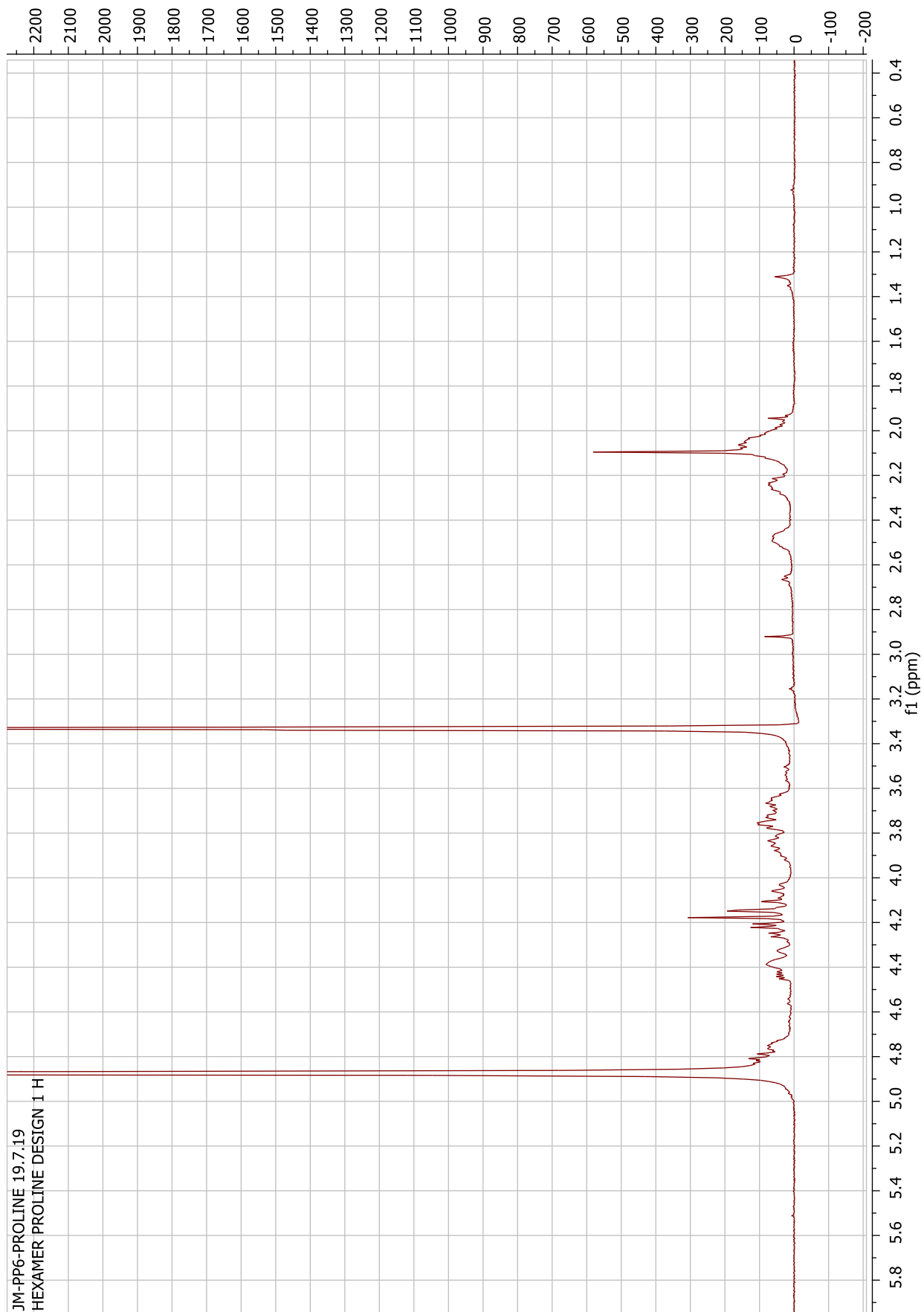
Title of current Chapter (in this example Appendix)



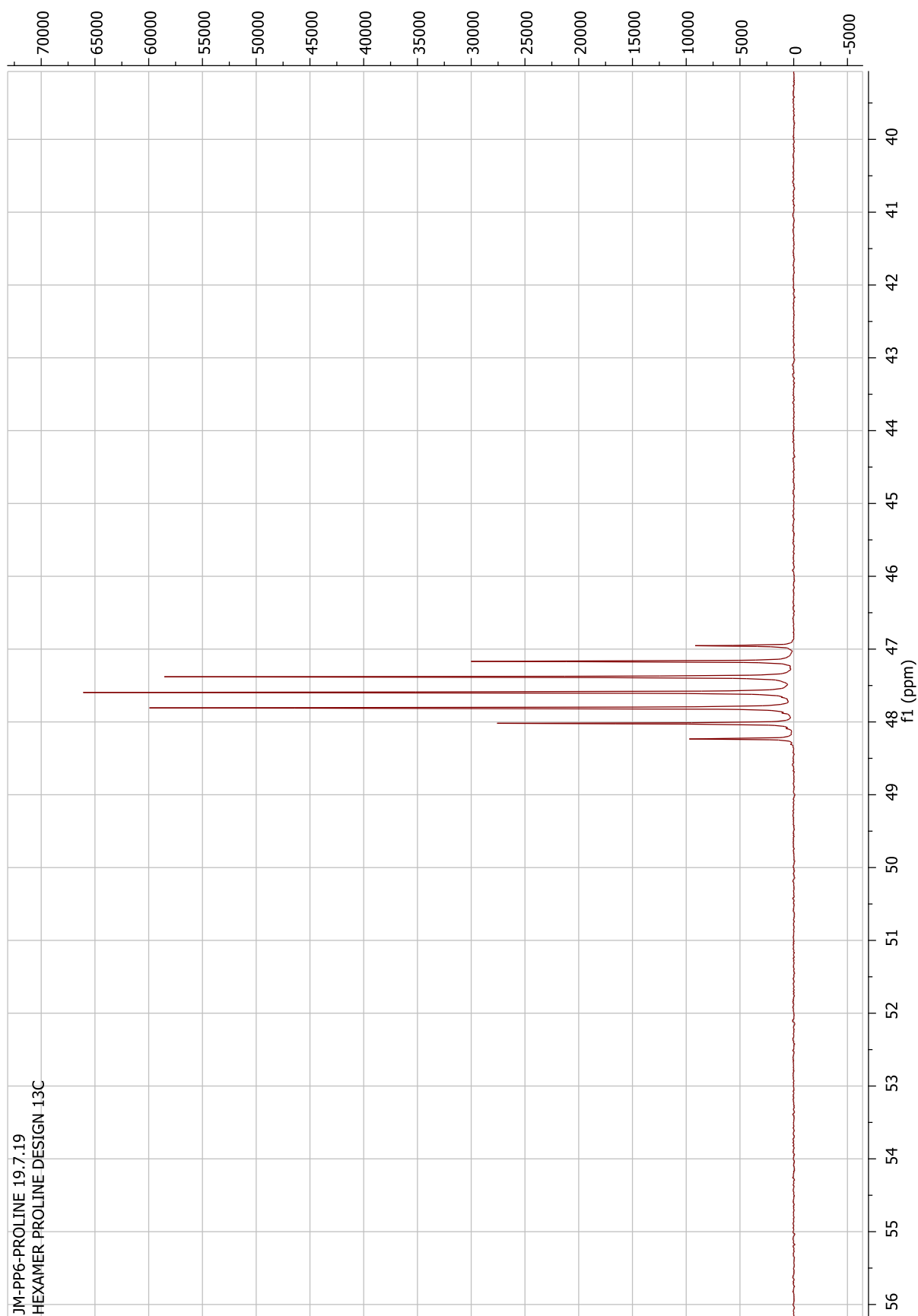
Appendix 13: IR spectra of product (5) text file data convert to excel graph. Chemical structure of proline with tert-butyl acetate group and Fmoc.



Appendix 14: ^{13}C spectra of product (5) Chemical structure of proline with tert-butyl acetate group and Fmoc.

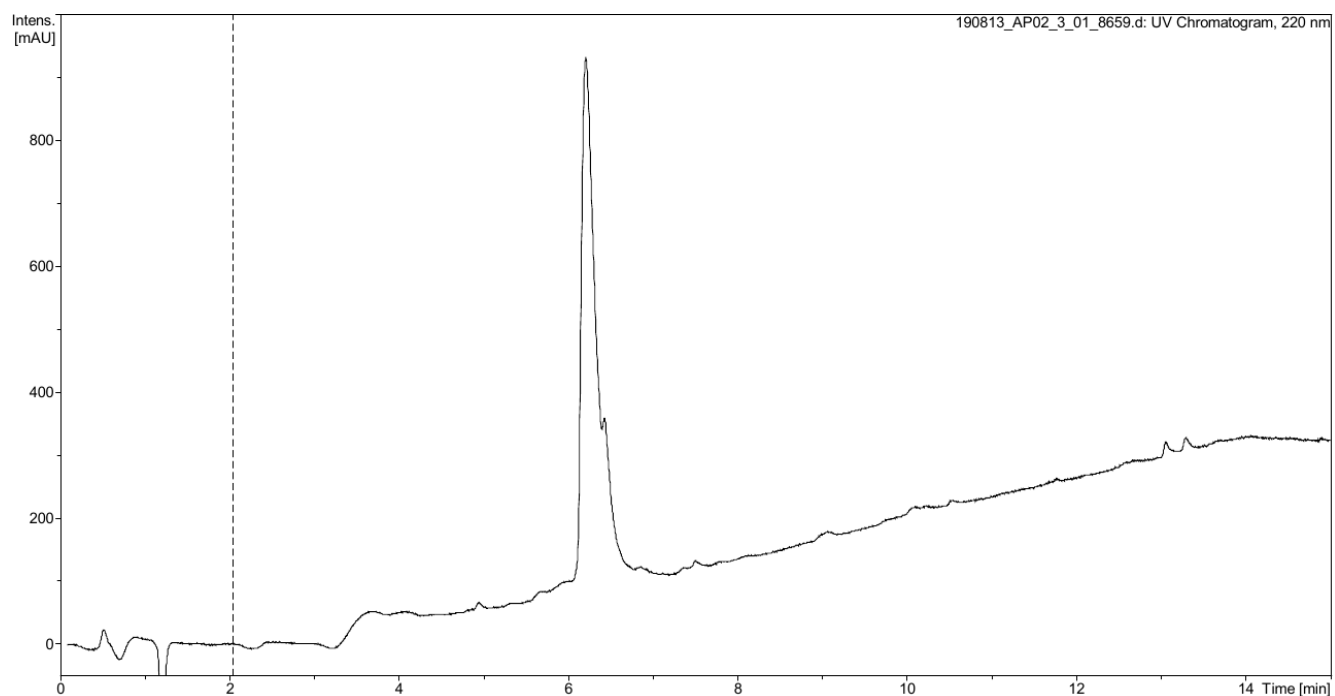
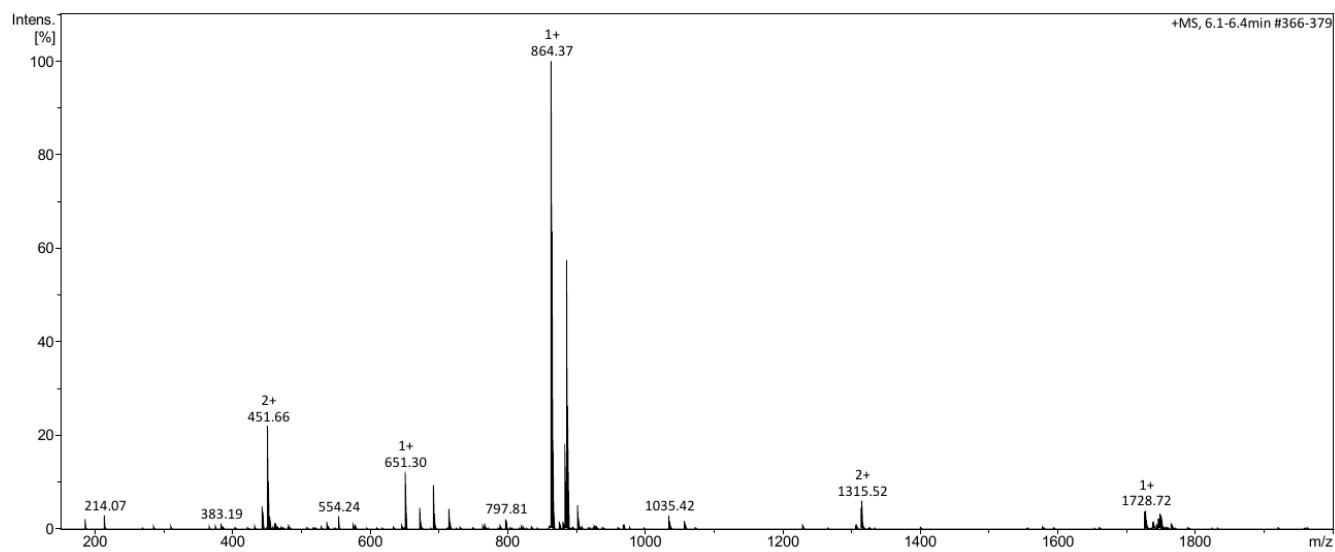


Appendix 15: ^1H NMR spectra of Hexamer PP6 design.



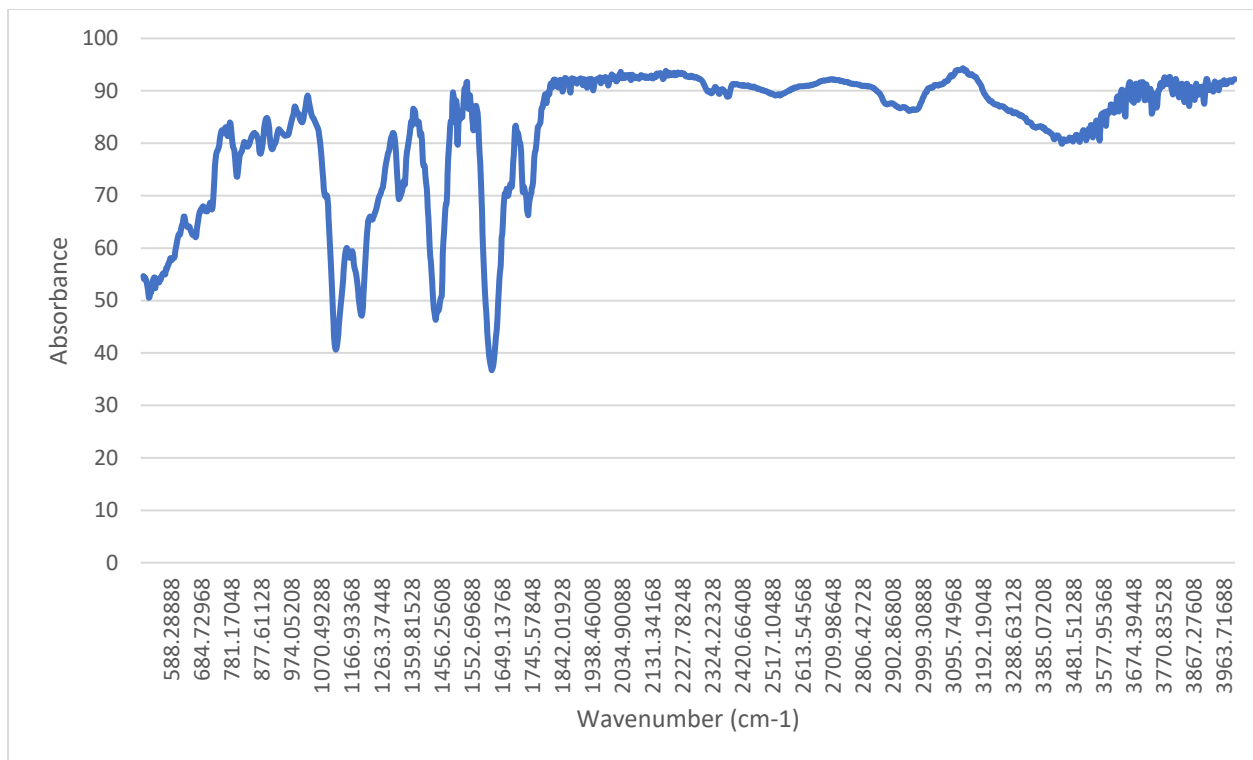
Appendix 16: ^{13}C NMR spectra of hexamer PP6 design.

Title of current Chapter (in this example Appendix)

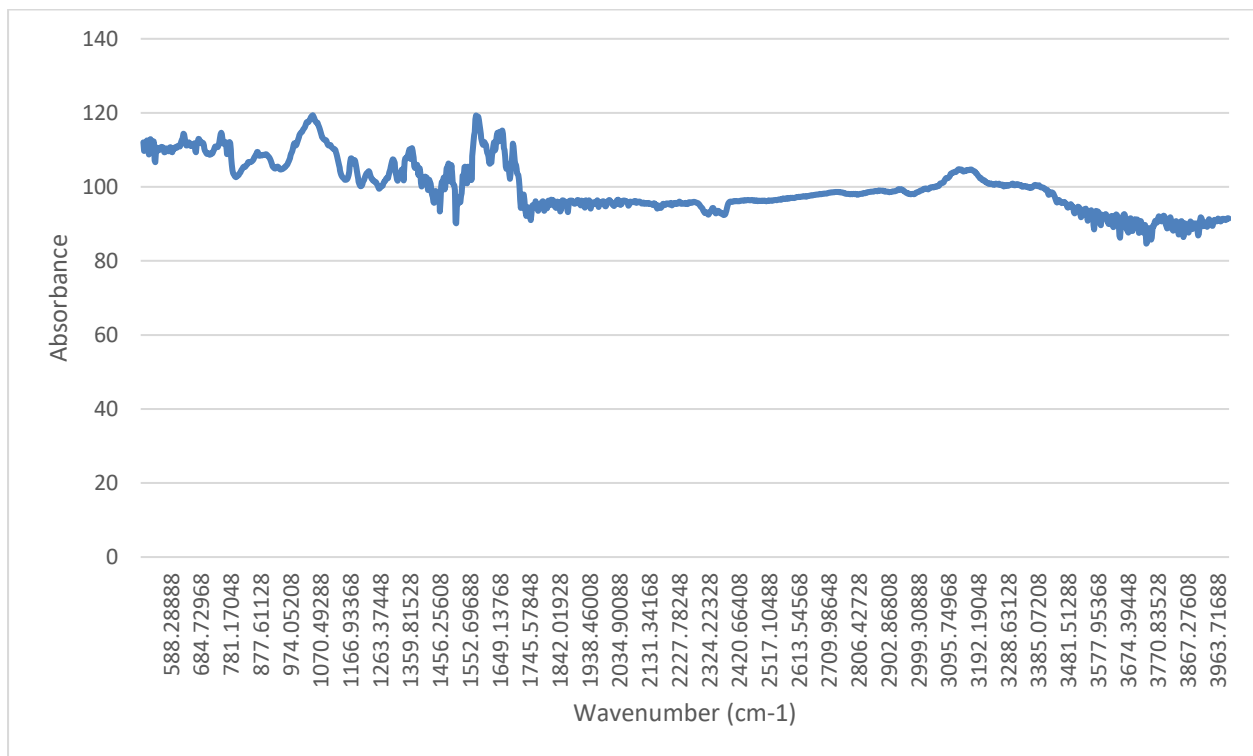


Appendix 17: MS spectra of hexamer PP6 design and retention time spectra of hexamer PP6 design.

Title of current Chapter (in this example Appendix)



Appendix 18: IR spectra of hexamer PP6 solid. text file data convert to excel graph



Appendix 19: IR spectra of hexamer PP6 in TFE solution. text file data convert to excel graph